DOT/FAA/TC-15/10

Development and Validation of Structural Usage and Loads Monitoring Methods for Use in Determining Rotorcraft Usage Credits

December 2015

Final Report

U.S. Department of Transportation
Federal Aviation Administration

NOTICE

This document is disseminated under the sponsorship of the U.S. Department of Transportation in the interest of information exchange. The U.S. Government assumes no liability for the contents or use thereof. The U.S. Government does not endorse products or manufacturers. Trade or manufacturers' names appear herein solely because they are considered essential to the objective of this report. The findings and conclusions in this report are those of the author(s) and do not necessarily represent the views of the funding agency. This document does not constitute FAA policy. Consult the FAA sponsoring organization listed on the Technical Documentation page as to its use.

This report is available at the Federal Aviation Administration William J. Hughes Technical Center's Full-Text Technical Reports page: actlibrary.tc.faa.gov in Adobe Acrobat portable document format (PDF).

1. Report No. DOT/FAA/TC-15/10	2. Government Accession No.	3. Recipient's Catalog No.	
4. TITLE AND SUBTITLE DEVELOPMENT AND VALIDATION OF STRUCTURAL USAGE AND LOADS MONITORING METHODS FOR USE IN DETERMINING ROTORCRAFT USAGE CREDITS		5. Report Date December 2015	
		6. Performing Organization Code	
7. Author(s) Ray Beale and Mark Davis		8. Performing Organization Report No.	
9. Performing Organization Name and Address Sikorsky Aircraft Corporation 6900 Main Street Stratford, CT 06615-9129		10. Work Unit No. (TRAIS)	
		11. Contract or Grant No. DTFACT-11-D-00004 (DO-0001)	
12. Sponsoring Agency Name and Address U.S. Department of Transportation Federal Aviation Administration Southwest Region-Aircraft Certification Service Directorate 2601 Meacham Boulevard Fort Worth, TX 76137		13. Type of Report and Period Covered Final Report July 13, 2011–July 15, 2014	
		14. Sponsoring Agency Code ASW-112	

15. Supplementary Notes

The Federal Aviation Administration William J. Hughes Technical Center Aviation Research Division CORs were Paul Swindell and Traci Stadtmueller.

16. Abstract

The Federal Aviation Administration has funded research and development efforts to establish and demonstrate viable approaches for validating and certifying health and usage monitoring systems (HUMS) regime recognition (RR) enabled usage-based maintenance (UBM) credits. In a previous contract, Sikorsky Aircraft Corporation defined an end-to-end UBM process that fulfills the objectives of Advisory Circular (AC) 29-2C and works with available HUMS. This effort included the development of an RR clustering approach for addressing identified shortcomings of current RR algorithms that can be applied through post-processing of HUMS data without having to modify existing RR onboard software.

This new research builds on the previous work, culminating in a flight test and fleet demonstration of several virtual usage monitoring technologies, including RR with clustering, virtual monitoring of loads, and gross weight estimation that can provide valuable insight into actual fleet usage and loads using existing HUMS aircraft parametric state parameters and without needing to integrate physical sensors. Under separate funding, a flight test program on a UH-60M aircraft was conducted by the Army Communications-Electronics Research, Development and Engineering Center. This provided a unique set of validation flight data using the baseline production Integrated Vehicle Health Management System along with independent truth measurements of key dynamic component loads. The RR clustering algorithms were then applied to operational UH-60M fleet data and compared to the design usage spectrum. This research shows how these usage monitoring technologies can be validated, applied to fleet data, and post-processed to arrive at meaningful results to inform a usage/loads-based fatigue life management process.

17. Key Words Structural usage and loads monitoring, Regime recognition, Structural usage credit, Usage-based maintenance, Retirement-time adjustment, Life extension	18. Distribution Statement This document is available to the U.S. public through the National Technical Information Service (NTIS), Springfield, Virginia 22161. This document is also available from the Federal Aviation Administration William J. Hughes Technical Center at actlibrary.tc.faa.gov.		
19. Security Classif. (of this report) Unclassified	20. Security Classif. (of this page) Unclassified	21. No. of Pages 89	22. Price

Form DOT F 1700.7 (8-72)   Reproduction of completed page authorized

TABLE OF CONTENTS

LIST OF FIGURES

LIST OF TABLES

LIST OF ABBREVIATIONS AND ACRONYMS

AC	Advisory Circular
AED	Aviation Engineering Directorate
AOB	Angle of bank
ARL	Army Research Laboratory
CERDEC	Communications-Electronics Research, Development and Engineering Center
CG	Center of gravity
CONOPS	Concept of Operations
CRT	Calculated retirement time
CWC	Composite worst case
Deg	degree
DO	Delivery order
DOE	Design of experiment
ESSS	External stores support system
FAA	Federal Aviation Administration
FLS	Flight loads survey
GW	Gross weight
HUMS	Health and usage monitoring systems
IGE	In ground effect
IMD-HUMS	Integrated mechanical diagnostics-health and usage monitoring systems
IVHMS	Integrated Vehicle Health Management System
LLP	Life-limited part
MRLSS	Main rotor lateral stationary swashplate
MRSEBL	Main rotor shaft extender bending load
NOE	Nap-of-the-earth
NR	Rotor rpm
NZ	Vertical acceleration
OEM	Original equipment manufacturer
OGE	Out of ground effect
R&D	Research and development
RR	Regime recognition
S/N	Stress-life
SAC	Sikorsky Aircraft Corporation
UBM	Usage-based maintenance
UMRF	Usage monitor reliability factor
VH	Maximum air speed
VML	Virtual monitoring of loads

EXECUTIVE SUMMARY

Monitoring of actual aircraft structural usage would increase rotorcraft safety enhancements provided by health and usage monitoring systems (HUMS) and could potentially reduce operating costs via usage-based maintenance (UBM) credits. Though flight regime recognition (RR) algorithms have been demonstrated, none have been fully validated or used to obtain UBM credit approval because of complex certification issues. The Federal Aviation Administration (FAA) has funded research and development (R&D) efforts to establish and demonstrate viable approaches for validating and certifying HUMS RR-enabled UBM credits. In a previous contract, Sikorsky Aircraft Corporation (SAC) defined an end-to-end UBM process that fulfills the objectives of Advisory Circular (AC) 29-2C and works with available HUMS. This effort included the development of an RR clustering approach for addressing identified shortcomings of current RR algorithms that can be applied through post-processing of HUMS data without having to modify existing RR onboard software.

The subject FAA-funded R&D effort builds on the previous work, culminating in a flight test and fleet demonstration of several virtual usage monitoring technologies, including RR with clustering, virtual monitoring of loads (VML), and gross weight (GW) estimation, which can provide valuable insight into actual fleet usage and loads using existing HUMS aircraft parametric state parameters and without needing to integrate physical sensors.

The technical work herein started with a component, load, and regime selection. From this analysis, two key loads were selected for instrumentation in the Army Communications-Electronics Research, Development and Engineering Center (CERDEC) flight test that covered several life-limited dynamic components: the main rotor lateral stationary swashplate (MRLSS) axial load, which can be used to substantiate the gearbox housing, and the main rotor shaft extender bending load, which can be used to substantiate the main rotor shaft, shaft extender, and hub. Important regimes for these substantiating parameters, based on the component life sensitivity study, were turns and climbs. These regimes and loads became the focus of the flight test evaluation.

Under separate FAA funding, a flight test program on a UH-60M aircraft was conducted by CERDEC. The primary objectives of this program were to provide validation data for RR, GW/center of gravity (CG), and VML algorithms, and to generate design of experiment data for the Army Research Laboratory to support a pilot sensitivity study. Climb and banked turn maneuvers were flown to support the development of RR clustering algorithms. These maneuvers differed from typical flight loads survey (FLS) maneuvers in that they included unique techniques to explore the boundaries of the regime definitions. The GW/CG estimation algorithms required level flight and out of ground effect (OGE)/in ground effect (IGE) hover maneuvers at several vehicle configurations. The VML algorithm validation for key substantiating parameters required focusing on the turn, climb, and dive regimes, which were identified as key fatigue life drivers.

The RR clustering methods were applied to the CERDEC test data to show how raw RR data can be processed and refined in a way that is consistent with the UH-60M composite worst case (CWC) usage spectrum. Several RR clustering validation methods were demonstrated that use

parametric truth regime definitions, flight regime load analysis, and flight test run log data. The flight test run log validation approach is demonstrated on existing UH-60M FLS test data.

The VML and GW estimation algorithms were also applied to the CERDEC flight test data. Use of these models was shown to be a viable approach for monitoring actual aircraft usage and loads. While neither of these virtual methods is perfect, the error distributions are reasonable and well-behaved such that error models can be created for use in a probabilistic framework for establishing reliability factors to ensure safety and reliability associated with UBM processes and credits.

An overview of UBM processes is provided, which describes current fatigue life management practices and relates the current process to various approaches to UBM. A proposed serial number UBM credit process is described, which includes a framework for maintaining equivalent reliability.

The RR clustering algorithms developed from the CERDEC testing were then applied to fleet data and compared to the UH-60M CWC usage spectrum. To support this task, the U.S. Army Aviation Engineering Directorate provided SAC with three populations of sample fleet data from operational UH-60M aircraft. The RR clustering algorithm was shown to be a viable approach for refining raw RR output data to support both fleet-wide usage calculated retirement time (CRT) adjustments or individual tail number CRT adjustments without having to modify existing onboard software. The clustering algorithm provides a more realistic picture of helicopter usage than the baseline Integrated Vehicle Health Management System RR algorithms, even in the presence of a complex series of maneuvers.

Applying these usage monitoring technologies to fleet data uncovered some challenges that are unique to an operational fleet environment. The focus of the work conducted in delivery order (DO) 0002 will be to apply these methods to operational fleet data within a production framework in support of a specific mock UBM certification that will be shown to be in compliance with AC 29-2C, MG-15. This effort is ongoing and will be documented in a separate technical report for that DO.

1. INTRODUCTION

One of the central goals of usage-based maintenance (UBM) is to change the maintenance paradigm from one that is currently flight-hour or schedule based to one that is based on usage and loads. For example, life-limited parts (LLPs) are currently retired based on the number of flight hours flown, regardless of whether the aircraft is only flown benignly (e.g., VIP transport) or is flown much more aggressively (e.g., cargo transport with many ground-air-ground cycles per hour). A certified UBM process that accurately monitors usage and loads would enable the attainment of retirement time credits (or debits) for LLPs based on measured aircraft configuration, usage, and loads rather than flight hours and the use of underlying conservative design assumptions. Virtual sensing methods that use measured aircraft state parameters have been developed previously by Sikorsky Aircraft Corporation (SAC) to monitor key parameters, including: regime recognition (RR) algorithms with associated clustering techniques; virtual monitoring of loads (VML); and gross weight (GW) and center of gravity (CG) estimation. The research documented herein focused on the application of these methods and algorithms to real flight test and fleet data to show the potential benefit of UBM and to identify challenges relevant to the certification of UBM processes and credits using these virtual usage and loads monitoring methods.

Dynamic component retirement times are currently set by a rigorously defined fatigue damage calculation process that computes a calculated retirement time (CRT) from three basic inputs: component strength with reliability-based safety factors, a composite worst case (CWC) usage spectrum, and a load spectrum derived from flight tests. Component strength is generally derived from full-scale component fatigue testing. The CWC spectrum combines conservative assumptions on aircraft usage with high envelope loads. The usage typically is given in the form of a list of flight regimes, each of which is assigned either a percentage of total flight time or a rate of occurrence (maneuvers per 100 flight hours). Flight loads are developed in the flight loads survey (FLS), a comprehensive flight test program that exercises the extremes of aircraft performance to develop the highest expected loads for each regime. Each component is assigned one or more substantiating load parameters, which characterize the load states for that component's critical failure mode. Common substantiating parameters for dynamic components are derived from calibrated bending and axial bridges, such as a main rotor shaft bending bridge or a push rod axial load bridge. They can also be based on more local stress/strain measurements when necessary. The three inputs (i.e., strength, usage, and loads) are then combined in a stress-life fatigue calculation, which results in the CRT.

The Integrated Vehicle Health Management System (IVHMS) is the next generation system derived from the integrated mechanical diagnostics-health and usage monitoring systems (IMD-HUMS). The IVHMS is standard equipment on the SAC UH-60M aircraft, and the IMD-HUMS is standard equipment on the S-92 aircraft. Aside from recording a large quantity of aircraft-state parameters, such as airspeed, engine power measurements, and pilot control inputs, both the IVHMS and IMD-HUMS execute similar RR algorithms from these state parameters. These algorithms translate aircraft state measurements into regime classifications (e.g., climbing left turn or level flight at 0.8 VH), which can be used to better understand aircraft usage, which drives component retirement times. The result is a recorded time sequence of regimes flown for each flight.

Though the current onboard RR algorithms provide significant insight into the usage of operational aircraft, some shortcomings have been identified that must be overcome to develop a practical UBM process that can be certified for securing credits and benefits. One such issue is the frequent toggling of RR output data due to the precise second-by-second classification using state parameter data. To overcome some of the shortcomings of this system, additional off-board processing of these data is desired to enable existing onboard software capabilities to be exploited without the need to invest in costly onboard software changes. One such technique is called regime clustering. After being trained on a given dataset, this additional processing gathers regime time sequences into contiguous maneuvers or target regimes, which more accurately represent the aircraft usage both in terms of pilot intent and CWC design assumptions than the fine, second-by-second, granularity regime sequences produced by the IHVMS, IMD-HUMS, and similar systems. The regime clustering algorithms work by reprocessing the IVHMS RR sequence outputs into broader target regimes based on statistical and physics-/experience-based rules.

The state parameters collected by the IVHMS and IMD-HUMS can also be processed off-board to estimate additional aircraft configuration parameters, such as GW and CG location. The algorithms involved can be grouped into two classes—physics-based and mathematical models. Both classes of algorithms operate only on a small subset of aircraft regimes, which are chosen to enhance algorithm accuracy. This typically is limited to hover and steady-level flight. In another off-board processing application of aircraft state parameter data, individual loads can be estimated in continuous time through VML algorithms. After being trained, these mathematical models recreate the readings of individual strain gages, bending bridges, or other load measurements that were included in the aircraft FLS as a substantiating parameter. If a given load is also a component substantiating parameter, it is possible to gain a better understanding of the remaining fatigue capacity of a component subjected to field usage.

This report documents several tasks that were conducted to achieve a flight test and fleet demonstration of these usage and loads monitoring technologies. Because the FAA-funded research is in part collaboration with the Army Research Laboratory (ARL) and the Army Communications-Electronics Research, Development and Engineering Center (CERDEC) flight test organization, the UH-60M served as a representative application vehicle. Section 2 focuses on the selection of UH-60 components, regimes, and loads that would best demonstrate the application of these usage and loads monitoring technologies. Section 3 describes the CERDEC UH-60M flight test planning and execution effort that generated unique data for which to demonstrate the usage monitoring technologies. Section 4 documents the application of regime clustering algorithms using the CERDEC flight test data with a focus on the validation process. Section 5 describes the application of VML and GW algorithms to the CERDEC flight test data. Section 6 describes the general process for achieving UBM credits on a serial number basis. Finally, section 7 describes the culminating task for which the RR clustering methods developed in section 4 were applied to a set of operational UH-60M fleet data. Results from this task were then compared to results from a similar effort conducted by the Army-Aviation Engineering Directorate (AED) on the same set of fleet data.

2. COMPONENT AND REGIME SELECTION

2.1 SELECTION OF CANDIDATE COMPONENTS—UH-60M

The retirement times of dynamic components are generally set by either a fatigue damage methodology, commonly based on a stress-life (S/N) curve, or a maintenance concern. Those parts that have lifetimes set by maintenance concerns are usually marked as on-condition. Regardless, each component is assigned a CRT. The UH-60M has approximately 50 such components.

If potential fatigue retirement-time benefits are desired as a result of the collection of actual loads or usage data, the list of 50 life-limited dynamic components can be narrowed down by eliminating all components that have been assigned unlimited retirement times with CRTs over 20,000 flight hours. Any components which are replaced on-condition for reasons other than a CRT are also eliminated. Many such components are relatively low-value items, which are replaced during maintenance actions for higher-value components. Finally, any low-value components, such as bolts or bearings, are eliminated. Using this elimination process for the UH-60M results in the list of ten components, shown in table 1. These are not the only components to which usage and loads monitoring can provide benefit; rather, these are the components to which these methods can potentially provide significant retirement-time increases. Additional benefits can be obtained by increasing the fatigue lives of other low-value components. Such benefits are possible through, for instance, allowing improved synchronizing of required maintenance actions. These types of benefits are not considered in this report.

Table 1. High-value low-lifetime UH-60M dynamics components

Life-Limited Component	Part Number	Failure Mode	Substantiating Parameter
IDGB Main Rotor Shaft	70351-38131-042	Potential, Non-Chafing	Upper Main Rotor Shaft Bending (in-lb) (MRSBU1)
Main Rotor Shaft Extender	70351-08186-043	Attachment Shoulder, Chafing	Upper Main Rotor Shaft Bending (in-lb) (MRSBU1)
Main Rotor Growth Spindle (with Tierod)	38023-10374-041	Thread Mode, Non-Chafing	Main Rotor Spindle Undercut Stress (SPNT1R-4R, SPNTOR1R-1L)
MR Cuff	70150-09209-042, 70150-09209-043	Potential Lug, Non-Chafing	Main Rotor Cuff Lug Stress (MRCTELL)
Expandable Pin	70103-08107-104	Potential Steel, Non-Chafing	Main Rotor Cuff Lug Stress (MRCTELL)
Main Rotor Hub	70103-08112-042	Hub Arm Observation Hole (Lag Side), Non-Chafing	Derived Main Rotor Blade Flapping Angle, (Deg) (MRFLAPDP)
MR Rotating Swashplate	70104-08001-045	Pushrod Attachment Mode, Chafing	Main Rotor Pushrod Load (lb) (MRPR1)
Main Gearbox Housing	70351-38110-044	Main Support Bridge Attachment, Chafing	MR Lateral Stationary Star Load
Main Support Bridge	70400-08162-042	Chafing	MR Lateral Stationary Star Load
Left Tie Rod	70400-08115-046	Chafing	Left Tie Rod Load (MRSCBCSL)

2.2 COMPONENT AND REGIME MAPPING TABLES

Under the fatigue life management program funded by the Army AED, component and regime mapping tables were constructed for the UH-60M. In these tables, all pertinent information regarding the damage calculations of the critical components were collected and organized in a manner that aided in conducting quantitative sensitivity analyses. Focusing mainly on usage-monitoring applications, this information included the following parameters for all high-value, life-limited components: component name and part number; critical failure mode; substantiating parameter; retirement time; the calculated damage for any damaging regime in the CWC spectrum with non-zero damage; and supporting information for those regimes. The supporting information for each regime includes binary data on whether or not conservatism was removed through the use of cycle counting or pro-rating methodologies as well as flags for the GW class of a regime (high, low, or any). The component mapping table contains this

4

information for the collection of all component damage calculations. In the more detailed regime mapping table, this information is reduced to only those damage calculations belonging to the critical failure mode of the component. This information was essential in identifying key critical regimes as initial usage monitoring candidates and in determining the overall sensitivity of lifetimes with usage.

For the subject FAA project, these tables were augmented to include information pertinent to loads monitoring and to increase the fidelity of the sensitivity analyses. Both the component and regime mapping tables were first updated to the most current version of the UH-60M substantiation report at the time (SER-703333 V4). The updating was completed for the ten components listed here, which correspond to those selected in paragraph 2.1: 1) main rotor shaft, 2) main rotor shaft extender, 3) main rotor growth spindle, 4) main rotor cuff, 5) expandable pin, 6) main rotor hub, 7) main rotor swashplate, 8) main gearbox housing, 9) main support bridge, and 10) left tie rod. Damage calculations from only the critical failure mode were included. This means that for each component, two damage calculations were completed; both with and without external stores.

Additional information, which is required for loads monitoring and sensitivity analysis, were also built into the tables, including the following parameters: material S/N curve data, endurance limit data, and regime load data. An excerpt from the updated component mapping table is included in table 2 for the left tie rod. This table shows the detailed inputs that go into the component life-sensitivity analysis, including failure mode type, substantiating parameter, S/N curve parameters (beta, gamma), fatigue endurance limit, and damage sources from the basic mission spectrum, nap-of-the-earth (NOE) spectrum, and cargo spectrum for the UH-60M. In table 3, an excerpt from the regime mapping table is included, which refers to a portion of the damaging regimes for the main rotor shaft. This table includes additional information, such as whether regime damage is calculated with cycle counting (CC), prorating (PR), (N/Y = No/Yes), and the assumed GW range for the maneuver (A = Any GW, L = Low GW, H = High GW). Because it is the regime mapping table that allows regimes to be easily sorted in a number of categories and is set up for computational analysis, it will be the primary tool for subsequent work.

Table 2. Excerpt from component mapping table

Component	Part Number(s)	Failure Mode(s)	Substantiating Parameter (Mnemonic)	Beta	Gamma	Fatigue Limit (Working at Infinity)	CRT (Hours) MNS	Regimes by Mission Type (with Associated Damage) MNS			NOE/ Cargo Inc.
								Basic Mission	NOE	Cargo	
Left Tie Rod	70400-08115-046	Non-Chafing	Left Tie Rod Load (MRSBCSL)	0.483	0.5	1967	10000	E&R Turn 60 R (.0001, 2240), E&R Turn 60 L (.0000, 2100), E&R Turn 60 R (.0002, 2560), MOD P.O. (.0000, 2220), SEV P.O. (.0016, 3870), P 3.3G-SD (.0000, 4460), GAG/FLT (.0078, 7340)	-	7 (.0000, 2220), 30 (.0000, 2220)	No/No
		Chafing	Left Tie Rod Load (MRSBCSL)	0.893	0.5	1496	4600	Dive (.0053, 1860), E&R Turn 45 R (.0001, 1660), E&R Turn 60 L (.0000, 1710), E&R Turn 60 R (.0005, 2240), Climb (.0015, 1860), Dive (.0016, 1730), Turn 45 L (.0003, 1690), Turn 45 R (.0015, 1950), Turn 60 L (.0001, 1970), Turn 60 R (.0001, 1850), E&R Turn 30 R (.0001, 1670), E&R Turn 45 L (.0000, 1700), E&R Turn 45 R (.0005, 1940), E&R Turn 60 L (.0002, 2100), E&R Turn 60 R (.0006, 2560), MOD P.O. (.0001, 2220), SEV P.O. (.0016, 3870), Extr Man (.0000, 1840), P 3.3G-SD (.0000, 4460), GAG/FLT (.0054, 7340)	1 (.0000, 1640), 4(.0000, 1670), 5 (.0030, 2000)	2 (0.0002, 1860), 4 (0.0000, 1670), 7 (0.0001, 2220), 19 (0.0018, 1860), 21 (0.0000, 1670), 25 (0.0002, 1860), 26 (0.0000, 1670), 30 (0.0000, 2220)	Yes/Yes

Table 3. Excerpt from regime mapping table

Component	Part Number(s)	Failure Mode(s)	Substantiating Parameter (Mnemonic)	Beta	Gamma	Endurance Limit (Working at Infinity)	CRT (Hours) MNS	Basic Mission	Damage	Load	NOE	Damage	Load	Cargo	Damage	Load	NOE Inc.	GW	Critical	Appendix	CC	PR	Endurance Limit Proximity	Life Sensitivity with Load	Life Sensitivity with Cycles	Load/Cycle Power Factor	Maximum Life % Change	Maximum Life Change
IDGB Main Rotor Shaft	70351-38131-042	Potential non-chafing	Upper Shaft Bending (MRSBU1)	0.032	1	423500	5200	SEV P.O.	0.0027	626000								A	Y	B	Y	N	0.48	-0.43	-0.14	3.09	0.16	849.33
IDGB Main Rotor Shaft	70351-38131-042	Potential non-chafing	Upper Shaft Bending (MRSBU1)	0.032	1	423500	5200	REC AUTO	0.0001	425000								A	Y	B	N	N	0.00	-1.47	-0.01	283.33	0.01	27.18
IDGB Main Rotor Shaft	70351-38131-042	Potential non-chafing	Upper Shaft Bending (MRSBU1)	0.032	1	423500	5200	DRP STOP	0.0014	550000								A	Y	B	N	Y	0.30	-0.32	-0.07	4.35	0.08	408.28
IDGB Main Rotor Shaft	70351-38131-042	Potential non-chafing	Upper Shaft Bending (MRSBU1)	0.032	1	423500	5200	PO 3.3G-SD	0.0001	626000								A	Y	B	Y	N	0.48	-0.02	-0.01	3.09	0.01	27.18
IDGB Main Rotor Shaft	70351-38131-042	Potential non-chafing	Upper Shaft Bending (MRSBU1)	0.032	1	423500	5200	GAG/FLT	0.0024	637000								A	Y	B	N	Y	0.50	-0.37	-0.12	2.98	0.14	741.50
IDGB Main Rotor Shaft	70351-38131-042	Potential non-chafing	Upper Shaft Bending (MRSBU1)	0.032	1	423500					7	0.0064	460000				Y	A	Y	B	Y	N	0.09	0.00	0.00	NA	0.00	0.00
IDGB Main Rotor Shaft	70351-38131-042	Potential non-chafing	Upper Shaft Bending (MRSBU1)	0.032	1	423500					8	0.0064	460000				Y	A	Y	B	Y	N	0.09	0.00	0.00	NA	0.00	0.00

CC = cycle counting
PR = prorating
A = Any GW
L = Low GW
H = High GW

2.2.1 Life Sensitivity Metrics

To investigate which of the more than 250 regimes on the ten critical components should be targeted as potential load monitoring candidates, six metrics were defined and calculated: 1) endurance limit proximity, 2) life sensitivity with load, 3) life sensitivity with cycles, 4) load cycle/load power factor, 5) maximum life change (%), and 6) maximum life change (hrs). These metrics, coupled with analyses of the component life as damage calculation parameters change, can aid in quickly prioritizing where additional investigation into potential UBM benefits can be obtained.

2.2.1.1 Endurance Limit Proximity

The Endurance Limit Proximity is a simple measure of how close a regime load is to the endurance limit used in a given damage calculation. It is calculated as the regime load divided by the endurance limit minus 1. Values above zero signify a regime that causes some damage to the component, with increasing values accruing damage at a faster rate. Just because this parameter is high does not mean that the regime is highly damaging, because damage is also a function of usage. For instance, a very high load for one cycle will not be a key regime. Values less than or equal to zero signify a regime that is below the endurance limit and, therefore, does not cause any damage.

This parameter has limited use for metallic components, which have S/N curve shapes with significant curvature. For these parameters, the damage accrual rate near the endurance limit is generally very small. However, composite curve shapes are almost always flat and horizontal. Damaging loads on these curve shapes, which are close to the fatigue limit, can accrue damage at a very high rate. This is where the endurance limit proximity is useful—to quickly scan regimes in a composite damage calculation to find those for which the load can be reduced slightly (using VML or other load-monitoring techniques) while still making a large lifetime improvement.

2.2.1.2 Lifetime Sensitivity Factors

The second two metrics define the sensitivity of the calculated lifetime to both the regime load and the number of cycles at that load. Defined as point elasticities, these parameters can be interpreted as follows: Given a 1% change in load (cycles), the lifetime would change by this percent. Using these parameters, all regimes can be quickly scanned to determine which might provide benefit faster than others. The life sensitivity with load and cycles for the main rotor hub is shown in figure 1. An additional parameter, termed the load/cycle power factor, measures the relative power of load to cycle reduction and is simply the ratio of the two point elasticities. This final factor is mainly for diagnostic use because it can be difficult to interpret in a manner that is meaningful to the damage calculations.
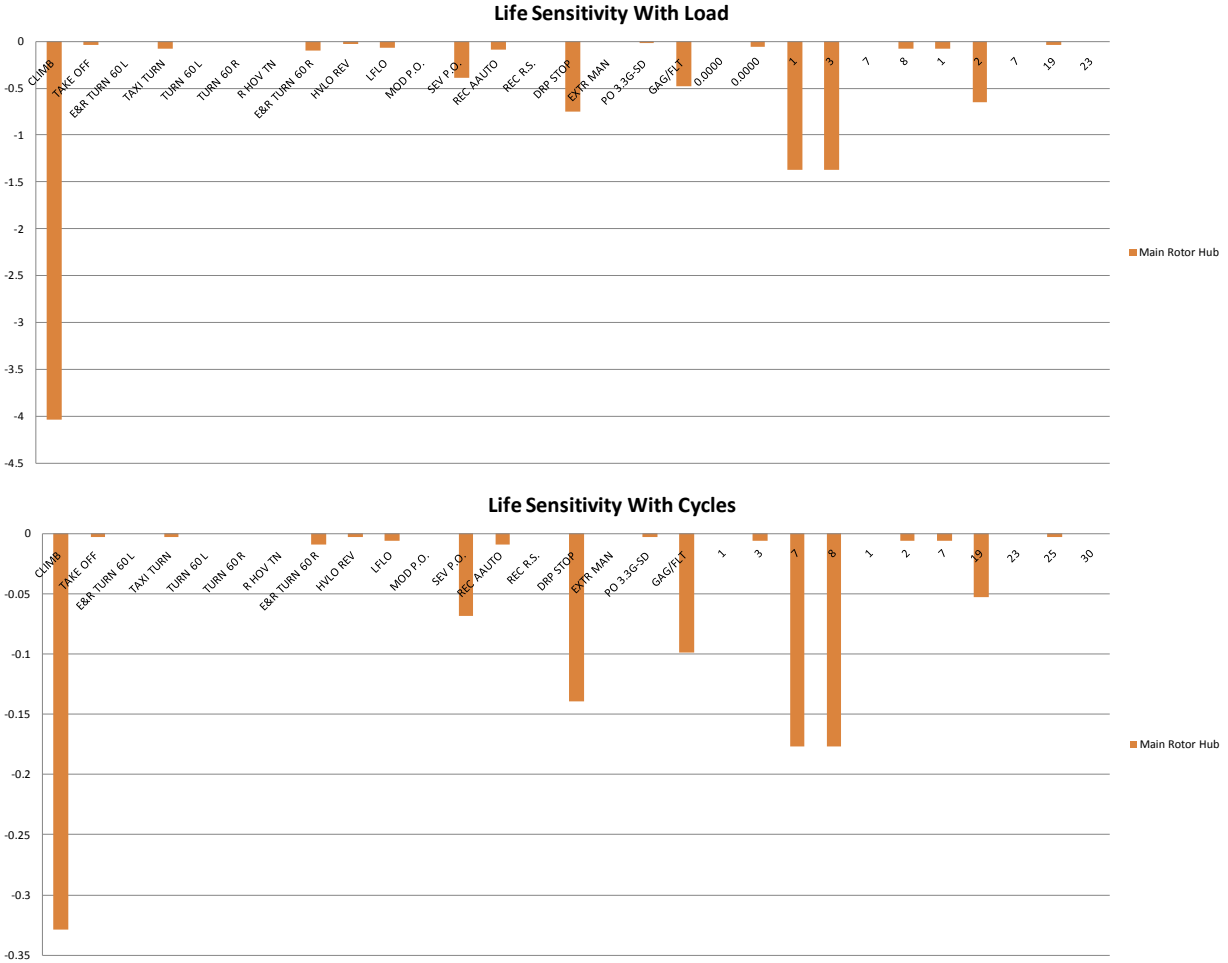
Figure 1. Life sensitivities with load and cycles for MR hub

The calculation of both sensitivity factors flows from a generalized derivation of component retirement time. This derivation begins with the standard SAC form that represents all S/N curves:

$$N = \left[\frac{\beta}{\left(\frac{S}{e}\right)-1}\right]^{1/\gamma} \tag{1}$$

In this formulation, S is the load, e is the endurance limit, N is the number of cycles to fracture in millions, and β and γ are material constants provided for each structural material. This curve shape is used for the vast majority of materials considered in aircraft substantiations, including titanium, steel, aluminum, fiberglass, graphite, and most adhesives. One notable exception is the reflexive curve shape used for annealed, low kt shot-peened Ti-6Al-4V.

The second step in the derivation is to invoke Miner's rule of damage summation. This rule allows the damage from each regime to be calculated, based on a single S/N curve, separately, then linearly summed together to obtain a total damage. The part is assumed to fracture when

9

this damage summation is equal to 1. An important note is that all SAC damage calculations use a baseline of 100 hours. This means that the number of cycles or occurrences provided in the CWC table of a damage calculation is really the number of cycles/occurrences per 100 flight hours. With this modification, the calculated lifetime of a part can be calculated as:

$$L = \frac{100}{\sum_i D_i} \tag{2}$$

where L is the CRT and D_i is damage for regime i. The damage for a single regime can be calculated from the generalized S/N curve shape as follows:

$$D_i = \frac{t_i \cdot \omega / 10^6}{\left[\frac{\beta}{\left(\frac{s_i}{e}\right)-1}\right]^{1/\gamma}} = \frac{O_i \cdot L_i \cdot \omega / 10^6}{\left[\frac{\beta}{\left(\frac{s_i}{e}\right)-1}\right]^{1/\gamma}} \tag{3}$$

In the first of these two formulations, t_i is the number of seconds spent within a regime per 100 flight hours, s_i is the regime load, and ω is the loading frequency (1/rev main and 4/rev tail). Note that the total number of cycles is divided by one million, as the S/N curve constants are derived with this scaling. The second formulation, which is used for transient maneuvers, calculates the number of seconds per 100 flight hours by multiplying the occurrences per 100 flight hours (O_i) by the length of each occurrence (L_i).

An intermediate step in the sensitivity calculation is to evaluate the derivative of the single regime damage with respect to both time per 100 hours (t_i) and regime load (s_i). These are:

$$\frac{\partial D_i}{\partial t_i} = \frac{\omega / 10^6}{\left[\frac{\beta}{\left(\frac{s_i}{e}\right)-1}\right]^{1/\gamma}} \tag{4}$$

$$\frac{\partial D_i}{\partial s_i} = \frac{(t_i \cdot \omega / 10^6) \cdot \left((s_i/e)-1\right)^{1/\gamma - 1}}{\gamma e \beta^{1/\gamma}} \tag{5}$$

Two final parameters, the maximum life change % and the absolute maximum life change (hrs), provide the potential life change if all damages associated with a given regime are taken away. When observing the point sensitivities, it is essential to monitor the maximum benefit for a given regime as well because some high-sensitivity regimes might be sensitive over small changes but may not provide benefit over a large range.

The two most important metrics for ranking of potential components and target regimes are the elasticity of fatigue life with load and cycles. These parameters essentially represent the percentage change in life, with a 1% change in either the regime load or the number of cycles at a given load. Though these parameters immediately point out those damage calculation line items to which the life is most sensitive, they are limited in the fact that they are point estimations only. This means that as load/cycles move up or down, the point elasticity and this sensitivity also change.

To ensure that the perceived benefits themselves are not sensitive to reasonably large changes of either load or cycles, formulations of the fatigue life as a function of the two parameters were

created. The elasticity parameters were also termed in a way that allowed them to be plotted versus the input parameters as well. A MATLAB® program was created, which allows for these curves to be calculated and plotted quickly, and given simple inputs, such as the S/N curve parameters and initial damage calculation figures. Representative output taken from a single regime from the main rotor hub damage calculation is shown in figures 2 and 3.
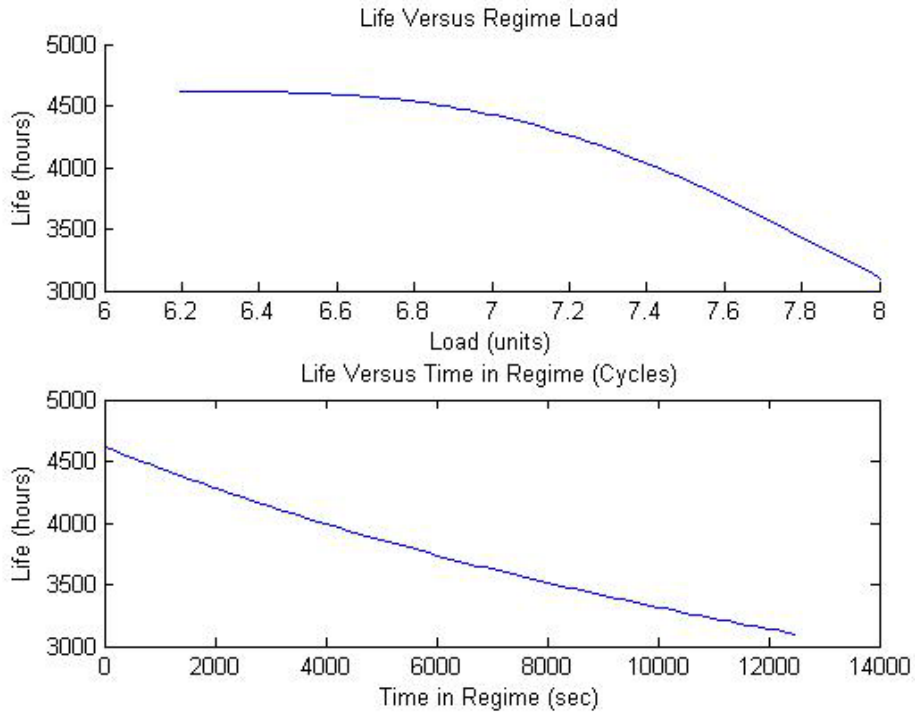
Figure 2. The MR hub life as a function of low GW climb load and cycle count
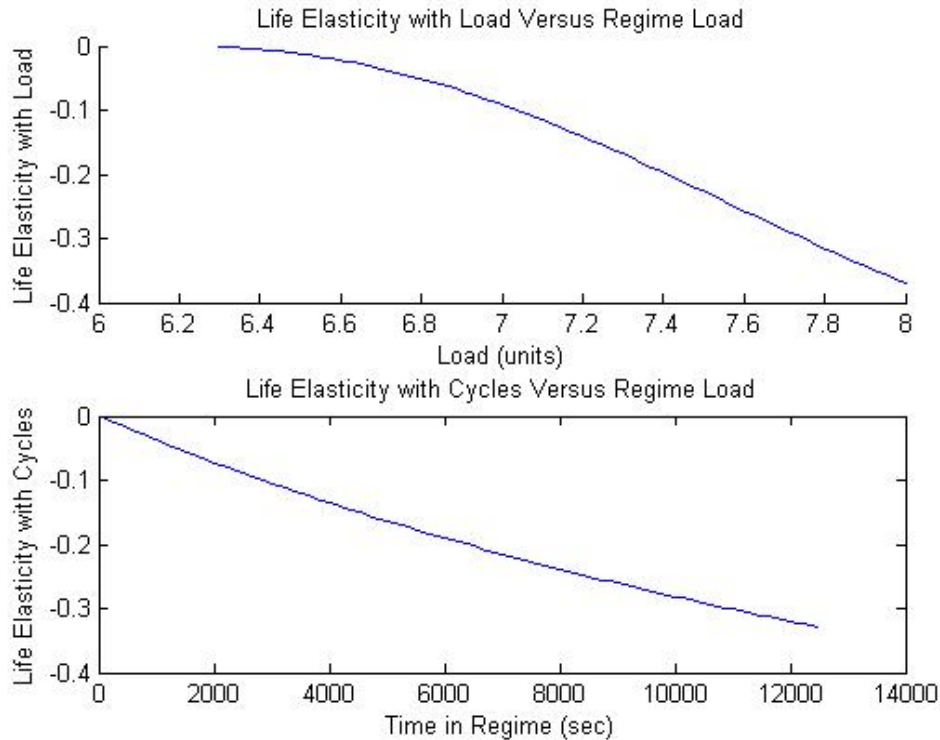
Figure 3. The MR hub life elasticities as functions of low GW climb load and cycle count

As shown in the figures, life elasticities exhibit nonlinear behavior with both load and cycles. For example, after a load reduction of approximately 10%, most of the benefit of load reduction has been used. For this reason, it is essential to be aware of this behavior when selecting potential targets for UBM applications.

From this analysis, two key loads were selected for instrumentation in the CERDEC flight test that cover several life-limited dynamic components: the main rotor lateral stationary swashplate (MRLSS) axial load, which can be used to substantiate the gearbox housing, and the main rotor shaft extender bending load (MRSEBL), which can be used to substantiate the main rotor shaft, shaft extender, and hub. Important regimes for these substantiating parameters based on the component life sensitivity study were turns, climb, and pullouts. These regimes and loads were the focus of the CERDEC flight test evaluation.

3. CERDEC UH-60M FLIGHT TEST SUPPORT

3.1 FLIGHT TEST OVERVIEW

An FAA-funded IVHMS flight test program was conducted by the Army CERDEC on a UH-60M from March–July 2013. The FAA/CERDEC IVHMS flight test program objective was to provide validation data for several load and usage monitoring methods. SAC provided a support role to assist in defining the flight test plan, instrumentation requirements, and data processing requirements. The primary objectives of this program were to provide validation data

for RR, GW/CG, and VML algorithms, and to generate design of experiment (DOE) data for the ARL to support a pilot sensitivity study.

Climb and banked turn maneuvers were flown to support the development of RR clustering algorithms. These maneuvers differed from typical FLS maneuvers in that they included unique techniques to explore the boundaries of the RR definitions. The GW/CG estimation algorithms required level flight and out of ground effect (OGE)/in ground effect (IGE) hover maneuvers at several vehicle configurations. The VML algorithm validation for key substantiating parameters required a focus on the turn, climb, and dive regimes, which were identified as key fatigue life drivers.

3.2 INSTRUMENTATION

The CERDEC flight test aircraft used an ACRA data-acquisition system with data-acquisition units installed in both the fixed and rotating systems. This system was selected based on input from SAC. The rotating acquisition system precluded the need for a slip ring and was time-synchronized to the fixed system through the GPS time. In addition to the ACRA data stream, data were acquired independently by the production IVHMS, which included RR sequence data. The IVHMS and ACRA data were time synchronized in post-processing using the yaw rate signal to enable joint analysis of RR performance with corresponding flight loads. The two key dynamic loads measured during this flight test program were the axial load on the MRLSS and the MRSEBL. These components are shown in their calibration fixtures in figures 4 and 5, respectively. Both of these components have extensive load measurement history from the UH-60M FLS test program, which enabled a meaningful comparative analysis of CERDEC-measured dynamic loads during scripted maneuvers. Both components were instrumented and calibrated by SAC Instrumentation Engineering in Stratford, Connecticut. A complete list of parameters recorded by the ACRA data system is shown in table 4.

Figure 4. Main rotor lateral servo link

Figure 5. Main rotor shaft extender

Table 4. The CERDEC flight test instrumentation list

Cabin Acquisition

Mnemonic	Sample Rate
EGI1_Belly_Vel_Zb_calc	10 Hz
EGI1_Calibrated_Airspeed_calc	10 Hz
EGI1_Lateral_Acceleration_calc	10 Hz
EGI1_Longitudinal_Acceleration_calc	10 Hz
EGI1_Nose_Vel_Xb_calc	10 Hz
EGI1_Pitch_Rate_calc	10 Hz
EGI1_Pitch_Attitude_calc	10 Hz
EGI1_Pressure_Altitude_calc	10 Hz
EGI1_Roll_Attitude_calc	10 Hz
EGI1_Roll_Rate_calc	10 Hz
EGI1_RW_Vel_Yb_calc	10 Hz
EGI1_Vertical_Acceleration_calc	10 Hz
EGI1_Wind_Direction_calc	10 Hz
EGI1_Wind_Velocity_calc	10 Hz
EGI1_Yaw_Rate_calc	10 Hz
EGI2_Belly_Vel_Zb_calc	10 Hz
EGI2_Calibrated_Airspeed_calc	10 Hz
EGI2_Lateral_Acceleration_calc	10 Hz
EGI2_Longitudinal_Acceleration_calc	10 Hz
EGI2_Nose_Vel_Xb_calc	10 Hz
EGI2_Pitch_Rate_calc	10 Hz
EGI2_Pitch_Attitude_calc	10 Hz
EGI2_Pressure_Altitude_calc	10 Hz
EGI2_Roll_Attitude_calc	10 Hz
EGI2_Roll_Rate_calc	10 Hz
EGI2_RW_Vel_Yb_calc	10 Hz
EGI2_Vertical_Acceleration_calc	10 Hz
EGI2_Wind_Direction_calc	10 Hz
EGI2_Wind_Velocity_calc	10 Hz
EGI2_Yaw_Rate_calc	10 Hz
GPS_Altitude	10 Hz
GPS_Ground_Speed	10 Hz
GPS_Heading	10 Hz
GPS_Lock	10 Hz
GPS_Speed_KPH	10 Hz
GPS_Speed_KTS	10 Hz
iHUD_Altitude_Rate_calc	10 Hz
iHUD_Baro_Altitude_calc	10 Hz
iHUD_Engine_1_Torq_calc	10 Hz
iHUD_Engine_2_Torq_calc	10 Hz
iHUD_Radar_Altitude_calc	10 Hz
iHUD_Indicated_Airspeed_calc	10 Hz
Satellites_in_Use	10 Hz
Satellites_in_View	10 Hz
MRLSS (Lat Servo Link Load, lb)	160 Hz

Rotating Acquisition

Mnemonic	Sample Rate
aaGPS_DOY	10 Hz
abGPS_Hours	10 Hz
acGPS_Minutes	10 Hz
adGPS_Seconds	10 Hz
aeGPS_Centiseconds	10 Hz
afGPS_Microseconds	10 Hz
Centiseconds	10 Hz
Day_of_Year	10 Hz
GPS_Altitude	10 Hz
GPS_Ground_Speed	10 Hz
GPS_Heading	10 Hz
GPS_Speed_KPH	10 Hz
GPS_Status	10 Hz
Hours	10 Hz
Minutes	10 Hz
Satellites_in_Use	10 Hz
Satellites_in_View	10 Hz
Seconds	10 Hz
Too_Few_Satellites	10 Hz
MRSEBL (Shaft Bending, in-lb)	160 Hz

3.3 FLIGHT TEST APPROACH

3.3.1 RR/Clustering

Two particular flight regimes, climb and 45-degree turns (left and right), were identified as key drivers of component retirement times. It was also determined that the effects of these maneuvers on component fatigue lives were particularly sensitive to the total number of cycles accounted for in the damage calculation. This makes these regimes prime candidates for IVHMS/HUMS usage-monitoring applications. The dive regime is also significant to certain components and was included because it can be used to balance out the climb maneuvers during the flight test.

To better design the regime cluster definitions, it is necessary to exercise the RR algorithms, specifically when they are weakest or have the greatest ambiguity relative to combining regime sequences into a contiguous maneuver. For this reason, both regime excursions and compound maneuvers (which are based on one of the selected key target regimes having the most impact on UBM benefit) were flown. Regime excursions happen when one or more state parameters of a regime are temporarily altered.

Regime excursions begin with a steady state regime, such as climb or coordinated turn, being flown by hand. It was important that the pilot was not assisted by the partial authority flight controls because they would eliminate much of the variation that is desired in this data set. Once the steady state was obtained, the pilot deliberately inputted manual control impulses, which forced the aircraft to deviate from the steady maneuver. These control inputs were intended to last a very short time (impulse) to several seconds and were generated by either the cyclic or collective sticks. The pilot then brought the aircraft back to the previously held steady state. These naturally flown dynamic excursions from the steady state maneuver were desired. The excursions were repeated with increasing severity until the data requirements were met. An example of a regime excursion is a climb flown with temporary changes to the climb rate (excursions) to attempt to induce the RR algorithms to falsely recognize a pullout or pushover. In this maneuver, a predetermined climb rate is achieved (at a predetermined forward speed). The pilot then made natural collective or cyclic inputs which altered the climb rate (the speed changed as well). Maintaining the predetermined climb rate and airspeed for the whole procedure was not as critical as the natural oscillations around some steady state maneuvers.

Compound maneuvers occur in a situation in which there is no clear entry or exit from one regime to the next. For instance, if an aircraft is in a level turn and begins to climb steadily, the CWC spectrum would at first recognize a turn, then a climb (climbing turns are part of the climb regime).

These maneuvers were flown at three GW and CG combinations. As with all test segments, all maneuvers and aircraft states remained within the normal operating envelope of the aircraft.

This testing not only simulated what conditions cause error in the RR output, but also allowed for a proper definition of entry and exit of the key regimes. Strategically important load measurements, described in section 4.3.3, were recorded alongside the RR output. This allowed a clear linking of entry and exit with load thresholds that are directly linked to the pertinent component damage calculations (e.g., endurance limits).

16

3.3.2 Loads Monitoring

As with usage-monitoring applications, a study was performed to identify regimes that had high lifetime sensitivity to load. The key regimes were climb, 45-degree turns (left and right), and the NOE mission. The possible benefits from these regimes stem from the cycle counting that loads monitoring enables and the reduction of the severity of the assumed CWC load spectrum. Because of the specialized nature of the NOE mission, these regimes were not part of this flight test program.

To obtain monitoring loads benefits in a component damage calculation, it is important to treat all sub-maneuvers, which are grouped into each regime. For instance, the climb regime actually consists of loads from best rate of climb, takeoff power climb, intermediate power climb, and climbing left and right turns. Likewise, 45-degree turns include turns at varying airspeed ranges and descending turns. During this flight test program, it was desired to collect data for as many of these sub-regimes as practical. Both the climb and turn maneuvers were flown at three GW and CG combinations. All maneuvers and aircraft states remained within the normal operating envelope of the aircraft.

The actual load measurements collected, as described in section 4.3.3, were compared to the VML output in a variety of manners to both train and validate the models. Applications included cycle counting, vibratory load assignment, and maximum/minimum load tracking.

3.3.3 GW/CG Estimation

To provide clean training and validation data for GW and CG estimation algorithms, the aircraft was held in steady state hover and level flight conditions at three GW and CG combinations. Steady hover and hover turns were performed at varying radar altitudes, in both IGE and OGE. Rotor rpm (NR) was also varied across hover data points. A full level flight sweep was conducted for each aircraft configuration.

3.3.4 Pilot Variability

A UBM process must maintain the level of reliability that is obtained with the current damage calculation process. A key input to this process is a distribution of the error involved in either usage or loads measurements. It would be simple to complete a flight test program with a single pilot, providing clean data on algorithm accuracy. However, this would ignore the possibility that human factors can result in variations in piloting techniques, which may lead to variability in how a pilot enters or exits any particular maneuver and peak loads for nominally the same regime, potentially resulting in additional uncertainties in the algorithm results.

To fully characterize this error, the variation due to human factors in each of the RR/VML inputs needs to be understood. This would necessitate a large data set that was beyond the scope of CERDEC's flight test budget. Instead, a DOE developed by the ARL characterized what this data set would look like, specifically for the climb regime, to examine whether such pilot variability was important. These results are described in an ARL report [1]. It is important to understand that the intent of such a study was not to characterize the variability of loads and usage due to pilot effects, but rather to characterize the sensitivity of error statistics related to usage and loads monitoring.

The program flight log is shown in table 5. Two basic configurations were tested, which consisted of a clean, low GW configuration and an external stores support system (ESSS) high GW configuration. The GW and CG of these test points relative to the UH-60 envelope and FLS conditions are shown in figure 6.

Table 5. The CERDEC/FAA IVHMS test program flight log

Flight #	Date	Flight Time (hrs)	Takeoff GW (lb)	Takeoff CG	Configuration	Fuel Load
1	3/11/2013	1.50	16,000	363	Clean	Main
2	3/13/2013	1.00	16,080	363	Clean	Main
3	3/29/2013	1.10	21,400	353.5	ESSS	Main+External
4	4/16/2013	2.00	21,800	353.5	ESSS	Main+External
5	6/11/2013	1.80	21,900	353.5	ESSS	Main+External
6	7/24/2013	1.40	16,170	363	Clean	Main
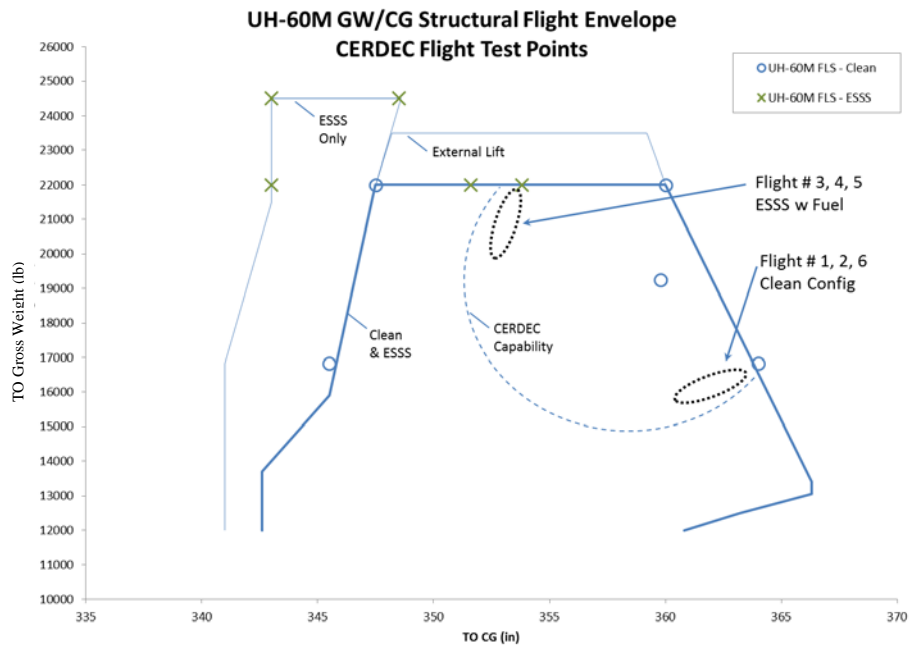
Figure 6. The CERDEC/FAA GW-CG test point diagram

3.5 FLIGHT TEST RESULTS

Results from the CERDEC flight test are analyzed in sections 4 and 5. Section 4 focuses on applying RR clustering methods using the CERDEC flight test data. Section 5 focuses on applying VML and GW prediction methods. The VML models are compared to the measured

shaft bending and servo loads, and the GW model is compared to the known GW configurations from the CERDEC aircraft.

4. RR ANALYSIS

4.1 OVERVIEW OF RR

HUMS RR algorithms are used to identify and categorize how the aircraft has been flown. These algorithms are a key element to short-term structural usage monitoring approaches being pursued by various original equipment manufacturers (OEMs) and Department of Defense Services to obtain approved UBM credits. Most RR inputs are also essential for flight control and pilot decision-making and originate from avionics units that have the highest levels of reliability for hardware and associated software. The RR data flow is shown in figure 7, which shows standard input and output data types. The RR input data can be grouped into the following six categories:

1.   Basic aircraft and system data, which include directly measured parameters and parameters that typically depend on some level of pilot input
2.   Derived air data parameters
3.   Aircraft attitude parameters
4.   Stick position
5.   Aircraft discrete parameters
6.   Aircraft rigid-body accelerations

Though the details of RR algorithms vary, the above types of required input data are typical for most OEM rotorcraft platforms. The RR output includes all raw parametric data, derived parameters, regime records, and event records. For RR algorithms that identify broader maneuver categories rather than detailed regimes, fewer input parameters may be required.

Most mature RR algorithms are based on hierarchal Boolean logic that compares input parameters against a set of predefined ranges to determine the general aircraft flight condition/maneuver, such as steady level, turn, climb, or pullout. For the UH-60M, these rules are documented in reference 2. An example of a regime definition for Intermediate Power Climb is shown in table 6. Further detailed regime definition is possible with knowledge of aircraft configuration, such as GW, CG, external load, and external stores. This enables prorating of component loads within finer regime categories rather than allocating the most severe peak load for all instances of a general maneuver. This prorating is frequently used in fatigue substantiation for military rotorcraft and less so for commercial rotorcraft, which typically use only maneuver severity to form prorated regimes.

Inputs

Basic Aircraft Parameters

External Cargo Weight, GW, APU Speed, Main Rotor Speed, Engine NP, Engine Turbine Temp, Engine Torque, Groundspeed, Radar Altitude, Velocity

Air Data Parameters

Outside Air Temperature, Barometric Altitude, Calibrated Airspeed, Barometric Rate of Climb

Aircraft Attitude Parameters

Heading Attitude, Pitch Attitude, Roll Attitude, Yaw Rate

Stick Positions

Longitudinal Cyclic Position, Lateral Cyclic Position, Pedal Position, Collective Stick Position

Aircraft Discretes

WOW, MR Brake Applied, ADC ID, AHRS ID

Acceleration

Longitudinal, Lateral, Vertical Acceleration

IVHMS Onboard RR Process

Outputs

Regime Packet Data

A record of each regime containing the start time and duration.

Prorates applied to each regime (optional).

Logged Data

Basic aircraft parameter data and derived parameter data.

Event Data

A record of each event.

Derived Parameters

Ground Speed, Aircraft heading, etc.

Figure 7. The RR algorithm data process

Table 6. Example regime definition for intermediate power climb

Regime:	Intermediate Power Climb		
Category	Steady State		
Parameter	Operator	Threshold	Hysteresis
WOW Delayed	=	False	None
Landing Flag	=	False	None
Takeoff Flag	=	False	None
Roll Attitude	>=	-10	None
Roll Attitude	<=	10	None
Altitude Rate	>	600	200
Lateral Acceleration, Filtered	>=	-0.08	None
Lateral Acceleration, Filtered	<=	0.08	None
Yaw Rate	>=	-5	None
Yaw Rate	<=	5	None
Corrected NZ	<=	1.2	None
Corrected NZ	>=	0.8	None
Derived TGT	>=	775	None
Derived TGT	<	850	None
VH Fraction	<=	1.05	None
Calibrated Airspeed	>	43	5
Turn Entry Recovery ID	=	0	None

TGT = turbine gas temperature, WOW = weight on wheels

4.2 RR CLUSTERING

A fundamental requirement that must be satisfied before component retirement times can be influenced by RR data is to demonstrate, with direct evidence from flight tests, that the algorithms correctly classify the flight regimes being pursued in a particular credit application. This requirement is the validation of RR algorithms. Several previous efforts have focused on RR validation, most notably a previous FAA-funded SAC effort documented in reference 3. Through these efforts, it was discovered that onboard RR classifications for many critical maneuvers do not correlate directly to independent pilot-declared maneuvers, which traditionally serve as the truth classification that RR performance is measured against. Two common issues that lead to these errors are: 1) regime thresholds are not adequately designed to align with flight test data and 2) truth regimes and predicted regimes are defined with different levels of abstraction. For example, table 7 shows a real example from flight test of the RR-predicted sequence during a 60-degree right turn. During this flight test maneuver, RR detected four unique types of turn regimes and two rolling pullouts. Both of the above-mentioned issues with

RR can be observed in this example. The detection of pullouts during the turn is due to inadequate definitions of thresholds, and the multitude of predicted turn regimes are because the predicted regimes are defined more narrowly than the flight test truth regime.

Table 7. Example of RR prediction during 60-degree right turn

Pilot-Declared Truth Regime	RR Prediction
60-Degree Right Turn	Right Climbing Turn
	Right Climbing Turn Exceeding 45-Degree AOB
	60-Degree AOB Level Right Turn
	60-Degree AOB Descending Right Turn
	Right Rolling Pullout
	60-Degree AOB Descending Right Turn
	Right Rolling Pullout

AOB = Angle of bank

Though these issues are often perceived as errors in the output of RR, the output during these maneuvers is not random. RR properly classifies the regimes based on the definitions that were provided to the software and the dynamic nature of certain key state parameters, such as roll attitude, rate of climb, and load factor during transient maneuvers. Though it is possible to define these regimes to be more consistent with flight test definitions, a simpler post-processing approach called clustering was developed to take advantage of hundreds of thousands of hours of existing RR data. Clustering works by identifying the patterns in RR output that occur during targeted regimes and defining the logic for broadening or clustering the RR output into larger groups that correctly capture both the occurrence and duration of the intended regime. The objective of clustering is to find occurrences and duration of a particular CWC regime within existing RR output data.

Cluster definitions consist of a set of target regimes and a set of cluster regimes. Because the IVHMS RR definitions were designed with a higher degree of specificity than the UH-60M CWC, several different RR target regimes can be associated with a single CWC regime. However, examination of actual RR output shows that many other nonassociated cluster regimes are in close proximity to or cluster within and around the CWC regime. In processing a cluster definition, any contiguous set of cluster and target regimes that contain at least one target regime will satisfy the definition. Cluster regimes can be defined with persistence parameters so that only very short duration cluster regimes are included.

The process of designing a regime cluster involves a combination determining the desired target regime set that aligns with the CWC regime, and observation of RR test data to determine the cluster regime set that occurs within the CWC regime. In addition, a truth regime definition must be established to provide independent comparison data. A truth regime classification is traditionally established by a flight test pilot or engineer and documented in a run log, which

contains maneuver descriptions and maneuver codes. Maneuver codes are then mapped to a usage spectrum regime list.

4.3 APPLICATION OF RR CLUSTERING TO CERDEC FLIGHT TEST

4.3.1 Cluster Design Process for Climb Regime

4.3.1.1 CWC Mapping

Mapping of both standard flight test maneuvers and corresponding IVHMS Regimes to the UH-60M CWC climb regime is shown in table 8.

Table 8. The CWC climb regime mapping

Flight Test Maneuver	UH-60M Regime Definition	IVHMS Regime
Climb Steady Best Rate of Climb	CLIMB	31: Best Rate of Climb
Climb Steady Intermediate Power		32: Intermediate Power Climb
Climb Steady Takeoff Power		33: Takeoff Power Climb
Climbing Left Turn (Inc E/R, 180 Deg)		36: Left Climbing Turn
Climbing Right Turn (Inc E/R, 180 Deg)		37: Right Climbing Turn

4.3.1.2 Definition of Truth Regime

A parametric definition of the truth regime is required to generate error statistics for a given IVHMS regime or regime cluster set using the CERDEC test data. In the context of the UH-60M structural fatigue usage spectrum, the climb regime is composed of various climb power levels and climb maneuvers that can be referred to as sub-regimes, which are listed in table 8. Of interest in a UBM credit application is the total duration spent in the broader CWC regime, not necessarily the duration spent within each sub-regime. Sub-regime durations would be of particular interest in developing a more refined usage spectrum or in defining a climb prorate, for example, to reduce the overall contribution of takeoff power climb within the CWC climb regime. Though the goal of RR is to be able to detect all sub-regimes with sufficient accuracy, that is not the objective of clustering. The clustering algorithm was intended to enable monitoring of broad regime classifications that map directly to the CWC.

Defining a unique truth regime for each of the six components of the climb regime is not necessary if a single set of truth criteria can be defined that encompasses all the components of the CWC climb regime. Truth criteria for the CWC climb regime were developed based on a review of existing onboard RR software and input from subject matter experts. Examination of the three steady state climb sub-regimes reveals that grouping these into a common truth regime would simplify the criteria by broadening the definition so that it would rely only on the airspeed, climb rate, and roll attitude. Grouping the transient turns during climb would open up

the roll attitude limits to include turns up to 45 degrees. The resulting parametric truth regime definition for the CWC climb regime is shown in table 9. This CWC truth regime captures the most important threshold in defining a climb regime: the altitude rate.

Table 9. The CWC climb truth regime definition

Parameter	Expression (Hysteresis)
Roll Attitude (deg)	$\geq$ -45
Roll Attitude (deg)	$\leq$ 45
Altitude Rate (fpm)	> 600 (200)
Calibrated Airspeed (kts)	> 43 (5)

fpm = feet per minue; kts = knots

4.3.1.3 Definition of Climb Target Regimes

Target regimes for the cluster definition are the IVHMS regimes that map directly to climb in the UH-60M usage spectrum. These regimes are shown in table 10.

Table 10. The CWC climb target regime set

Target Regime	Minimum Duration
31: Best Rate of Climb	0
32: Intermediate Power Climb	0
33: Takeoff Power Climb	0
36: Left Climbing Turn	0
37: Right Climbing Turn	0

4.3.1.4 Baseline Climb RR Performance

With the CWC climb regime defined parametrically and an RR target set defined, the baseline performance of RR can be assessed. At this point, the clustering algorithm is not being exercised beyond the simple task of grouping the target regimes. Summary results on the CERDEC test data are shown in table 11. The total count of climb regime occurrences is 1.8 times the occurrences of the truth regime, and the total duration is 87% of the truth regime duration. This tendency to over-count occurrences and undercount duration is a known characteristic of raw RR output data. One reason for this can be seen in figure 8, in which a single continuous climb regime is flown while the roll attitude is oscillated around the 10-degree threshold for turn classifications. In this plot, the regime sequence is shown at the top with the target regimes highlighted in red blocks. The true regime duration, according to the parametric definition, is shown by the dark red portion of the curves that represent the parametric data. By performing these unique maneuvers, the RR output classifies many short-duration turn-entry and turn-recovery regimes, which do not get counted as part of the climb. The mapping of these short transient regimes to the CWC is dependent on the context in which they occur. For the example shown, grouping them with the climb regime is desired because they occur adjacent to a

climbing turn and are, therefore, integral to the climbing turn. This is precisely what the clustering algorithm was designed to do.

Table 11. Baseline RR performance for climb from CERDEC testing

Statistic	Target Regimes	Truth Regime
Mean Duration(s)	17.2	37.3
Median Duration(s)	7.5	8.3
Duration Standard(s)	27.9	68.0
Minimum Duration(s)	1.0	0.05
Maximum Duration(s)	299	343
Total Duration(s)	6456	7458
Counts	376	200
Percentage	14.38	15.94
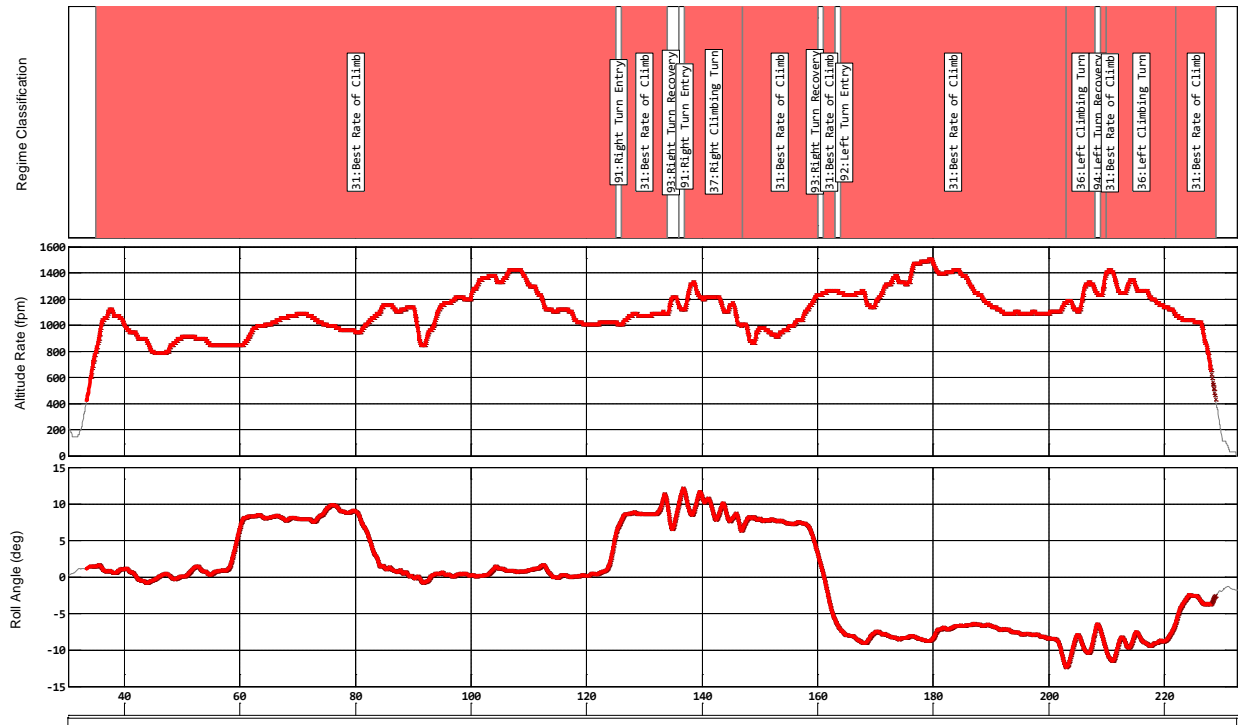
Figure 8. Example of climb RR before clustering

4.3.1.5 Selection of Climb Cluster Regimes

Defining a cluster set starts with analyzing the neighboring regimes from the existing target set defined in table 10. All neighboring regimes from the target set and associated frequency of occurrence within the CERDEC test data are shown in table 12. Examination of table 12 shows that moderate pullouts/pushovers and turn entry and recovery were frequently occurring immediately before or after a climb regime. This is as expected because the flight cards

contained stick excursion maneuvers in both the pitch axis and roll axis to induce these types of regimes during climbs. In a similar analysis of fleet data, these regimes occurred among the top-ten neighboring regimes adjacent to a climb regime.

Selection of the cluster regimes and their associated persistence (the maximum cluster regime duration that will satisfy the definition) required a combination of observation and engineering judgment. Two general criteria were applied in the selection of cluster regimes. First, regimes that should be grouped with a target set (regardless of duration), but that do not belong in any target set themselves, were selected. Turn entry and recovery regimes fall into this category. These regimes were assigned an arbitrarily high persistence threshold, such that any realistic duration would satisfy the threshold. Second, steady state regimes that occur very frequently and in very short duration were also selected. This is a means of imposing persistence logic into the RR classification process, which is not currently done onboard. The second criterion does not generally apply to transient regimes because they are, by nature, very short duration regimes.

Additional consideration was given to clustering moderate pullouts and pushovers with the climb regime using the minimum persistence threshold of 1 second. There are two reasons for including these short, transient regimes in the cluster definition. First, the truth definition was broadened by not including corrected load factor. This means that pullouts and pushovers occurring during a climb will not draw time away from the climb duration. Second, it was desired to mitigate the fact that pullouts are over-counted in RR output because of excessive noise in the onboard measured vertical acceleration parameter that is used to classify pullouts. By including these regimes in the cluster definition for climb, the resulting climb statistics are protected from false positives of nuisance regimes that can otherwise significantly reduce the total time within the CWC climb regime. The resulting set of cluster regimes is shown in table 13.

Table 12. The IVHMS regimes bordering climb target regimes

Regime	Before (%)	After (%)	Total (%)
82: Pushover to 1.2 VH, 0.3 to 0.8 G	12.418	15.033	13.725
73: Symmetrical Pullout to 1.2 VH	12.418	13.072	12.745
91: Right Turn Entry	8.170	13.072	10.621
93: Right Turn Recovery	11.765	9.150	10.458
94: Left Turn Recovery	7.843	9.804	8.824
92: Left Turn Entry	7.516	8.824	8.170
21: Level Flight Between 0.5 VH	8.497	7.516	8.007
22: Level Flight Between 0.6 VH	6.536	4.575	5.556
23: Level Flight Between 0.7 VH	4.902	4.575	4.739
24: Level Flight Between 0.8 VH	3.595	2.941	3.268
20: Level Flight Between 0.4 VH	2.288	3.268	2.778
55: 30 AOB Level Left Turn, 10 to 35 AOB	3.268	2.288	2.778
59: 30 AOB Level Right Turn, 10 to 35 AOB	2.288	0.980	1.634
56: 45 AOB Level Left Turn, 35 to 50 AOB	1.961	0.980	1.471
76: Left Rolling Pullout to 1.2 VH, Up to 1.8 G	1.634	0.327	0.980
79: Right Rolling Pullout to 1.2 VH, Up to 1.8 G	0.980	0.980	0.980
19: Level Flight Between 0.3 and 0.4 VH	0.980	0.327	0.654
25: Level Flight Between 0.9 and 1.0 VH	0.654	0.654	0.654
95: Unrecognized	0.654	0.327	0.490
60: 45 AOB Level Right Turn, 35 to 50 AOB	0.654	0.000	0.327
86: Other Maneuver 1, Left Climbing Turn Exceeding AOB Limits	0.000	0.654	0.327
87: Other Maneuver 2, Right Climbing Turn Exceeding AOB Limits	0.000	0.327	0.163
8: OGE Hover	0.000	0.327	0.163
96: Undetermined	0.327	0.000	0.163
9: Forward Flight to 0.3 VH	0.327	0.000	0.163

AOB = Angle of bank

Table 13. The CWC climb cluster regime set

Cluster Regime	Persistence(s)
8: OGE Hover	1
9: Forward Flight to 0.3 VH	1
19: Level Flight Between 0.3 VH	1
20: Level Flight Between 0.4 VH	1
21: Level Flight Between 0.5 VH	1
22: Level Flight Between 0.6 VH	1
23: Level Flight Between 0.7 VH	1
24: Level Flight Between 0.8 VH	1
25: Level Flight Between 0.9 VH	1
73: Symmetrical Pullout to 1.2 V	1
82: Pushover to 1.2 VH , 0.3 to	1
91: Right Turn Entry	999
92: Left Turn Entry	999
93: Right Turn Recovery	999
94: Left Turn Recovery	999

4.3.1.6 Clustered Climb Regime Results

Table 14 shows the results after applying the cluster definition to the CERDEC flight test data. Relative to the baseline results, the total count of occurrences improved from 1.8 to 1.03 times the occurrence count of the truth regime, and the duration accuracy improved from 87% to 94%. Figure 9 shows the same example climb maneuver as figure 8, except the clustering definition has now been applied.

Table 14. Clustering RR performance for climb from CERDEC testing

Statistic	Target Regimes	Truth Regime
Mean Duration(s)	34.1	37.3
Median Duration(s)	12	8.3
Duration Standard(s)	56.3	68.0
Minimum Duration(s)	1.0	0.05
Maximum Duration(s)	356	343
Total Duration(s)	7024	7458
Counts	206	200
Percentage	15.64	15.94
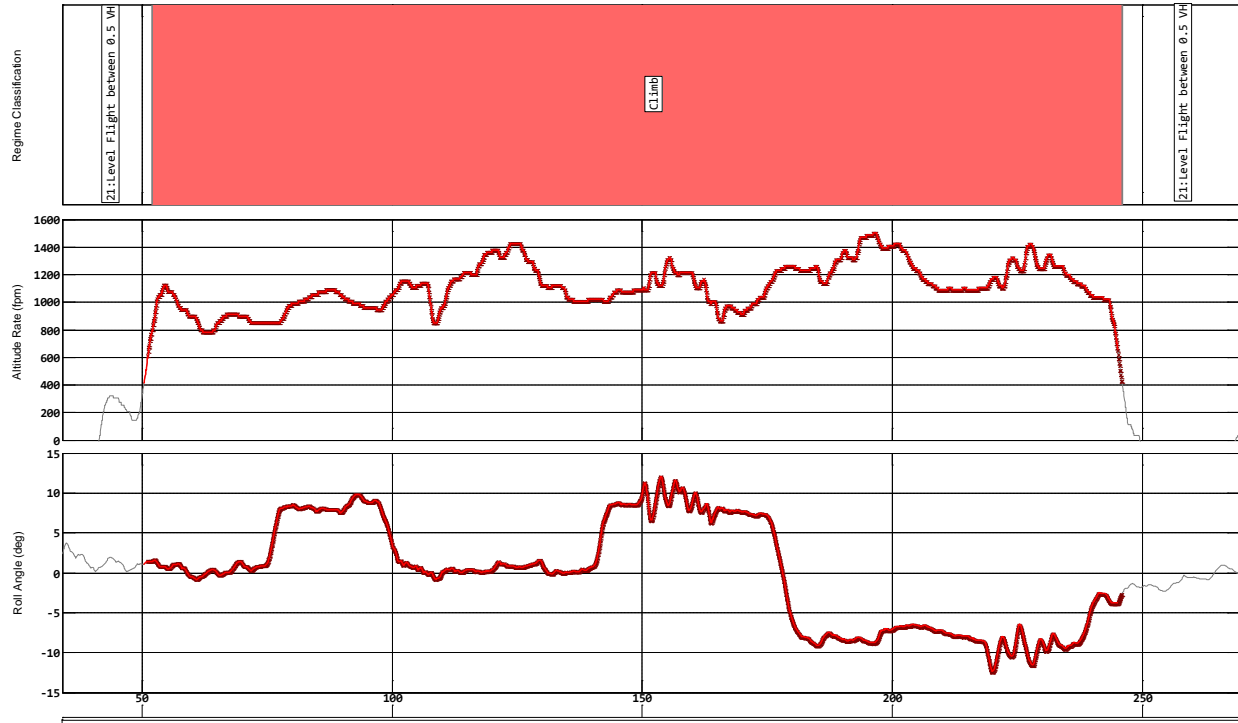
Figure 9. Example of climb RR with clustering

4.3.2 Cluster Design Process for 45-Degree Turn Regime

4.3.2.1 CWC Mapping

The mapping of both standard flight test turn maneuvers and corresponding IVHMS regimes to the UH-60M CWC generic turn regime is shown in table 15 for a 45-degree right turn.

Table 15. The CWC turn regime mapping

Flight Test Maneuver	UH-60M Regime Definition	IVHMS Regime
Steady Right Turn to 0.5 VH (45 DEG)	TURN 45 R	60:45 AOB Level Right Turn, 35° to 50° AOB
Steady Right Turn to 0.8 VH (45 DEG)		
Steady Right Turn to 1.0 VH (45 DEG)		
Right Turn to 0.8 VH (45 DEG) (Inc E/R)		68:45 AOB Descending Right Turn, 35° to 50° AOB
Right Turn to 1.0 VH (45 DEG) (Inc E/R)		
Descending Right Turn (45 DEG) (Inc E/R)		

AOB = Angle of bank

4.3.2.2 Definition of Truth Regime

A parametric truth regime definition was developed to represent the CWC turn 45 R regime, which is composed of both level and descending 45-degree right turns. Other types of turns that do not fall into this CWC regime are climbing turns and autorotation turns. As shown in section 4.3.1.1, climbing turns are considered to be part of the CWC climb regime and are not an explicit turn regime. Autorotation turns are represented explicitly in the CWC for left and right, but not by angle of bank (AOB). The approach for developing a truth parametric definition for generic 45-degree right turns (generic being the set of level and descending turns) is as follows: 1) identify all turns by a roll-angle threshold, 2) eliminate each identified turn that is either climbing (by a rate of climb threshold) or autorotation (by an engine torque threshold), and 3) prorate to 45-degree turns by AOB range. On the surface, this approach is very similar to how RR works. However, there is a key difference that is both an advantage of this method and a weakness in current RR software. The focus of the first step is to identify a single continuous turn from beginning to end, regardless of climb rate or torque levels. Then, the entire turn is classified as either generic, climbing, or autorotation turn and 30/45/60 AOB using the threshold criteria. This approach guarantees that each turn is counted as a single occurrence, which is very different from how RR works. RR decides which type of turn is being observed every second and when a climb rate or torque threshold is crossed during a turn, the classification is changed immediately, giving the appearance of two adjacent turns. When roll angle is also increasing or decreasing, the two adjacent classifications can have different AOB prorates as well.

Thresholds for the truth parametric definition were developed for level and descending 45-degree right turns. Because the climb rate and torque thresholds are imposed as a second step prorate of occurrence, they are not considered in the broad turn definition, but are imposed as a requirement on a statistic (max/min/average) of the climb rate and torque values across the entire occurrence.

Corrected NZ was not available in parametric data to include in the truth definition. Though this parameter could have been recalculated off board, it was also known through previous work that banked turns consistently cross moderate pullout thresholds, which trigger false-positive indications of a pullout during a turn. It was desired to eliminate this issue from the truth definition by removing the corrected NZ term. Further analysis of other UH-60M flight test data sources needs to be done to establish the proper criteria to distinguish banked turns from rolling pullouts. Given these considerations, the resulting truth definition for the CWC turn 45 R regime is shown in table 16.

Table 16. The CWC turn 45 R truth regime definition

Parameter	Expression (Hysteresis)	
Roll Attitude (degree)	> 10 (3)	
Prorates		
Parameter	Statistic	Expression
Roll Attitude (deg)	Max	< 50
Roll Attitude (deg)	Max	≥ 35
Altitude Rate (fpm)	Min	< 600
Total Engine Torque (%)	Max	> 10

fpm = feet per minute

4.3.2.3 Definition of Turn Target Regimes

IVHMS regimes that map directly to the CWC turn 45 R in table 15 were selected as the target regime set with a minimum duration of zero seconds.

4.3.2.4 Baseline Turn RR Performance

Baseline results of the target set compared to the truth definition are shown in table 17. Combining the target set into a single regime cluster and counting occurrences of the cluster resulted in a count accuracy of 93% of the truth regime. However, duration was very low at 27% accuracy, which is true for all measures of duration, such as mean duration and maximum duration. An example of a turn maneuver for which the duration was under-represented is shown in figure 10. In this plot, the regime sequence is shown at the top with the target regimes highlighted in red blocks. The true regime duration, according to the parametric definition, is shown by the dark red portion of the curves that represent the parametric data. Though the target regimes were correctly identified at some point during the turn, several other non-target regimes were also identified, which account for the inaccuracy in duration. There are also three occurrences of the target regime during this single turn contributing to a problem of over-counting occurrences. Note, however, that the occurrences were not over-counted when considering the total sum of target regime occurrences in table 17 as compared to the occurrences of the truth regime.

Table 17. Baseline RR performance for 45-degree right turn

Statistic	Target Regimes	Truth Regime
Mean Duration(s)	5.8	19.4
Median Duration(s)	5.0	16.1
Duration Std(s)	5.5	9.4
Minimum Duration(s)	1.0	7.1
Maximum Duration(s)	34.0	52.7
Total Duration(s)	306.0	1105.5
Counts	53	57
Percentage	0.77	2.65
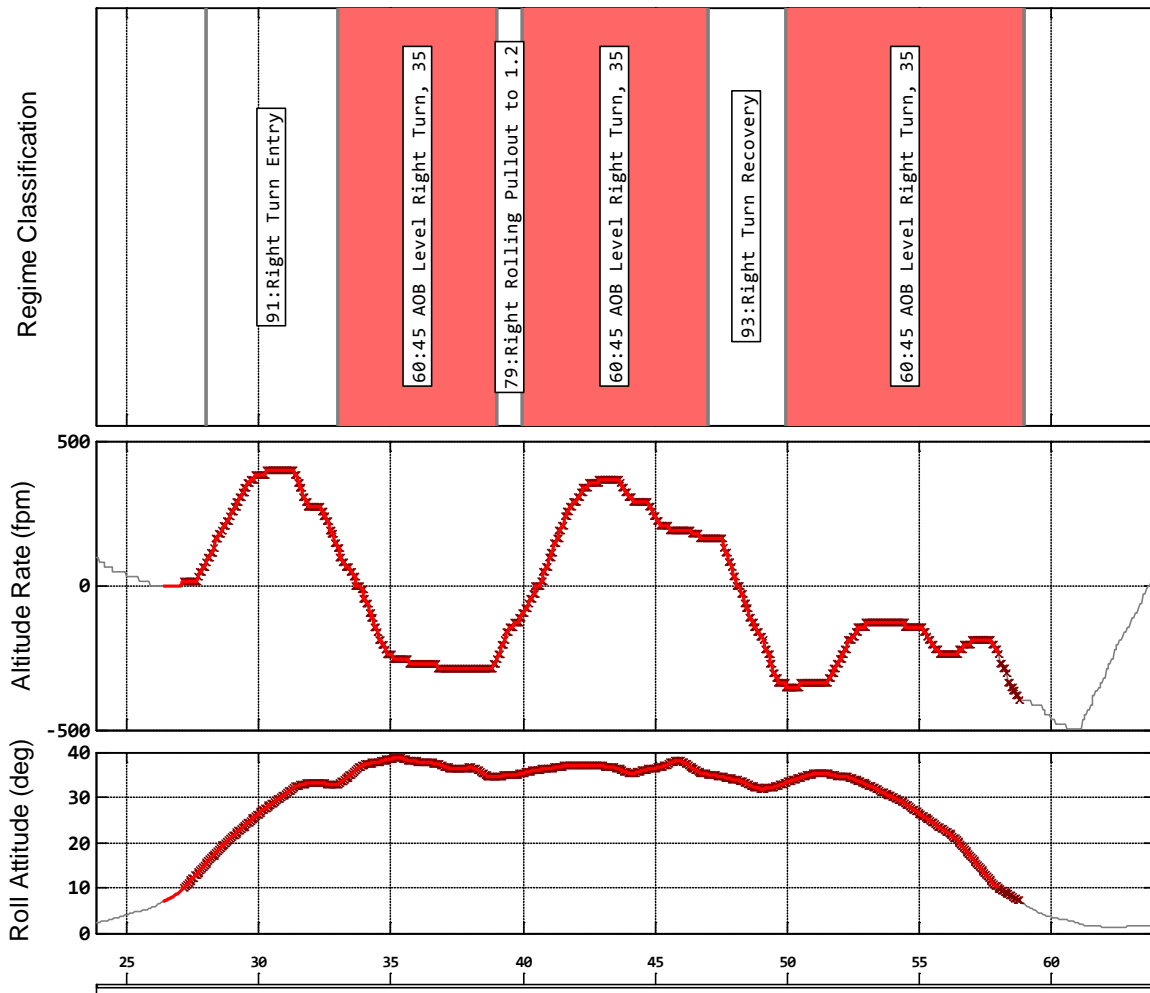
Figure 10. Example of turn RR before clustering

4.3.2.5 Selection of Turn Cluster Regimes

The frequency of adjacency of non-target regimes from the CERDEC testing is shown in table 18. Examination of these regimes and of individual turn maneuver plots revealed several issues affecting the inaccuracy in duration. These issues and proposed mitigation strategies are as follows:

1.   Turn entry and turn recovery regimes are explicit regimes in the UH-60M RR software and take up time from the turn. These regimes map directly to the CWC with an AOB prorate, but, when recognized, they are not associated with an AOB and, therefore, cannot be mapped to the CWC by themselves. The association of entry and recovery events to an AOB must be made by considering the middle portion of the turn. Rather than identifying entry and recovery independently from the turn maneuver, a simpler approach is to cluster recognized entry and recovery regimes with the turn maneuver and count entry and recovery occurrences implicitly by the occurrences of the turn itself. It is also noted that not every turn has a recognized entry and recovery. The proposed approach of implicitly counting entry and recovery guarantees that every recognized turn results in one count of an entry and one count of a recovery.

2.   Moderate rolling pullouts are often falsely triggered during turns because of inadequate thresholds for corrected NZ at high roll angles. Because the CERDEC flight test did not assess rolling pullouts, a means to detect them accurately still needs to be determined through further study of parametric data from other test data sources. However, a load factor threshold that varies with roll angle is a potential solution.

3.   Climbing and autorotation turns are frequently classified with level and descending turns. It was found that many turns have large variations in climb rate and engine torque, and can cross several boundaries in one continuous turn. A turn may start climbing but not maintain the climb rate throughout. It is proposed that turns are classified as climbing only if the climb rate is maintained throughout because a dropping off of climb rate is not characteristic of a true climbing turn. It is also proposed that a turn is classified as an autorotation only if it maintains autorotation throughout. Therefore, climbing and autorotation turns will be clustered with level or descending turns only if they occur adjacent to level or descending turns.

4.   Many 30-degree turns were observed to occur during an intended 45-degree turn. This problem is due to the reclassification issue when a torque or climb rate threshold is crossed while AOB is climbing or tapering. In the example from figure 10, the 45-degree turn starts out level but then starts descending. As it is descending, the roll angle tapers off below the minimum threshold for a 45-degree turn. Because RR treats level and descending turns as different regimes and classifies regimes on a second-by-second basis, it finds the descending turn and assigns it to 30-degrees AOB. The clustering approach can solve this by including all lower AOB turns as part of the cluster set of a given turn definition. This also introduces the need for prioritization of cluster definitions, which is discussed further in section 4.3.2.7.

The final set of cluster regimes is shown in table 19. Note that none of the clustering approaches previously discussed in this section require a persistence parameter.

Table 18. The IVHMS regimes bordering 45-degree right turn target regimes

Regime	Before (%)	After (%)	Total (%)
91: Right Turn Entry	81.132	0	40.566
93: Right Turn Recovery	3.774	67.925	35.849
79: Right Rolling Pullout to 1.2	9.434	18.868	14.151
37: Right Climbing Turn	0	5.66	2.83
21: Level Flight Between 0.5 VH	0	3.774	1.887
72: Autorotation Right Turns	1.887	1.887	1.887
59: 30 AOB Level Right Turn, 10	0	1.887	0.943
67: 30 AOB Descending Right Turn	1.887	0	0.943

Table 19. The CWC turn cluster regime set

Cluster Regime
37: Right Climbing Turn
59: 30 AOB Level Right Turn, 10° to 35° AOB
67: 30 AOB Descending Right Turn
72: Autorotation Right Turns
79: Right Rolling Pullout to 1.2 VH , Up to 1.8 Gs
87: Other Maneuver 2, Right Climbing Turn Exceeding AOB Limits
91: Right Turn Entry
93: Right Turn Recovery
59 62: Level Right Turns
67 70: Descending Right Turns

4.3.2.6 Clustered 45-Degree Right-Turn Regime Results

Results after applying the 45-degree right turn cluster definition are shown in table 20. These missed occurrences can all be properly captured as turns by clustering, but need further processing of roll attitude data to be properly mapped to the CWC during clustering post-processing. Ultimately, the onboard RR software should be refined to reduce the amount of post-processing necessary to properly classify all data.

The most significant improvement is that the clustered turn duration performance statistics, such as mean, standard deviation, and maximum and minimum duration, agree well with the truth regime. Both the total duration and the occurrence count of the clustered turns are 81% accurate relative to the truth regime, compared to 28% for the duration and 93% for the occurrences before clustering. The fact that clustering is consistently counting occurrence and duration means

that it is properly counting whole maneuvers and their durations for the maneuvers that were captured. The clustering approach appears to have reduced the accuracy of the occurrences from 93% to 81%, but closer inspection showed that the accuracy metric on occurrences calculated before clustering was flawed and fortuitous. While the pre-clustering result was 93% accurate (53 of 57) on counts, only 46 of the 57 occurrences of the truth regime were captured by the target regime, and an additional seven were over-counted during the same maneuver, leaving 11 occurrences that were misclassified by RR. By correcting the over-counting problem, the clustering approach revealed the full potential and allowed for a cleaner assessment of RR. This is best shown by comparison of the before-clustering example maneuver in figure 10 to the same maneuver after clustering in figure 11. The pre-clustering regime sequence counted three occurrences of the turn whereas the post-clustering regime sequence correctly counted a single occurrence for the entire turn.

Further investigation into the 11 misclassified occurrences of the 45-degree right turn revealed the following two primary scenarios that prevented RR from identifying the correct target regime:

1. The peak roll angle, which is ultimately used to classify the turn's AOB, was achieved briefly while the aircraft was climbing. When climbing, turns are not classified by AOB, so the peak AOB information is lost. This is not a problem for pure climbing turns because these maneuvers are not prorated by AOB. However, when a climbing turn briefly occurs at the peak roll angle, the entire turn is not considered a climbing turn and, therefore, needs to be prorated by AOB. In these cases, the turn is categorized into the next-highest AOB that was captured by RR. An example of this case is shown in figure 12. Here, a 45-degree turn maneuver is flown as shown by the roll attitude, but RR only classifies turn entry, 30-degree right turn, and right climbing turn. These regimes are shown in blue because they are cluster regimes for the 45-degree turn, but the 45-degree turn target regime was never classified. The 45-degree turn was achieved during a brief climbing portion, which prompted the climbing turn classification at that same point in time. Although the clustering approach for 45-degree right turns will not capture this maneuver, the maneuver would still be captured as a turn, but would be mapped to either climbing or 30-degree turns.

2. No turn event was actually identified by RR, but a turn entry and turn recovery were identified. In some cases, a turn entry and turn recovery occurred back to back and there was no time to identify the actual turn. In other cases, a moderate rolling pullout was identified between the entry and recovery, but no turn, as shown in figure 13. In this example, a rolling pullout was captured in the middle of a turn entry and turn recovery. It is possible that rolling pullouts would be clustered with adjacent turn entry and recovery regimes, in which case these would not be treated as misclassified turns. Further study of the difference between turns and rolling pullouts would be required to develop truth criteria that distinguish the two.

These missed occurrences can all be properly captured as turns by clustering, but further processing of roll attitude data is needed to be properly mapped to the CWC during clustering post-processing. Ultimately, the onboard RR software should be refined to reduce the amount of post-processing necessary to properly classify all data.

Table 20. Clustering RR performance for 45 degree right turn

Statistic	Target Regimes	Truth Regime
Mean Duration(s)	19.5	19.4
Median Duration(s)	17.0	16.1
Duration Standard(s)	9.5	9.4
Minimum Duration(s)	6.0	7.1
Maximum Duration(s)	51.0	52.7
Total Duration(s)	897.0	1105.5
Counts	46	57
Percentage	2.2	2.7
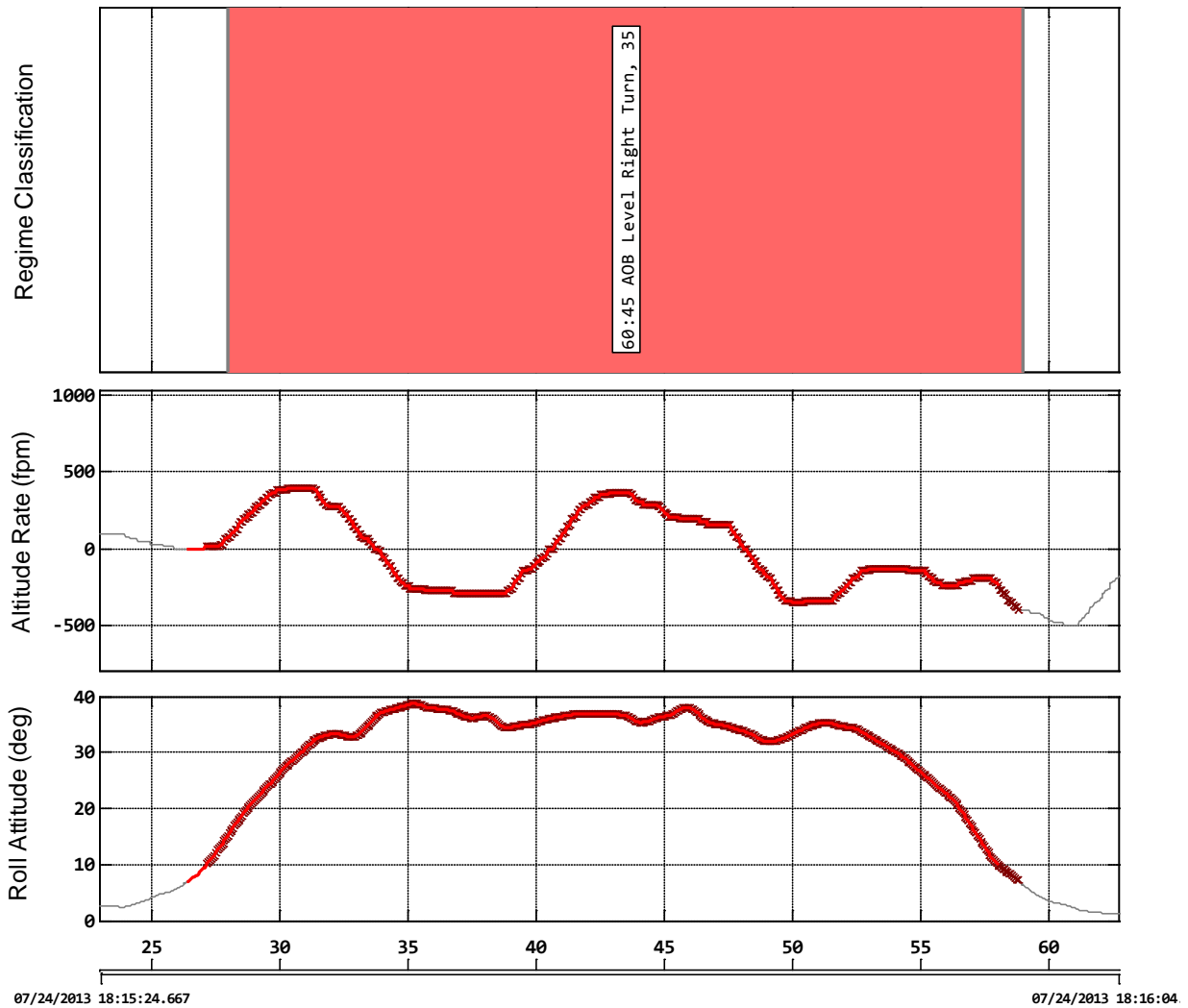
Figure 11. Example of turn RR after clustering

36
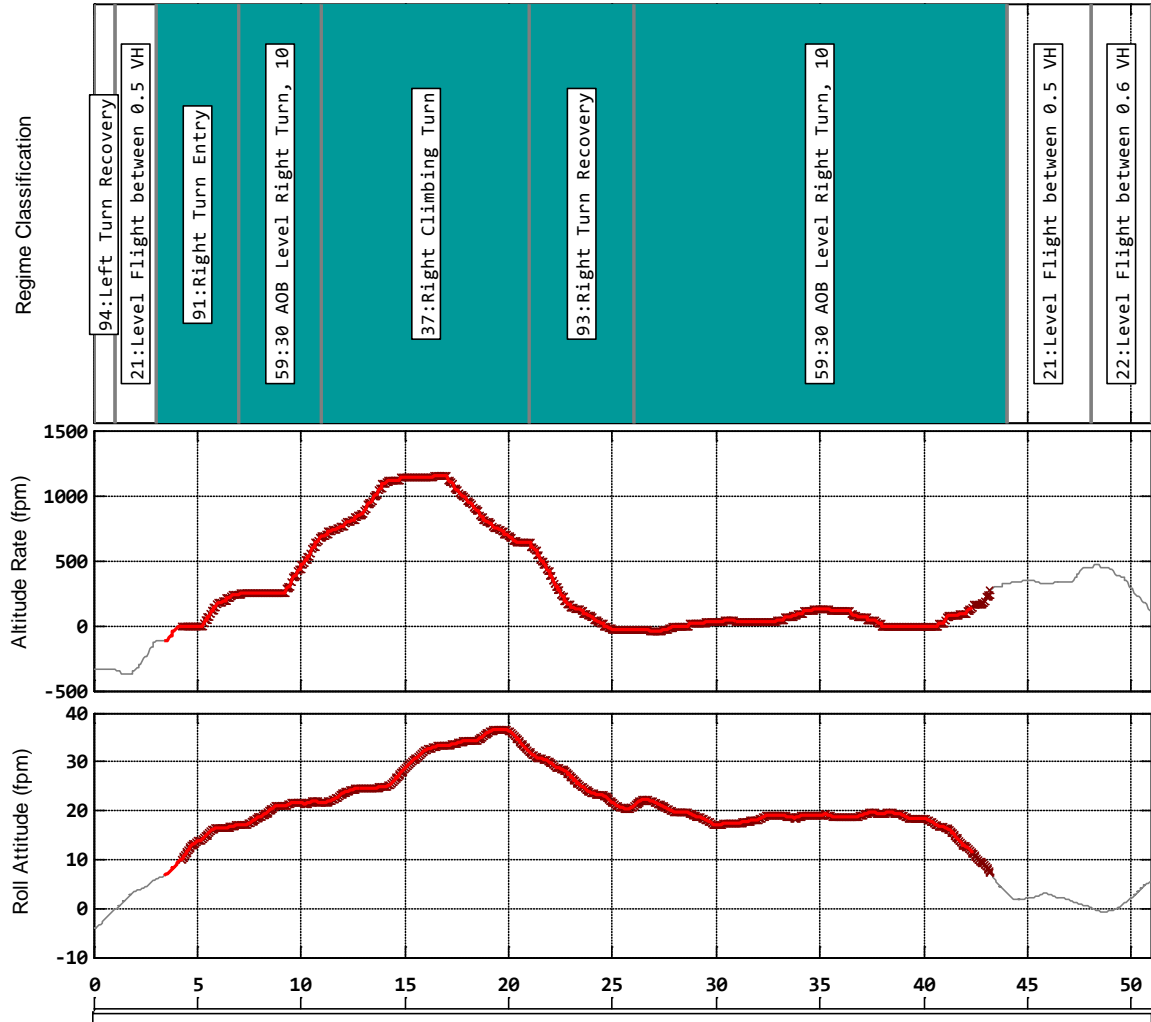
Figure 12. Example of a 45-degree turn classified as a 30-degree and climbing turn
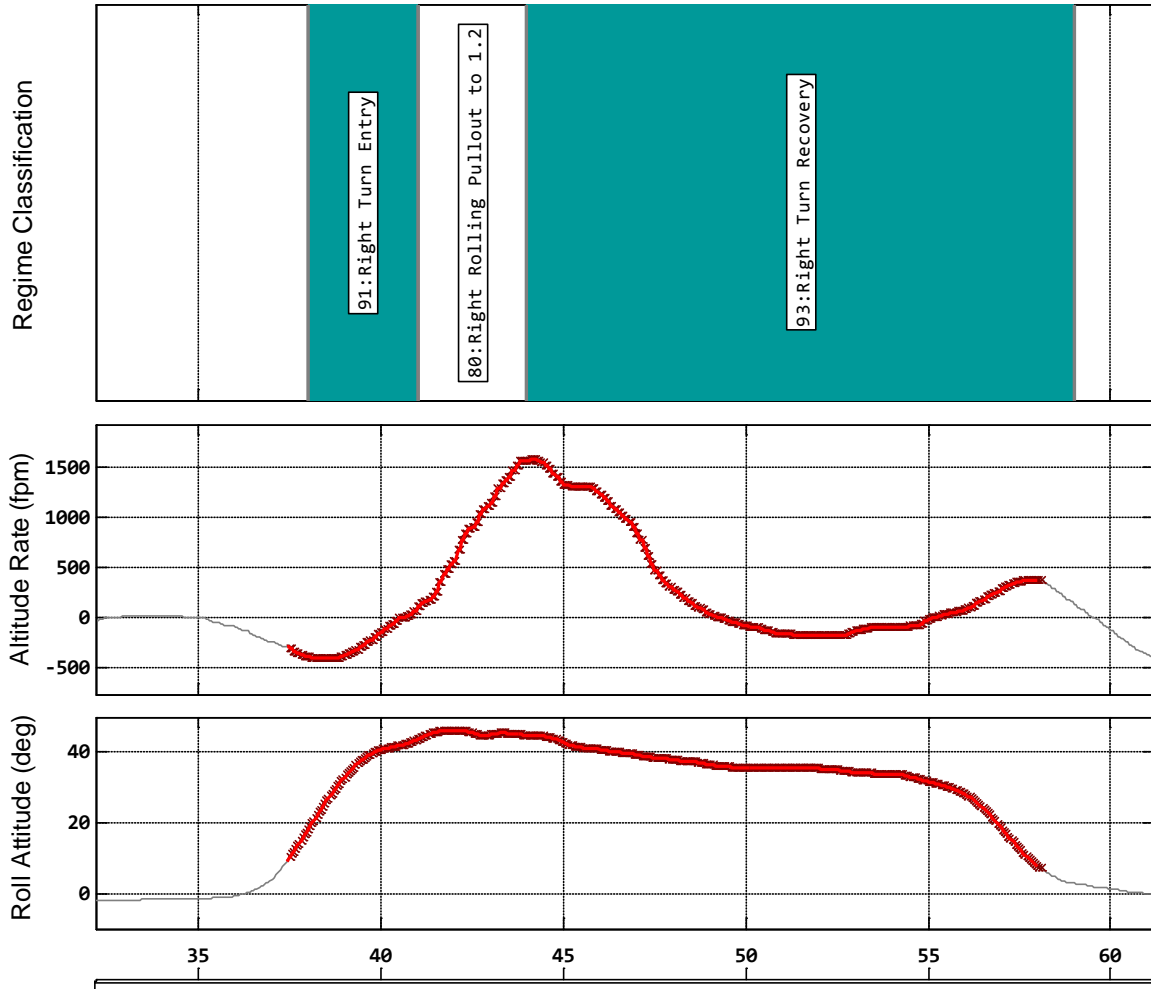
Figure 13. Example of a 45-degree turn classified as a rolling pullout

4.3.2.7 Turn Cluster Prioritization

It was noted in section 4.3.2.6 that when developing a cluster definition for 45-degree turns, a 30-degree turn was often identified during the 45-degree turn. In these cases, the 30-degree turns were clustered within the 45-degree turn. For the same reasons, the same issue can occur with 60-degree banked turns. Therefore, to develop and apply the 45-degree turn cluster definition to real fleet data, the 60-degree turns must be clustered before the 45-degree turns so that any 45-degree turn classifications that are really part of a 60-degree turn are not misclassified as a 45 degree turn. Clustering requires a hierarchical approach with which each cluster definition is assigned a priority rank. Though 60-degree and 30-degree turns were not validated in this effort, cluster definitions were developed for them using the same basic cluster regimes that were selected for the 45-degree turn to enable accurate clustering of the 45-degree turns.

4.3.3 Regime Load Analysis Using Clustering Capture Windows

Key dynamic system vibratory loads measured during the clustered turn and the climb regimes on the CERDEC test aircraft were compared to the baseline loads measured during the UH-60M

FLS for the same regime as another means to evaluate the clustering methodology. Comparisons were made only where the CERDEC GW/CG configuration matched or was in the vicinity of the FLS configuration. The two load measurements that were made on the CERDEC aircraft that enabled this analysis were the MRLSS link load and the MRSEBL. The load capture windows for the UH-60M FLS are based on pilot- or engineer-reviewed log cards. Load capture windows for CERDEC testing are based on clustered RR results. Figures 14 and 15 show a comparison of the maximum vibratory MRLSS load and MRSEBL load, respectively, during climb, turns, and pullouts from both tests.

Overall, the lateral servo loads compare favorably with flight test loads, shown in figure 14. For 45-/60-degree turns and moderate/severe pullouts, the baseline FLS conditions generated much more aggressive servo loads due to much higher speeds at the extreme conditions, which have a tendency to produce blade stall. This was expected because extreme FLS maneuvers were not included in the CERDEC flight test because their test pilots were not experienced in performing such maneuvers. Shaft bending loads from the CERDEC tests were also similar to previously measured loads with a few notable exceptions for the 45-degree turns, shown in figure 15. It was found that, in some cases, the CERDEC test aircraft achieved higher levels of VH airspeed at the high GW with ESSS configuration, which was accomplished during the descending phase of a 45-degree turn that started out level with high speed. Some other cases of higher shaft bending load were attributed to the longitudinal cyclic input required to generate an increased climb rate in the middle of the turn. The fact that the loads were higher for a few of these maneuvers is not surprising because of the intended complex nature of these maneuvers, which are not represented in the baseline FLS test data. The RR performance during these maneuvers was found to be satisfactory.

Below each scatter population in figures 14 and 15 is the number of data points contained within each population. Because the CERDEC load statistics were captured using RR with clustering as a capture window, the analysis was not bound to the run log in the same way the baseline FLS test data was. The turns captured in the CERDEC analysis were a combination of intended run log maneuvers, unofficial practice runs, and natural turns performed in the course of navigation. By using RR to define a capture window for loads acquisition, the quantity of load points made available is much higher. It took six test flights on the CERDEC aircraft to generate the maneuver quantity shown in these figures, compared to more than 20 test flights of the baseline UH-60M FLS test vehicle. Part of this is attributed to the high turn count within the CERDEC testing. However, the use of RR capture windows to gather load statistics means that each flight has 100% coverage of maneuver loads acquisition from takeoff to landing. As RR matures, there is a huge opportunity to integrate these methods into the flight test process to enhance structural maneuver load databases without any extra flying.

Also shown for each load in figures 16 and 17 is a comparison of maximum vibratory load for servo and shaft bending loads, respectively, versus cluster count for climb and 45-degree left/right turns conducted during CERDEC testing. Cluster count is the number of regimes that were combined into the target regime for each maneuver occurrence. A cluster count of 0 indicates there was no clustering applied to that maneuver, whereas a cluster count of 10 means 10 regimes were combined into the target regime for that maneuver. An evaluation of loads as a function of cluster count was done to understand if highly clustered maneuvers (exceeding 10) had any tendency to have higher loads associated with them. Figures 16 and 17 show that many

of the highest vibratory loads occurred with very moderate cluster counts of 2–4. Extremely complex maneuvers with many cluster counts do not have a greater tendency than simpler maneuvers to produce high peak loads.
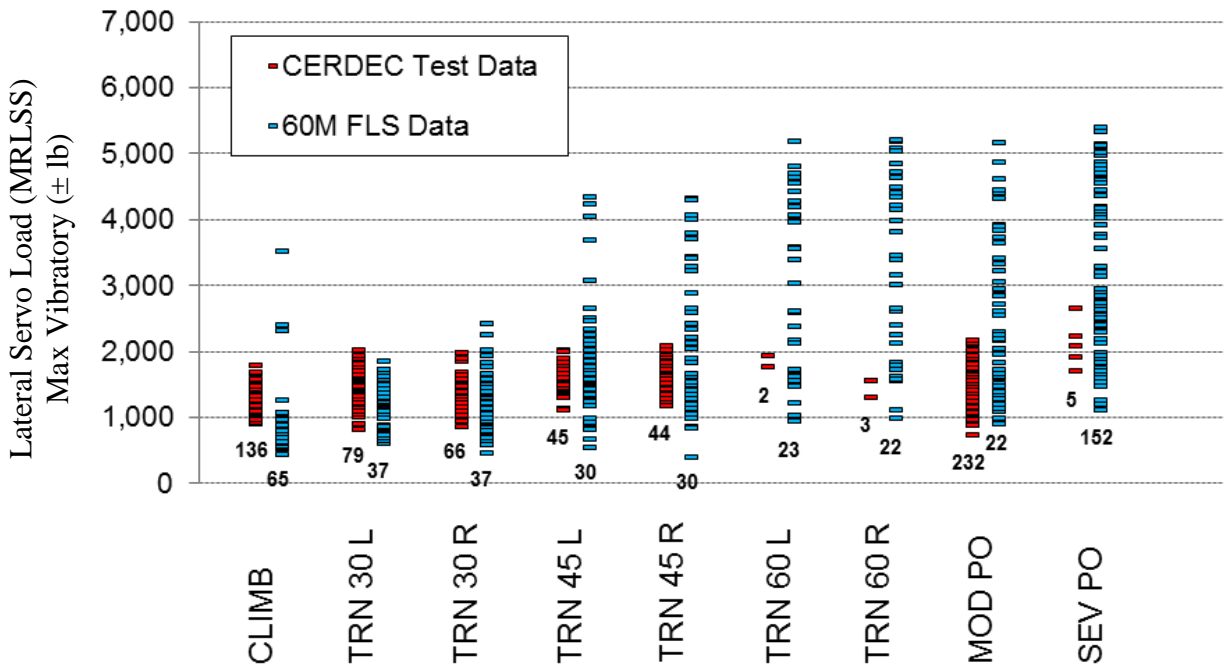
Figure 14. The MTLDD loads during CERDEC maneuvers
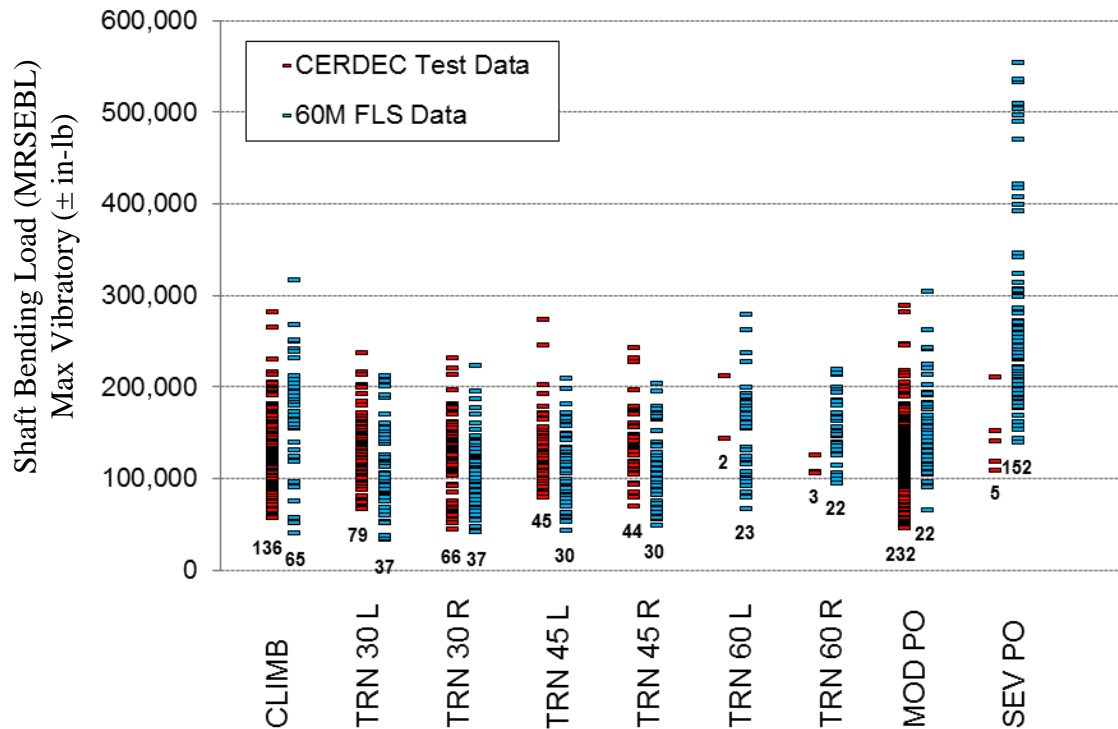
Figure 15. The MRSEBL loads during CERDEC maneuvers
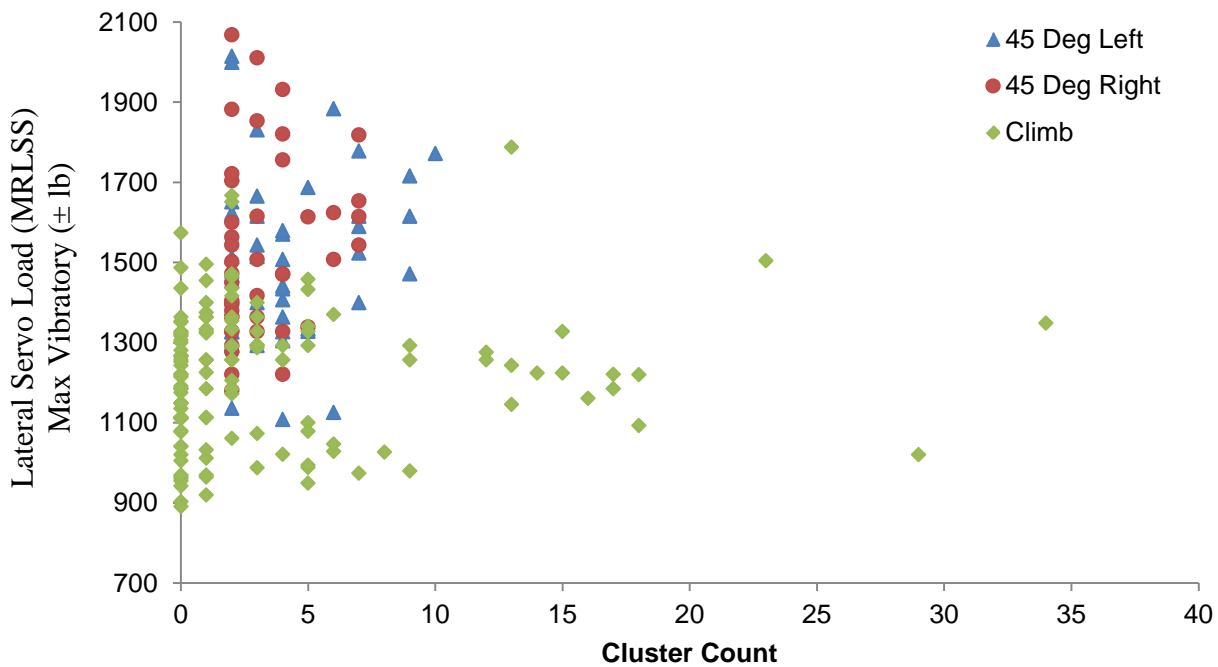
Figure 16. The MRLSS maximum loads versus cluster count per cluster from CERDEC testing
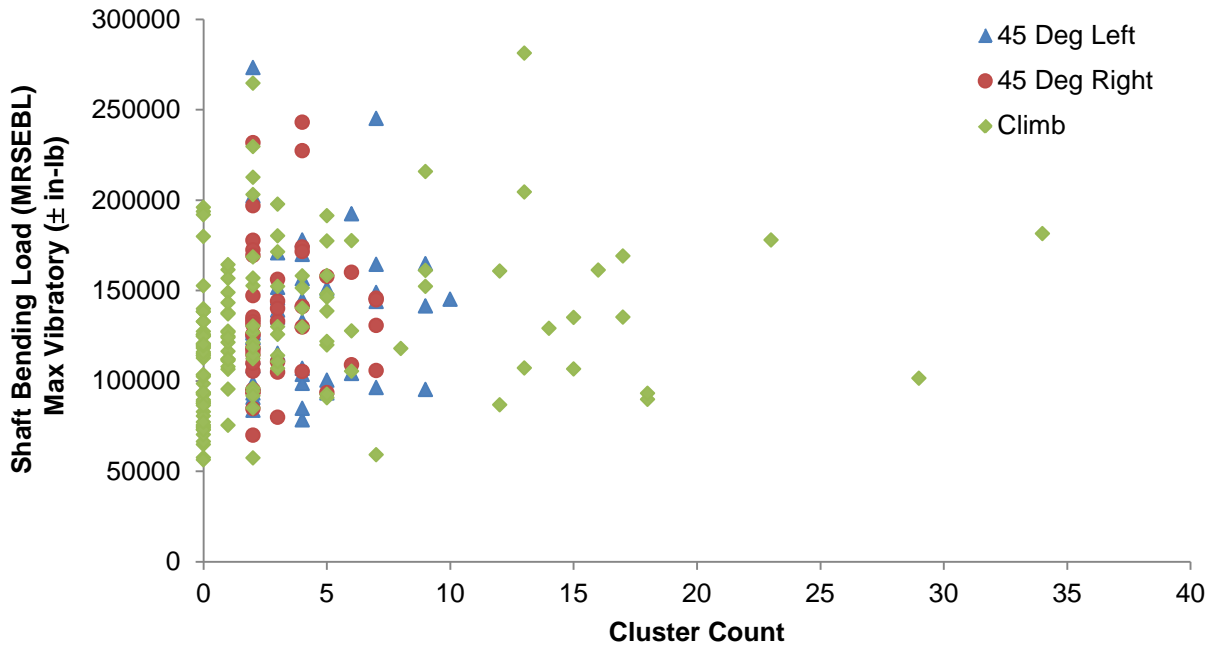
Figure 17. The MRSEBL maximum load versus cluster count per cluster from CERDEC testing

4.4 Enhanced RR Validation Approach

The validation approach followed thus far in the development of regime cluster definitions is useful in guiding the design of a cluster, but it has drawbacks. First, as discussed in section 2.1.1, the metrics used thus far in assessing accuracy can provide misleading results about the performance of a regime definition. Second, the parametric truth regime definitions themselves are essentially an independent RR approach and should also be validated against flight test data. This presents a problem because any truth parametric definition must have some prior validation against an even better set of truth data. At some point in the process, there must be a qualitative expert assessment of the maneuver. These expert classifications are made available in structural FLS test programs via maneuver-coded flight run logs. To use these expert classifications to assess RR performance, a few issues need to be sorted out relative to the uniqueness of FLS data.

The most unique aspect of the flight test log card approach is that the start/stop times of transient maneuvers capture a larger window than the start and end of the maneuver itself. An example of this is shown in figure 18. Here, a 45-degree left climbing turn maneuver is flown, but the capture window includes non-climbing turn data at the beginning and end. This makes the transient maneuver duration statistics difficult to attain because the true start and stop time of the maneuver cannot be achieved without laboriously going through hundreds of maneuvers and assigning them manually. Though algorithmic approaches may be used, the objective is to avoid the dilemma posed when validating an algorithm with another algorithm. Because transient regimes are traditionally quantified by occurrences rather than duration, it is proposed that the validation of transient regime classification methods be made on the basis of occurrence or detection accuracy and not on duration. It is far more useful to know the true occurrence rate of

transient regimes in the fleet than it is to accurately know their individual durations. For steady-state regimes, however, it is expected for a flight test pilot to hold a steady-state regime for the entirety of its recording. Therefore, duration metrics are possible and are valuable for the validation of steady-state regimes.
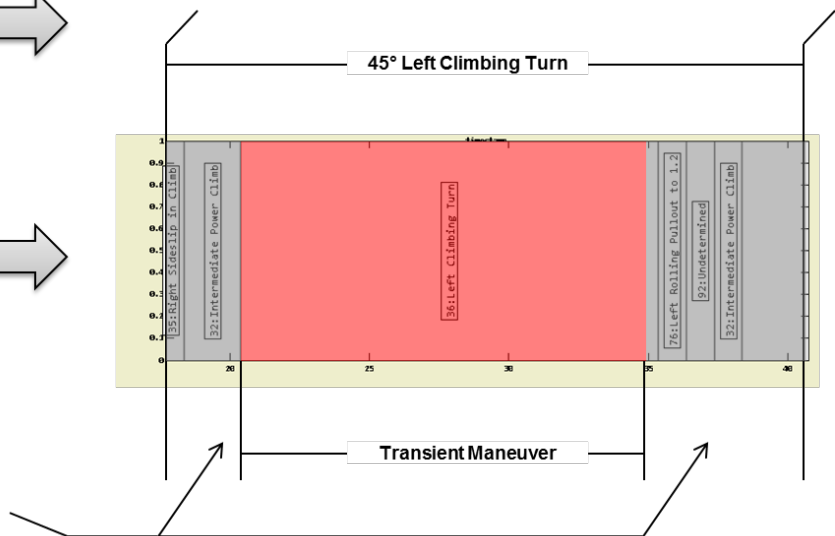
Figure 18. Example of run log markers for transient maneuver identification

Another challenge is that the truth regime labels are not equivalent to HUMS regime labels. However, this issue can be overcome by mapping both HUMS regimes and Advanced Data Acquisition and Processing System maneuvers to a common labeling system. This common regime labeling is found in CWC regimes.

From the lessons learned in developing the cluster definition for climbs and turns, it is necessary to clearly establish the definition of regime accuracy and the methodology behind assessing the accuracy. The previous approach of simply counting occurrences was problematic when there was a combination of mis-detects and over-counts, because the over-counts could mask the presence of mis-detects. Rather than counting the total number of detections, accuracy of detection should always be assessed by counting the number of mis-detects, or false negatives. If a truth regime is flown 100 times and four of those 100 occurrences are not detected, then the accuracy is (100–4)/100 or 96%. This does not necessarily mean that there were 96 detections, because there may still be the tendency to over-count in some cases. The tendency to over-count leads to the need for an additional metric for transient regime performance. This metric is the count ratio metric for transient regimes. The count ratio is the average number of detections per truth occurrence when at least one detection is made. When the count ratio is one, then the regime algorithm is perfectly detecting one occurrence per truth occurrence. A count ratio of 2 means the regime algorithm tends to double count. By only including the cases in which at least one detection is made, the count ratio does not account for mis-detects and, therefore, cannot be obscured by the combination of mis-detects and over-counts. A previous example for which this would be important to assess is shown in figure 10, in which three correct turns were classified

during a single turn. Using both of these metrics together was found to be very useful in revealing the underlying strengths and weaknesses in RR.

A simpler approach was taken for steady state regimes. Because flight test capture windows contain only the intended steady state regime, the accuracy metric was applied on a duration basis defined as the total time detected by RR divided by the total time spent in the flight test capture window. The time spent in all other regimes during the flight test capture window was also recorded so that the results not only indicated the accuracy of the target regime, but also highlighted areas of focus for regime definition improvements.

Though the accuracy metric is the most basic metric for assessing the performance of a regime definition, the frequency and the source of false positives are important in understanding regime performance. False positives are when a regime is recognized, but it has not actually occurred. In these cases, it is most likely that some other regime occurred that is very similar to the recognized regime, but not the same. It is conceivable that a particular regime definition can be 100% accurate and also have a tendency toward false positives associated with other similar regimes. The most important quality is that regime classification is conservative in the presence of false positives and sufficiently accurate (e.g., 95%) to instill confidence in algorithm performance and not unduly undermine benefit because of overly conservative methods. However, false positives will create a problem when the associated similar regime causing them becomes the subject of validation itself. In that scenario, the previously identified false positives will now be considered mis-detects for the new regime, and would likely require a change to both regime definitions to be correct. Therefore, it is important to understand false positives and what is causing them, and to minimize them in the development of the regime definition to avoid future algorithm changes and re-validation efforts as more regime definitions are refined, developed, and validated.

This approach to assessing regime accuracy was implemented on an existing set of UH-60M flight test data, from test flights conducted on aircraft M2 between July 11, 2006 and July 24, 2007 to support qualification of the UH-60M IVHMS. For these flights, the Goodrich IVHMS was installed and configured with a preliminary regime configuration. These are the best-known datasets that SAC has to validate UH-60M RR using flight test declared truth regimes during an FLS. The regime metrics described in this section were applied to the entire flight test data set with the pre-production regime configuration before clustering applied, and again after clustering was applied for the climb and turn regimes.

The validation results for transient turn regimes are shown in table 21 for both before and after clustering. The most significant improvement due to the clustering methodology is that the count ratio collapsed perfectly to 1 over all occurrences in the flight test data. When looking at the occurrence accuracy in table 21 for before and after clustering, however, it appears to have become worse with clustering. However, this is due to similar reasons, as discussed in section 4.3.2.6. Before clustering, RR was over-counting, with more than one classification for each turn and, therefore, had more than one opportunity to get the right classification at some point during the turn. An example of this is shown in figure 19, in which RR classified a 30-, 45-, and 60-degree turn during the same maneuver. Because clustering collapses the entire regime sequence into one maneuver during the turn, it has only one opportunity to get the right classification. By looking at all the turn events in a confusion matrix, as shown in table 22, it is

shown that the underlying cause of mis-detection is that RR is classifying some turns into the next-higher AOB prorate category. For example, this table shows that there were 85 (74+11) occurrences of 30-degree left turns, and 74 (87%) of them were correctly classified as 30-degree left turns, whereas 11 were conservatively classified as 45-degree left turns. For 60-degree left turns, 85 of them were flown, and 85 (100%) were correctly classified as 60-degree left turns. Because RR makes the AOB prorate decision directly on the roll angle, and because the flight test and RR prorate bands are identical, all of the cases for which RR classified into the next higher AOB category were correct classifications, and the perceived inaccuracy of RR is actually attributable to overshooting the target maneuver in the flight test. For the previous example in figure 19, clustering collapsed the sequence into a single 60-degree AOB turn. The flight test classification for this turn event was actually a 45-degree turn; however, the maximum AOB slightly crossed into the 60-degree band. This highlights the fact that any future uses of flight test truth classifications need to be thoroughly quality checked for consistency with established prorate thresholds to get a more accurate picture of RR performance against flight test truth data.

The validations results, before and after clustering, were found to be very low because of the pre-production version of the RR algorithms that were onboard at the time of this M2 test. The issue causing low accuracy for the climb regime was a poorly performing sideslip regime that was causing excessive false-positive sideslip indications. As a result of this baseline testing, production changes were made to the sideslip definition to eliminate the false positives that were interfering with the other regimes, such as climb. Because this same problem was not present in the CERDEC test data, the clustering approach was not designed to address it. Therefore, the benefits of clustering are not fully realized for the climb regime on this legacy test data.

Table 21. Turn validation statistics from FLS

	Total Occurrences	Before Clustering		After Clustering	
		Accuracy	Count Ratio	Accuracy	Count Ratio
Turn 30 L	85	93%	1.2	87%	1
Turn 30 R	85	93%	1.2	85%	1
Turn 45 L	85	95%	1.7	82%	1
Turn 45 R	85	81%	1.6	63%	1
Turn 60 L	85	98%	1.6	100%	1
Turn 60 R	82	91%	1.6	100%	1
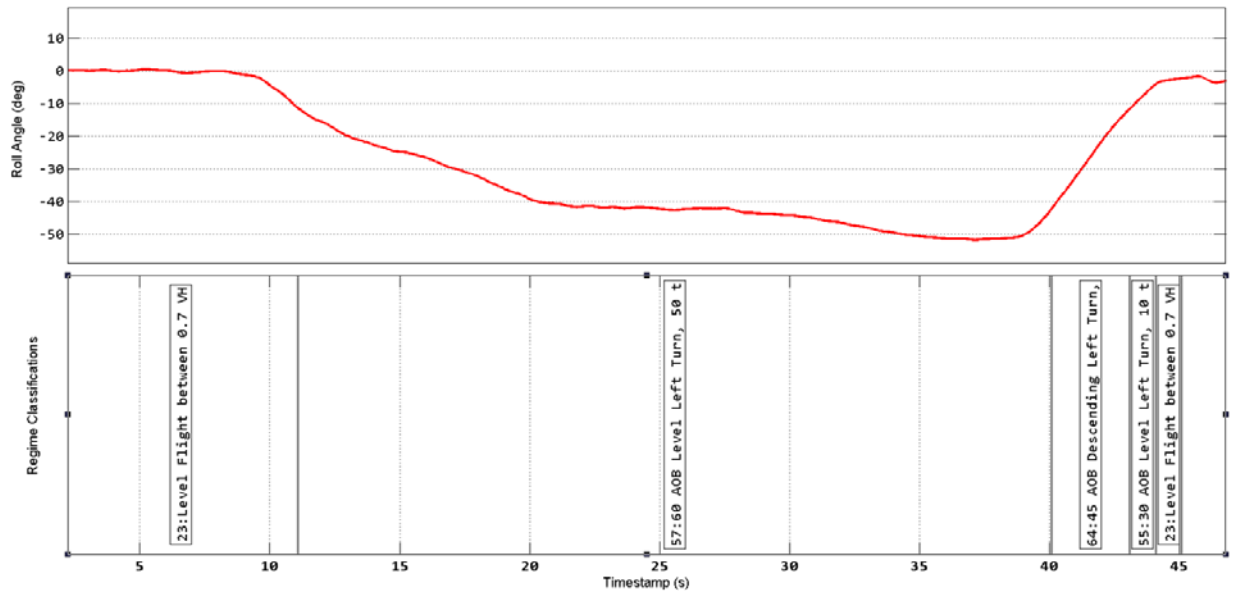
Figure 19. Sample turn regime classification before clustering

Table 22. Turn confusion matrix after clustering

		Regime Classification					
		Turn 30 L	Turn 30 R	Turn 45 L	Turn 45 R	Turn 60 L	Turn 60 R
Truth Regime	Turn 30 L	74		11			
	Turn 30 R		72		13		
	Turn 45 L	1		70		14	
	Turn 45 R				54		26
	Turn 60 L					85	
	Turn 60 R						82

5. VML AND GW/CG

5.1 VML

5.1.1 Background

The ability to measure key loads on operational rotorcraft could radically change the way rotorcraft are designed, qualified, and managed throughout their life cycles. The lack of such measurements is indicative of the perceived difficulties, increased weight, and reliability issues associated with deploying the many physical sensors that would be required to monitor all such local loads, especially in rotor systems. SAC has been developing an approach called VML that estimates rotorcraft loads using parametric data available from a state-of-the-art aircraft HUMS. VML is one of a few key technologies that will enable a transition from a simple flight-hour-based program to more advanced UBM programs for rotorcraft.

As a significant step toward achieving UBM, SAC has begun applying these methods to archived S-92® fleet data to support internal engineering decision-making processes that provide significant near-term value and build confidence in the methods. These steps are required before making the investment and making the decision to implement such a paradigm shift in product design and fleet management. Some of the near-term applications have been to: 1) support root-cause analysis for issues experienced in an aircraft to help determine whether the issue is aircraft- or operator-specific or a fleet-wide issue that may require a retrofitted engineering change, 2) assess loads incurred during a flight event to help determine appropriate maintenance actions, and 3) reassess the usage spectrum, especially applied pro-rates. Recently, a VML model was applied to more than 500,000 flight hours of archived historical fleet data for the S-92 rotorcraft, and the estimated tail rotor torque loads were used to support assessment of the actual fleet load spectrum to allow refinement of the prorating of severity of key critical regimes for use in design, testing, and certification of drivetrain components.

A VML model estimates high-frequency helicopter dynamic load profiles from once per revolution average helicopter state parameters. Training data for the model is comprised of measured dynamic loads and associated helicopter state parameters derived from structural FLS testing. During model training, important dynamic load waveform mode shapes are extracted from the measured load using proper orthogonal decomposition (also known as principal component analysis or singular value decomposition). A linear regression model is then developed to map helicopter state parameters to the mean load and mode shape coefficients. This process is shown in figure 20.

The result of model training is a library of fixed mode shapes and parameter-dependent mode coefficients that can be used to estimate the dynamic load waveform, steady load, and vibratory amplitude in real time or in a post-processing environment. To apply VML, the mode coefficients are estimated from operational HUMS-recorded helicopter state parameters and applied to the extracted mode shapes from training.
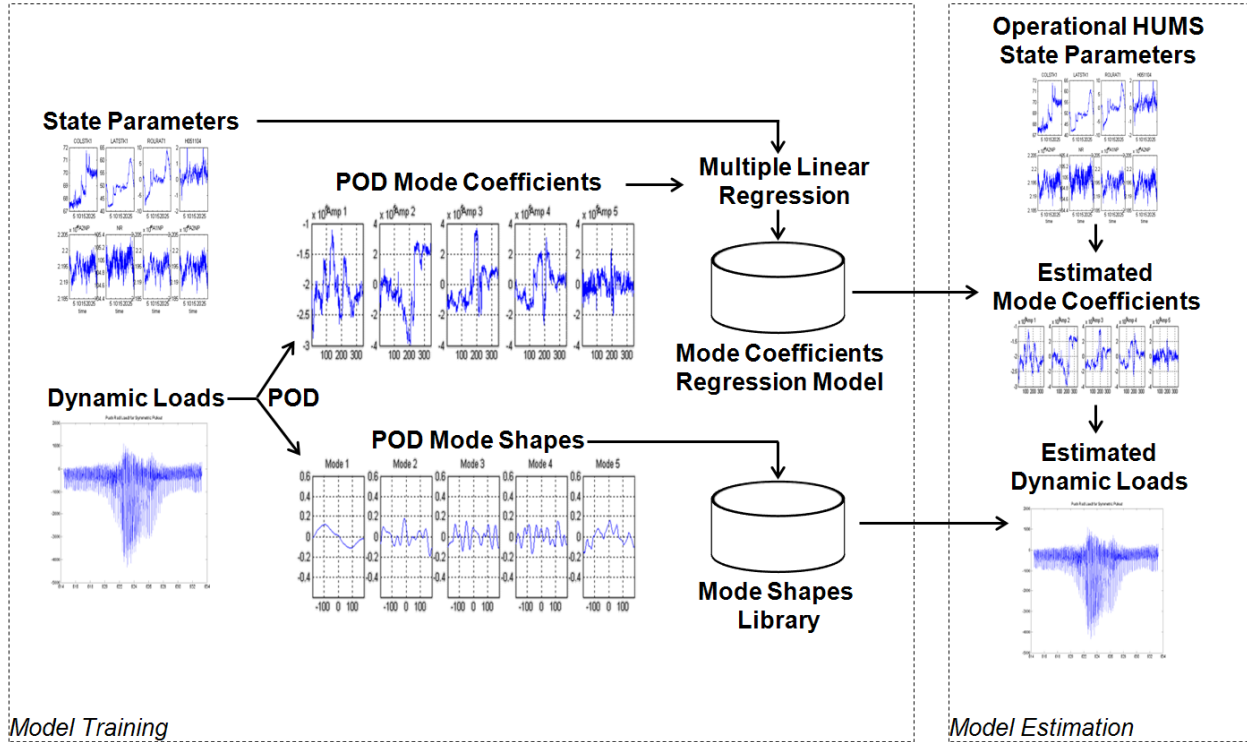
Figure 20. The VML process

5.1.2 Application of VML to CERDEC Flight Test

Two VML models were previously developed from UH-60M FLS test data for each of the two loads measured during the CERDEC flight test. The models were designed to be globally valid and operate on an IVHMS compatible set of parametric input data, which is listed in table 23. These models were demonstrated for the CERDEC aircraft using flight data from June 11, 2013.

Table 23. The VML input parameters

IVHMS Parameters	
NR	PITCHRATE
Outside Air Temperature	ROLLRATE
BAROCORRECTEDALT	YAWRATE
ALTITUDERATE	CYCLICLONGDCU
CAS	CYCLICLATCAL
VERTACCEL	PEDALCALIBRATED
TORQUE	COLLECTIVEDCU
PITCH	STABILATORPOSITION
ROLL	

When demonstrating the models, an issue was found that prevented analysis of data from an entire flight which, upon investigation, was found to be a known problem inherent within the UH-60M. Lateral stick position was found to become invalid many times throughout each flight, both intermittently and constantly. This parameter is important to many VML and CG models, and the invalid data affects how much meaningful model correlation data can be extracted from the CERDEC testing. Examples of the impact of this problem are shown in figure 21, where the time history of both the lateral stick position and the MRSEBL VML amplitude are plotted for the entire flight. Note the pervasiveness of the invalid stick position data that results in the solid red band where the VML model estimate intermittently goes out of range. The root-cause of this data problem remains unknown and there is no workaround available until this root-cause is established and fixed within the UH-60M avionics system that manages digital data bus traffic, which is the IVHMS data source for this parameter.
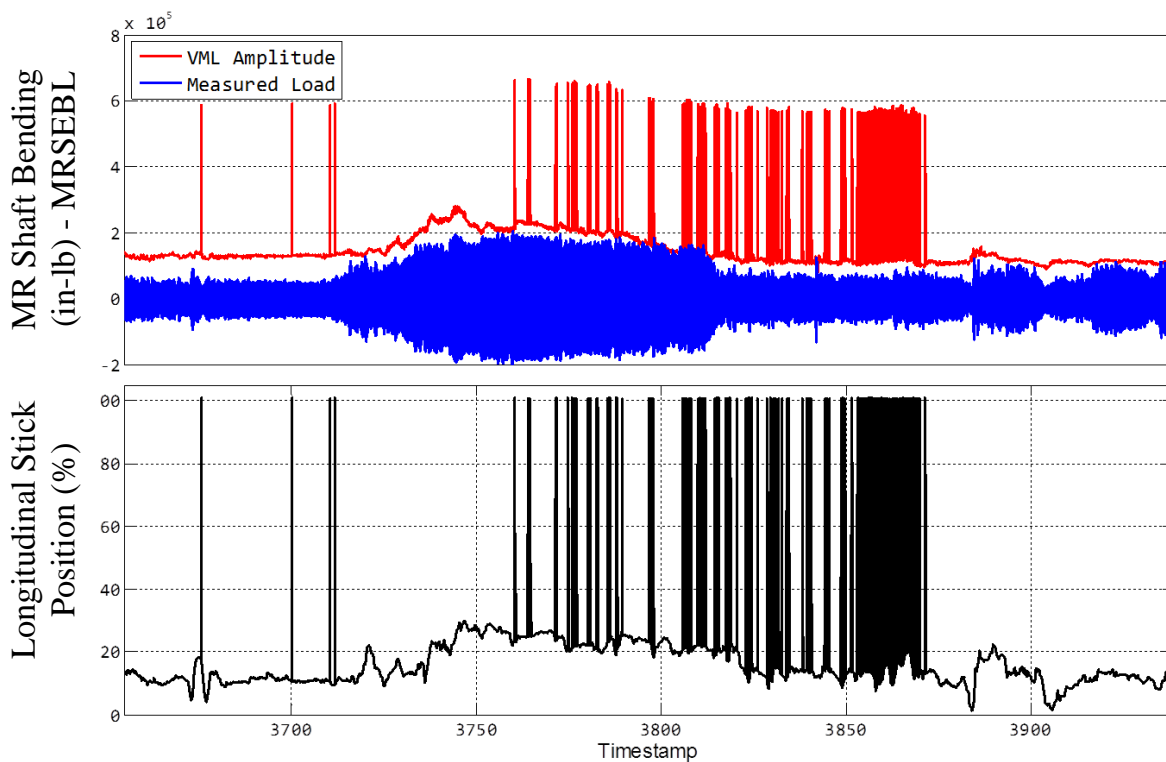
Figure 21. The UH-60M lateral stick position issue and resultant VML estimates

To enable a comparison of VML load performance, a segment of data from the 6/11 flight was selected that had both clean input data and interesting load excursions on both load measurements. This clean segment of flight test data is shown in figure 22. In this figure, the measured load of both the MRSEBL and MRLSS are presented as full-time history load waveforms. Below each direct measured load is the VML estimate of the load amplitude alongside the measured load amplitude.

49
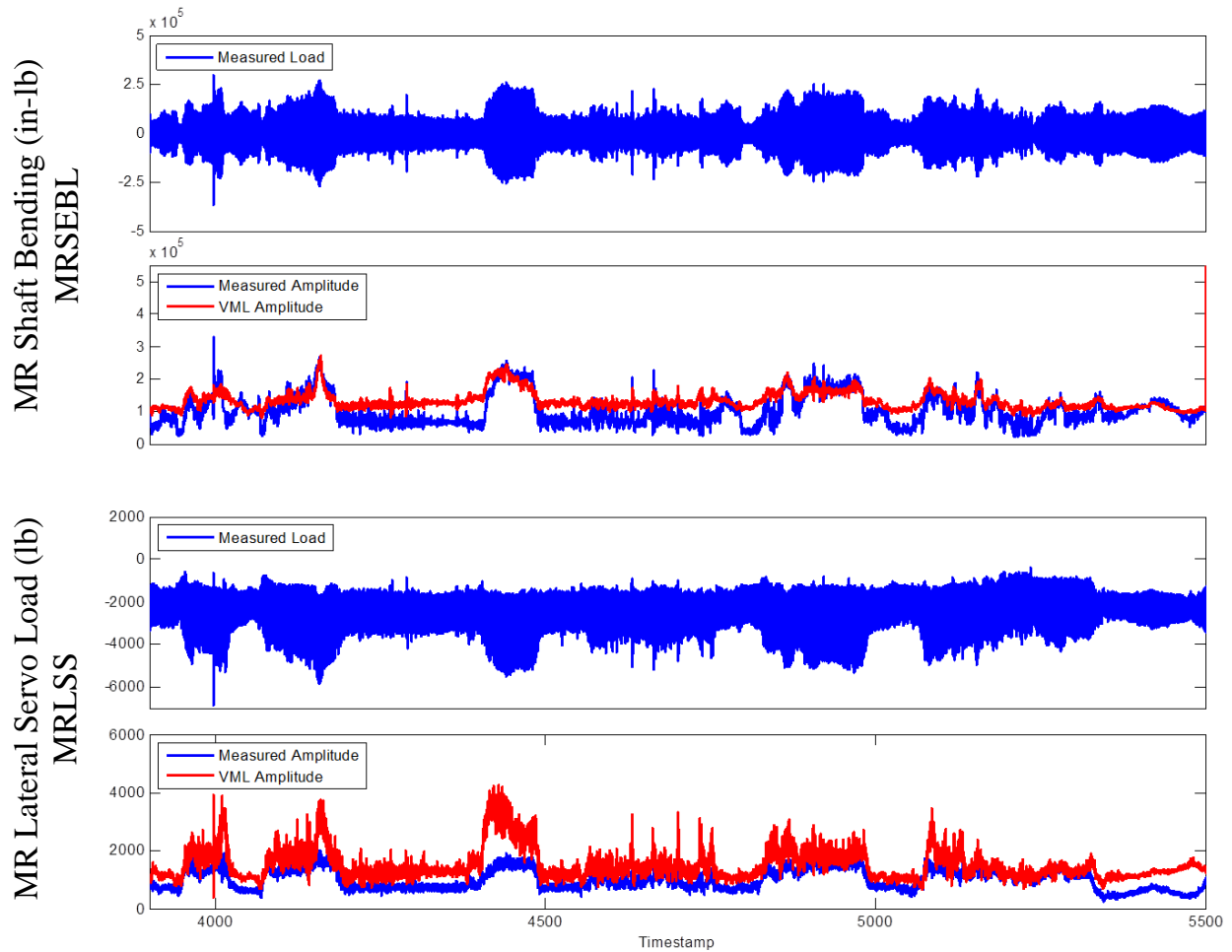
Figure 22. The VML model demonstration data—clean segment

The most important feature of these loads in UBM applications is the vibratory amplitude. A comparison of the VML estimated and measured amplitude is shown in the scatter plots in figures 23 and 24, respectively, for the shaft-bending and servo loads. In these plots, perfect agreement would result in all data being plotted on a 45-degree line. The desired behavior of uncertainty associated with VML loads estimates is for an equal likelihood of over- and under-prediction that statistically cancels out when calculating UBM benefit. As shown in figure 23, the VML estimate of shaft-bending vibratory amplitude agrees well at high loads, but generally over-predicts lower amplitudes. VML servo load estimates are generally over-predicted at higher amplitudes but are more accurate at lower amplitudes, as shown in figure 24. To further evaluate the accuracy of the vibratory amplitude prediction, both the measured and VML predicted loads were amplitude-cycle counted and ranked in a cumulative distribution. Accuracy was then evaluated against the highest amplitude cycles that were counted. This comparison is shown in figure 25. These analyses show different results for each load model. The servo load model does not perform as well as when it was originally developed on UH-60M flight test data, and over-predicts the highest vibratory loads. The shaft-bending model, however, over-predicts in the low-amplitude range but is extremely accurate in the

high-amplitude range. Analysis of the amplitude range in the top 1% of loads shows an accuracy of 97% on vibratory amplitude prediction.
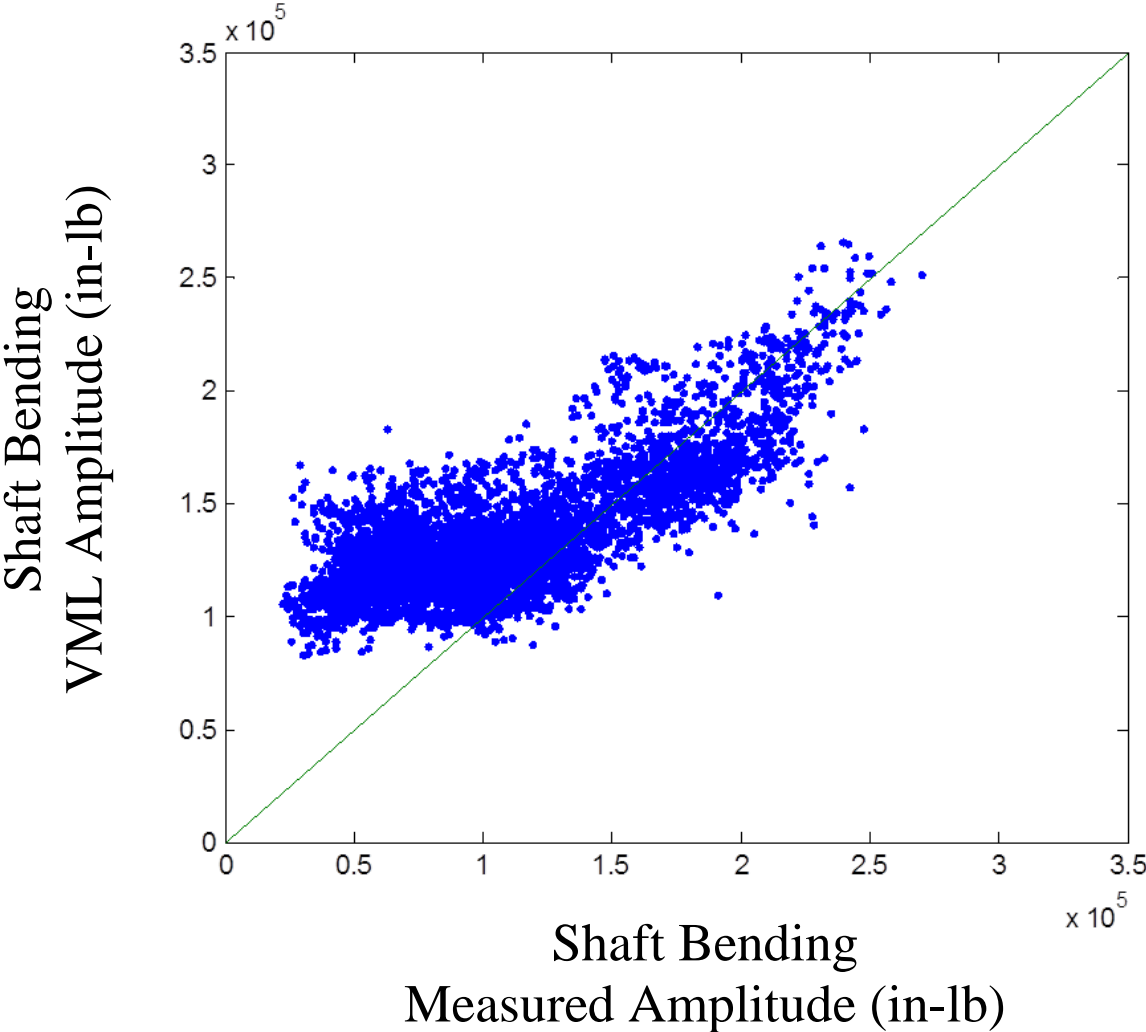
Figure 23. The MRSEBL VML vibratory amplitude correlation
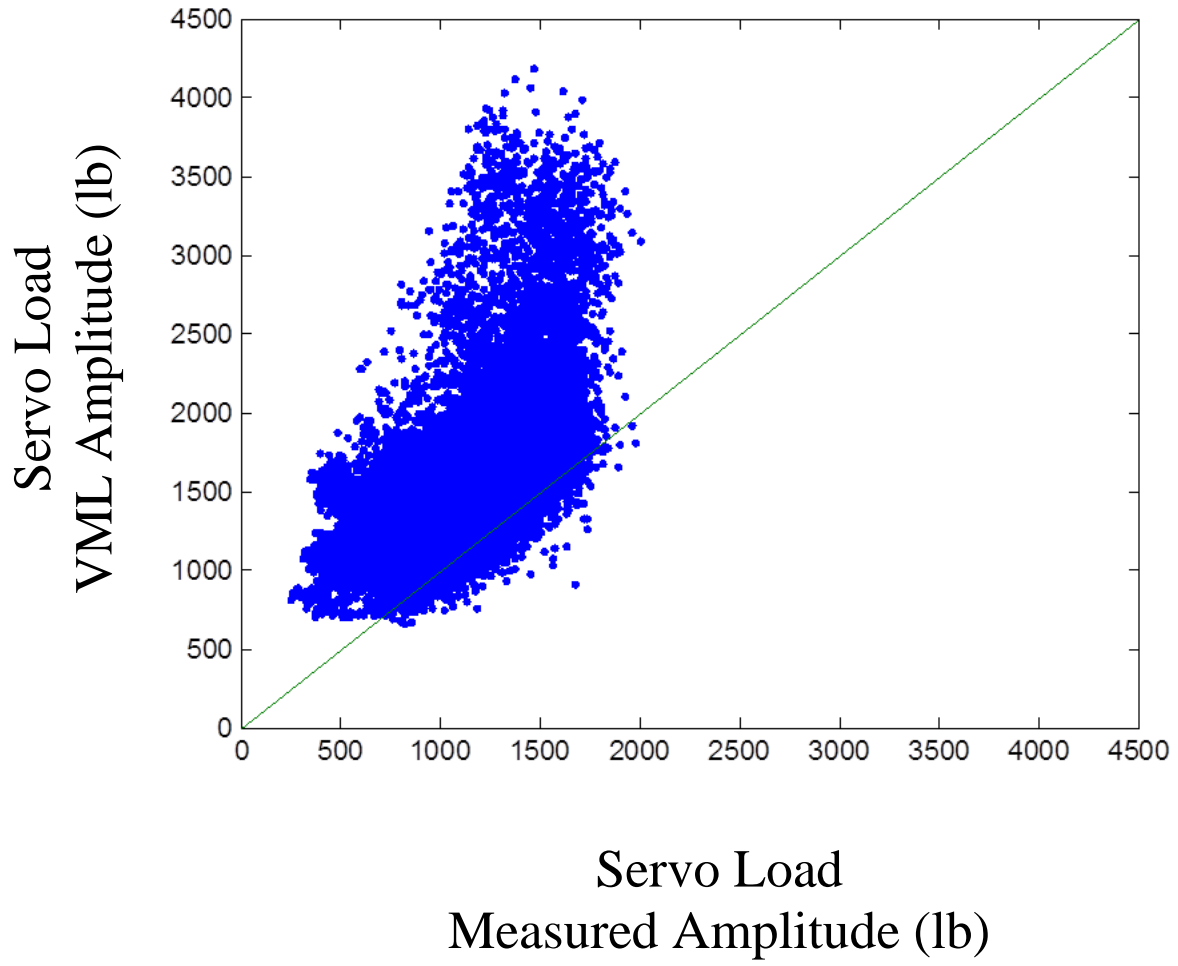
Figure 24. The MRLSS VML vibratory amplitude correlation
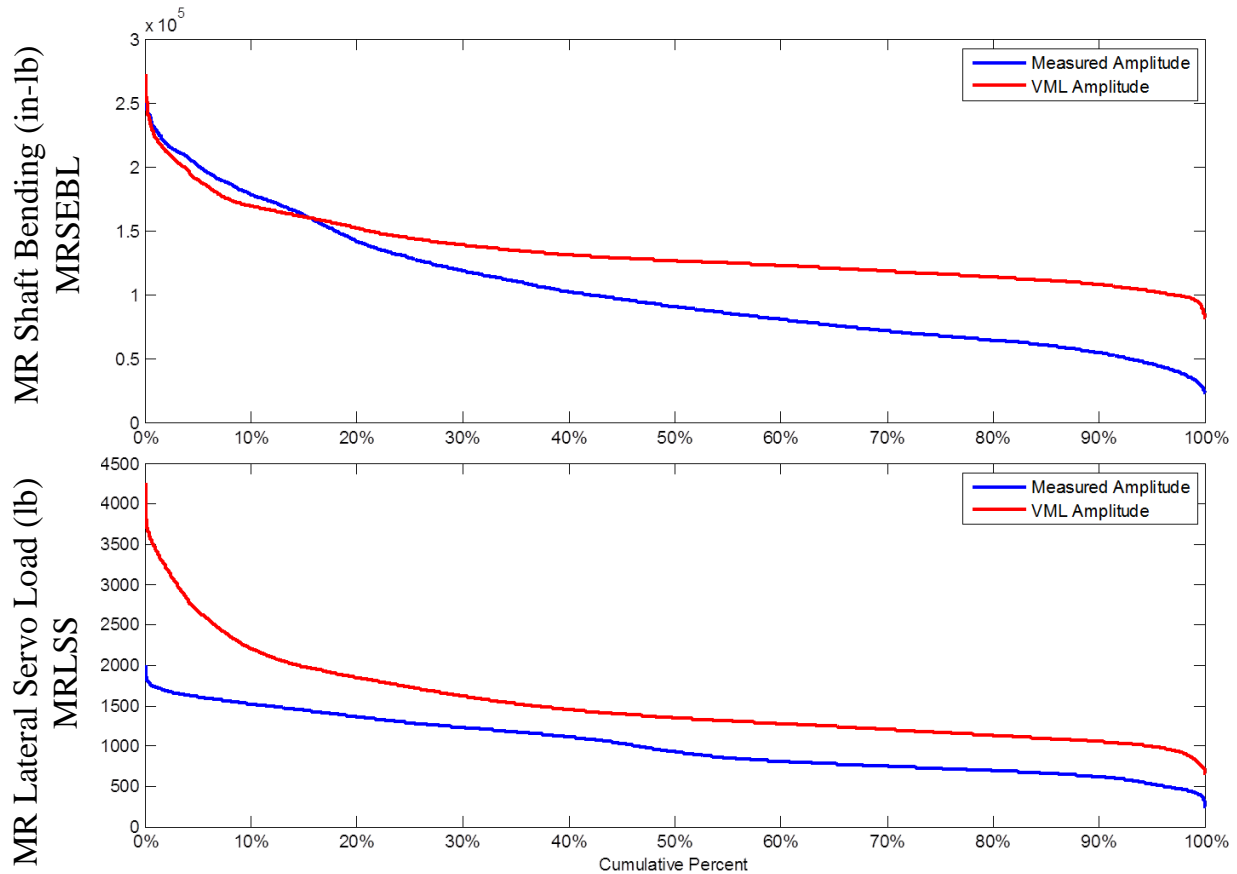
Figure 25. Measured load to VML cycle count comparison

Better results were obtained when demonstrating real-time VML load estimation on the Rotorcraft Aircrew Systems Concepts Airborne Laboratory aircraft, including results for main rotor shaft bending and lateral servo loads [4]. Though the results shown herein are overly conservative, they do show, along with the results documented in reference 4, the potential for load estimation methods, which will require a probabilistic framework to accommodate reasonable model error distributions to achieve UBM benefits. As shown in reference 4, the performance of VML models varies by component load. Model performance is much better for some component loads than others.

The level of accuracy required for models depends on the specifics of the UBM application. For example, excellent prediction of quasi-steady load values may be much more important than accurate prediction of vibratory amplitudes or vice versa for a particular component load and UBM application. Reference 5 summarizes one such UBM fleet analysis case study showing the viability of the use of these VML approaches and one method for accounting for model uncertainty. These errors can be evaluated either globally or focused on loads above a damaging threshold. Though the shaft bending model results shown herein do not predict well in the lower amplitude range, it may not be worth the additional engineering effort to improve the low amplitude prediction if the model can be shown to be accurate when loads are damaging. The servo load model results highlighted herein and in reference 4 show that some component loads are more difficult to predict than others, and may not be as suited for a UBM application until

further model development can be shown to improve the accuracy. In delivery order (DO) 0002, more effort will be expended in achieving VML results appropriate for a specific UBM application and the objective mock credit; whereas in DO 0001, the performance of existing VML models was demonstrated without any effort to refine the models for the CERDEC aircraft configuration.

5.2 GW AND CG ESTIMATION

5.2.1 Background

A unique aspect of GW and CG in fatigue life substantiation is that there is no single worst-case GW for all components and subsystems. Helicopter components may experience higher loads at low GW because of the increased maneuverability and capability of an aircraft, whereas other components may experience higher loads at high GW because of the increased weight. Likewise, variations in CG can affect fatigue life differently for different components. Nevertheless, component life analysis often employs the use of GW/CG prorates based on an assumed future GW usage distribution within broad high/low categories and CG within broad fore/aft categories. The ability to estimate GW and CG from operational HUMS data will enable a range of applications in UBM that can provide both component retirement-time benefits and improved safety. For example, existing usage prorates that depend on assumed GW and CG distributions can be updated to account for actual distributions on a global fleet-wide scale or can be adjusted for sub-fleets or individual aircraft that have different distributions than the rest of the fleet. It is also envisioned that the ability to estimate GW and CG in real time has applications beyond UBM that can enhance operational awareness and improve the safety of flight. There have been a number of accidents throughout the helicopter industry in which the root-cause was the attempt to fly aircraft outside operational limits on GW/CG. To this end, SAC has developed a set of regime-specific models for the UH-60M to predict vehicle GW and CG from HUMS parametric data. Models were developed to operate in level flight, hover IGE, and hover OGE, and were trained on UH-60M production FLS test data. Ultimately, logic will be developed to fuse estimates from these three regimes to provide a seamless time history of GW and CG.

5.2.2 Application of GW Modeling to CERDEC Flight Test

The data quality issues with longitudinal stick position that were discussed in section 5.1.2 and shown in figure 21 severely impact the ability to predict CG in flight as the CG model relies on clean stick position data. Therefore, this section focuses on the demonstration of the GW models on the CERDEC flight test data.

Applying the UH-60M GW models to operational HUMS data requires two checks on the parametric data, which are conducted once per second (i.e., the same rate as parametric data is recorded). First, for the model estimate to be considered valid, the aircraft must be within one of the three valid regimes (i.e., level flight, hover IGE, or hover OGE) within which the models were developed to operate. The result of this check is recorded in a Concept of Operations (CONOPS) parameter, which indicates whether the aircraft is in level flight, hover IGE, or hover OGE. Second, the input data is compared against the domain of the training data to determine if the model is interpolating or extrapolating. A STATUS parameter indicates whether the input data resides within the domain (i.e., interpolation) or outside the domain (i.e., extrapolation). The

STATUS parameter takes on a value of zero when the model is interpolating, and positive integers indicate that the model is extrapolating, with each positive integer indicating more information about the nature of the extrapolation. These parameter checks act as a capture window to restrict the application of the models to the operational space over which the models were developed and validated. Model estimates are considered valid only when CONOPS and STATUS are both zero.

GW models were developed from UH-60M FLS test data, which took place between September 2003 and August 2004 at the Sikorsky flight test facility in West Palm Beach, Florida. These GW models were evaluated against the CERDEC flight test using GW truth data provided for each flight by the CERDEC test team. Truth GW was recorded by CERDEC by weighing the vehicle empty and using a standard weight and balance program to calculate the initial GW for each flight from the known configuration, fuel, and payload weight. Truth GW through time was calculated by HUMS from fuel burn and was stored in the HUMS parametric data. A visual example of the model estimate, STATUS, and CONOPS output parameters over an entire flight (from Flight #2) is shown in figure 26 for the level flight and hover IGE model. In this example, the level flight model outputs are shown as the red curves and the hover IGE model outputs are shown as the blue curves. The GW is shown in the first plot, with the truth GW shown as a light gray curve. For the level flight and hover IGE models, GW output is shown only when the models are valid. The second and third plots from the top show the CONOPS and STATUS output values, respectively, which combine to determine model validity. The last two plots show calibrated airspeed and engine torque, respectively. These figures show how frequently and briefly each of the model capture windows are valid through the flight, and the level of post-processing required when distilling the results into a best estimate of GW.
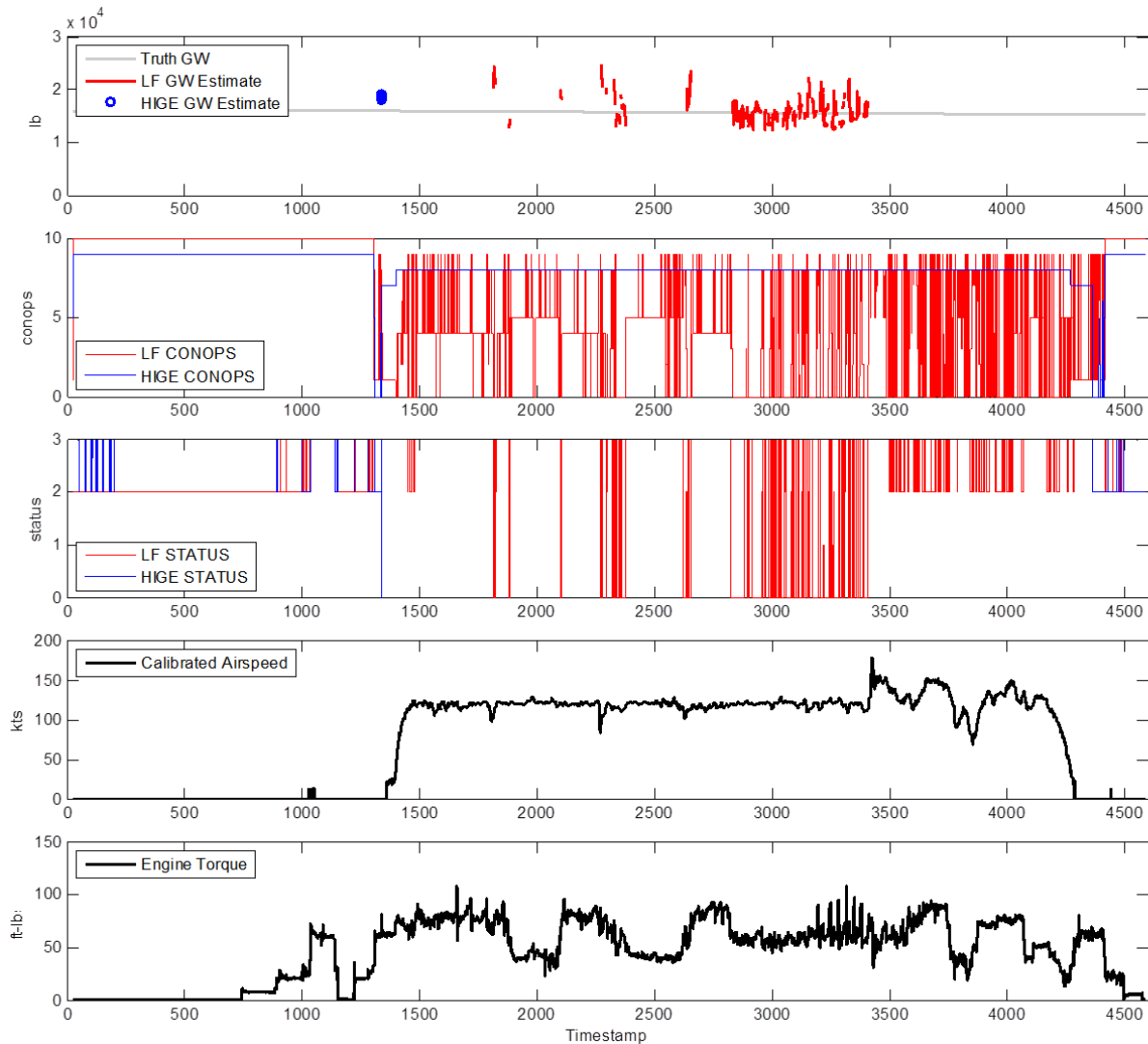
Figure 26. Level flight and hover IGE GW model output across an entire flight

Because the three GW/CG models are designed for specific regimes, valid estimates from each model are available only as frequently as the aircraft is in one of the three regimes. The collection of all GW estimate durations over the CERDEC testing is broken out by percentage from the three target regimes, as shown in figure 27. The level flight model is valid 45% of the flight time, the hover IGE model is valid 4% of flight time, and the hover OGE model is valid 0.35% of flight time. For each regime, there is a smaller portion that corresponds to the frequency of simultaneously being in the target regime and being within the bounds of the training data. For both the level flight model and the hover IGE model, the models were interpolating approximately 12% of the time that they were being called by the CONOPS. This is because the flight test data that were used to train the models only covered a small space within the defined CONOPS. The hover OGE model, however, never interpolated over the entire six flights of CERDEC test data. This was found to be a limitation of the training database for the hover OGE model in that it did not include a broad enough range on density altitude, which is compounded by the fact that all training data were collected in a warm and humid climate. This

56

highlights the need for a more robust set of training data that includes real-world variations in operating environments to transition this technology.

Valid Flight Duration by GW Model
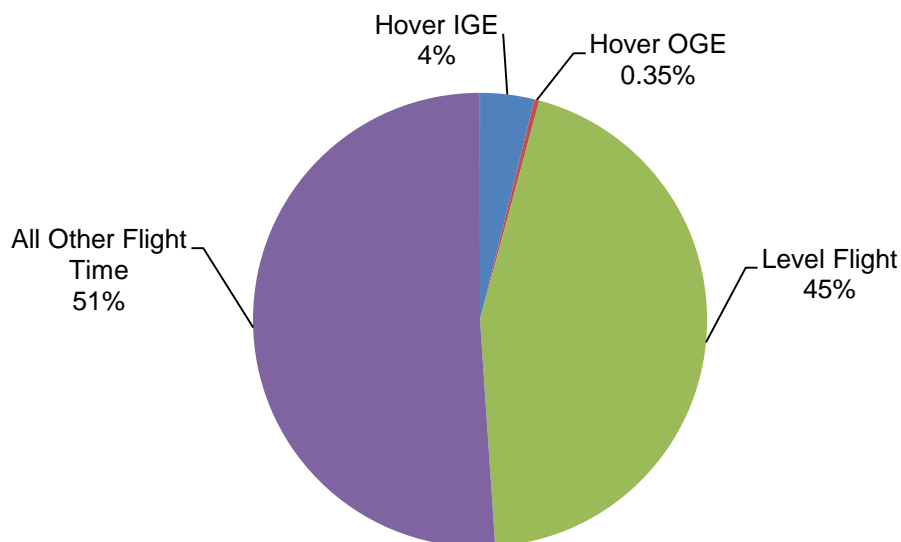
Figure 27. Valid flight time by GW model

To evaluate the capability and potential of GW modeling, the level flight model results were analyzed for prediction accuracy across all valid estimates for all CERDEC flights. The result of this analysis is an error distribution for the level flight model, shown in figure 28. This includes absolute error as large as 50%, mean error of -5%, and root mean square error of 12%, all of which are much higher than that observed on previous blind evaluations of flight test data. Over the course of analyzing these results, it was discovered that the primary root cause of the large modeling errors was unsteady vehicle dynamics during the steady state model captures windows. This phenomenon is due to the use of broad state space assigned to the capture window, derived from RR definitions, which does not sufficiently account for vehicle dynamics. For example, many large errors were spot checked and found to be due to an accelerating or decelerating level flight condition. Figure 29 shows a zoomed-in example from figure 26, which focuses in on one of the largest errors from the level flight model. Here, it is shown that the large error is associated with unsteady airspeed and engine torque. Airspeed rate of change is not currently evaluated by the CONOPS and was not an issue in early model development and evaluation because of the nature of clean steady state FLS test data used to train the models. Based on this analysis, it is hypothesized that increased accuracy could be achieved by defining more sophisticated capture windows that also monitor rate of change of key parameters to ensure GW estimates are calculated for sufficiently steady-state data.

Given the larger-than-expected modeling errors, the evaluation of the model's predictive capability was desired when mapping GW to high/low categories, which is the initial application intended for this technology. A method was previously developed to bin GW into high/mid/low bins with an emphasis on getting high accuracy for high/low bins and treating the middle bin as

unknown. This middle bin can then be mapped to the worst case bin in component analysis, depending on the sensitivity of particular component loads to GW. To perform the analysis, truth GW is mapped to high and low categories and estimates are mapped to high/mid/low categories. Binning accuracy is defined as the probability that the truth GW is in the high bin, given that the model estimate is in the high bin and vice versa. For now, estimates in the middle bin are treated as unknown estimates and are not evaluated for accuracy. The high/low threshold was set to the middle of the GW range from this test, which is 19,000 lb. The width of the middle bin was varied to assess high/low bin accuracy for several width settings. A middle bin width of zero is equivalent to having no middle bin; increasing the middle bin width further separates the high and low bins. This methodology is shown in figure 30. As the middle bin width increases, more estimates are essentially thrown out, meaning the quantity of valid estimates decreases. The results in figure 31 show that, as the middle bin width increases to 2000 lb, the high/low binning accuracy converges to 97% at a cost of approximately 40% of the estimates being thrown away. This analysis demonstrates that there is great potential for GW models to accurately predict the time spent in broad GW usage categories, even if the desired precision in pounds is not yet achieved. The accuracy requirements of the model depend on the specifics of the UBM application. In DO 0002, more effort will be expended in achieving GW/CG results appropriate for a specific UBM application and the objective mock credit.
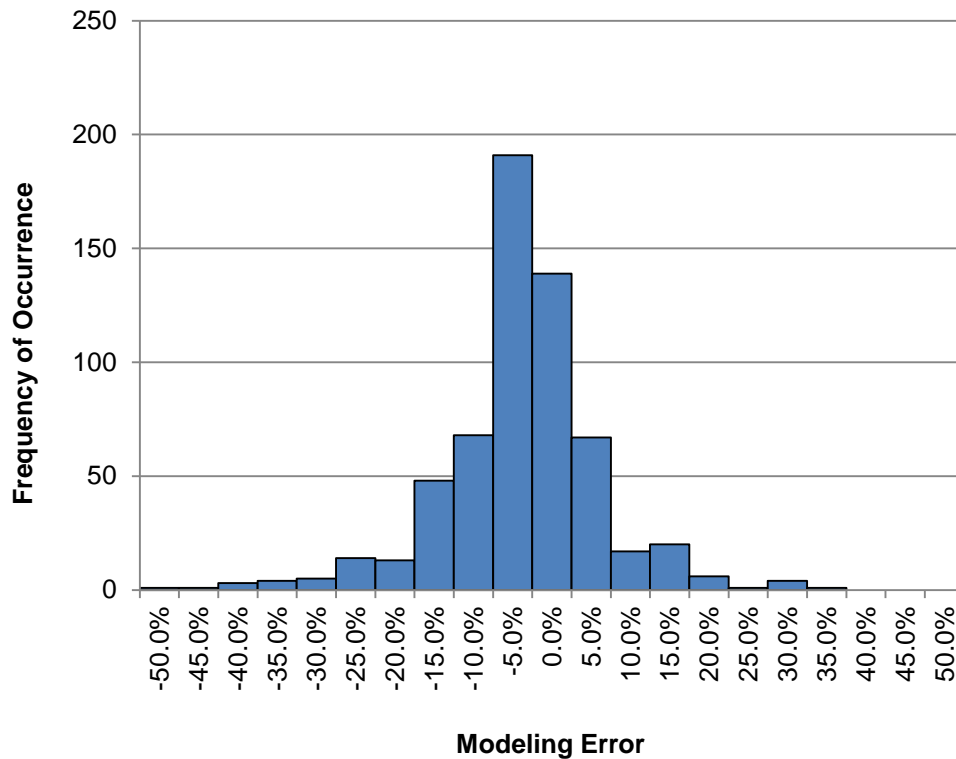
Figure 28. Level flight GW modeling error distribution
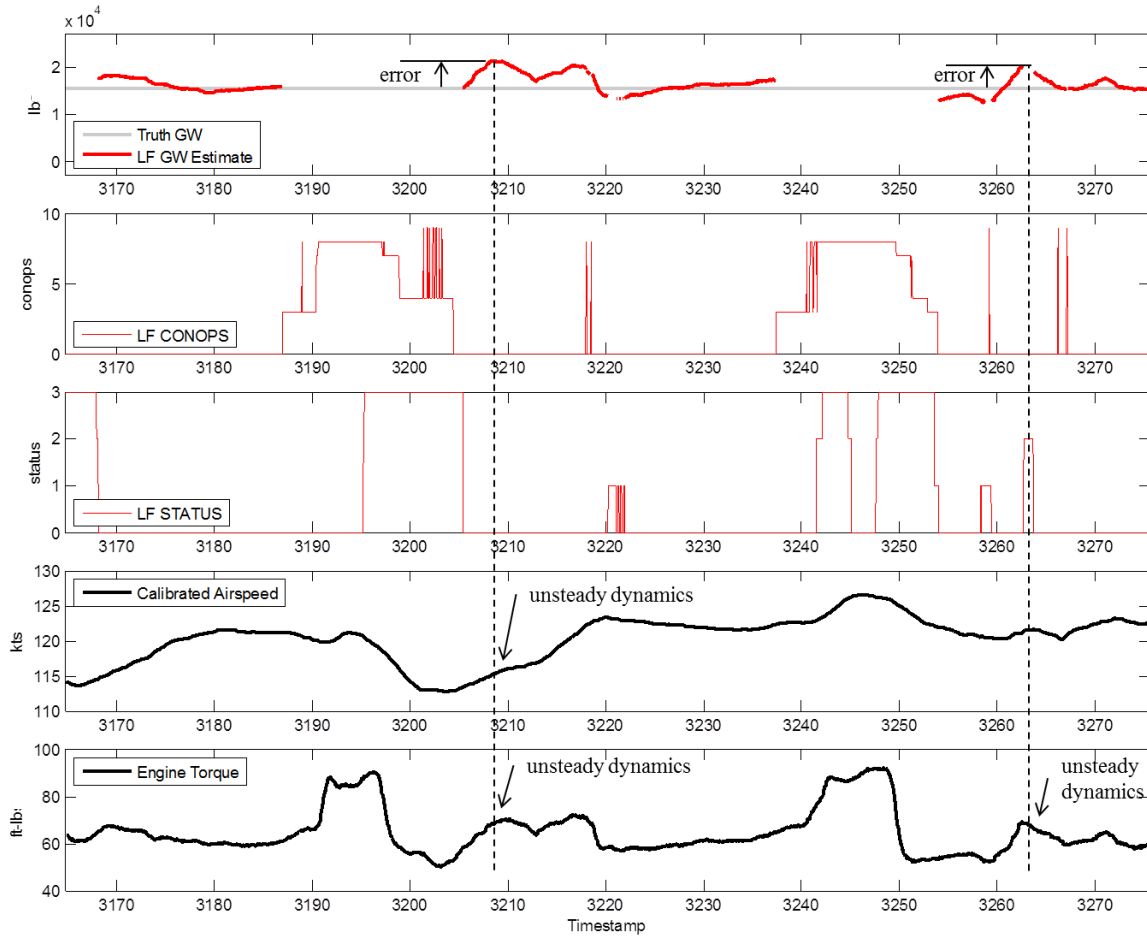
Figure 29. Example of large level flight model error due to vehicle dynamics
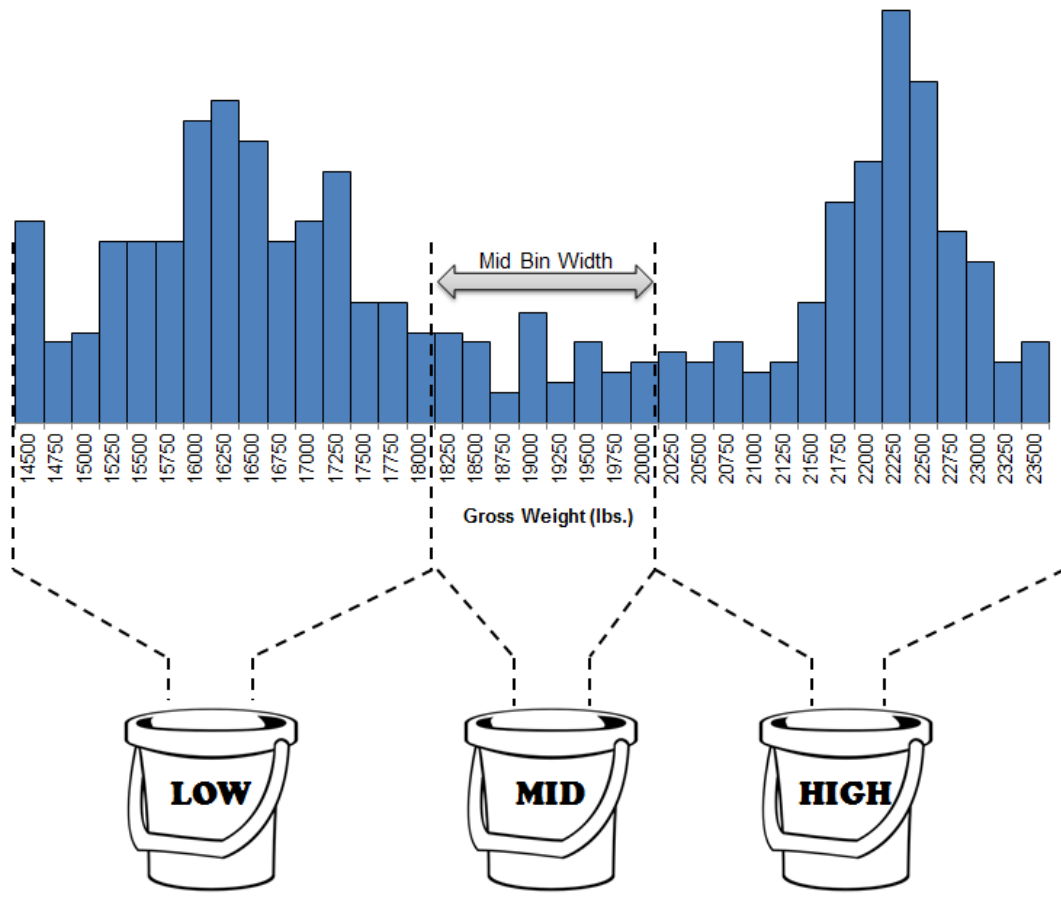
Figure 30. The GW binning methodology
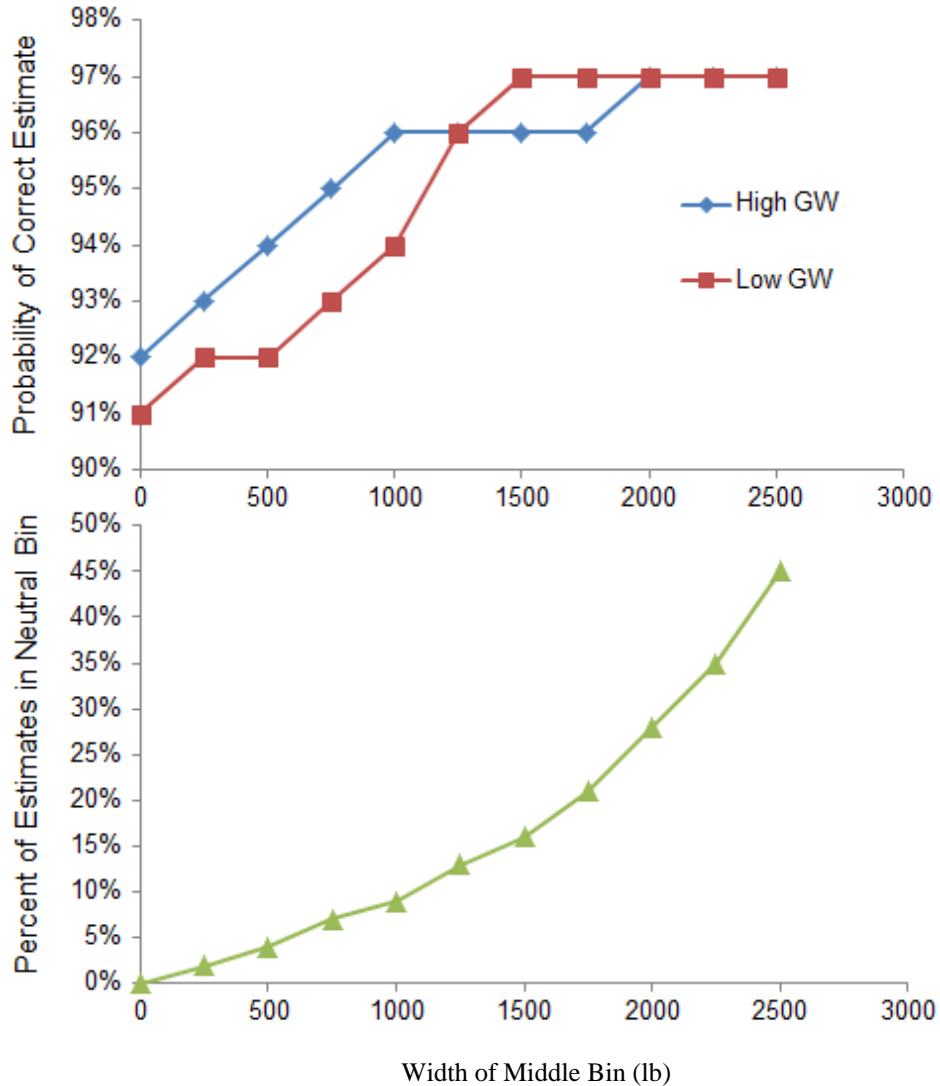
Figure 31. The GW binning accuracy

6. UBM PROCESS REVIEW

6.1 CURRENT FATIGUE SUBSTANTIATION PROCESS

Component fatigue life limits are established by helicopter OEMs using a traditional fatigue methodology based on Miner's rule of cumulative damage to achieve 6–9's reliability. Reliability of 6–9's means that less than 1 part in 1 million will fail within its retirement time. To achieve this level of reliability, conservatism is allocated to each of the three fundamental uncertain quantities that determine the fatigue life of an aircraft component: strength, loads, and usage. The fatigue substantiation process consists of correlating laboratory fatigue test strength data with measured flight test loads and the customer's usage spectrum to produce dynamic component retirement times and inspection intervals that reduce the chance of catastrophic fatigue fracture to an extremely remote possibility. This process is shown in figure 32.
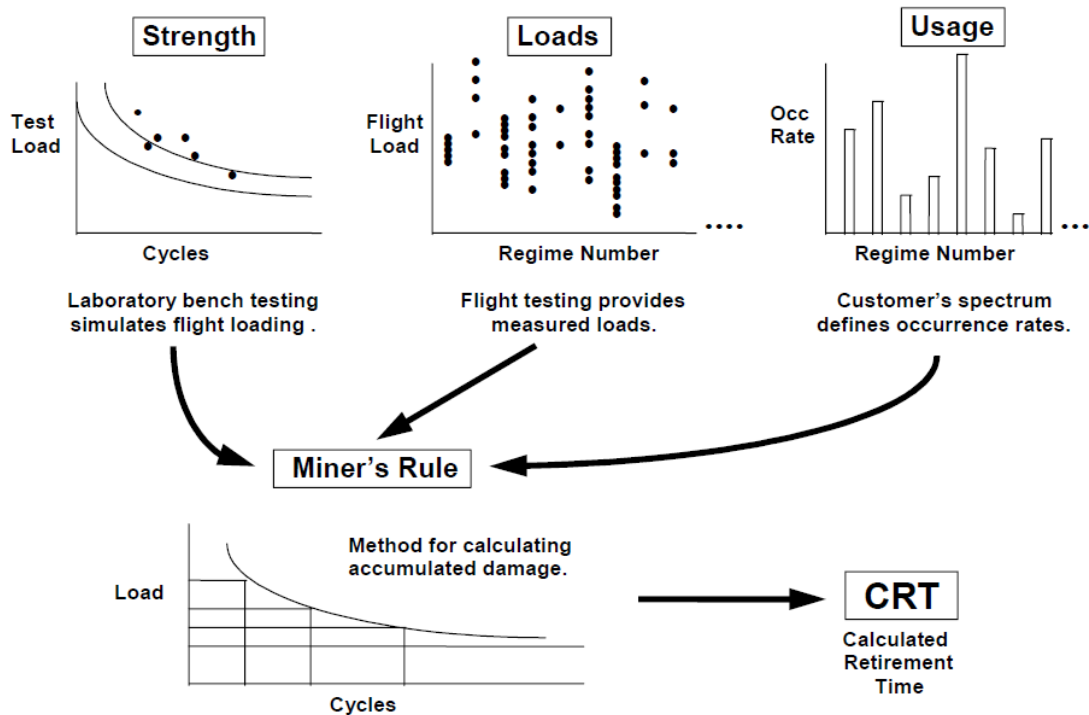
Figure 32. Traditional fatigue substantiation process

6.2 UBM Approaches

UBM is broadly defined as making maintenance decisions, including component retirement, based on structural usage data, including regimes and loads. Usage data can either be measured, derived, or predicted, and can characterize the load history of a component, the maneuver history of an aircraft, or both. The objective of UBM is to collect more data at the aircraft or component level in the customer fleet to reduce the uncertainty in the component fatigue life associated with maneuver history and loads. By reducing uncertainty in the fatigue life, the retirement time of a component can be extended (or reduced) while maintaining 6–9's reliability.

UBM can be implemented either at the fleet level (part number) or the aircraft level (serial number). Fleet level approaches can involve the monitoring of sub-fleets that are characterized by a particular mission, customers that operate in specific environments, or can be applied to the entire customer fleet as a whole. Aircraft level approaches go one level deeper and treat individual aircraft by their unique usage history.

UBM can also be implemented in different ways, which will likely be phased in over time because of different levels of complexity of the end-to-end UBM process. The long-term vision is that the UBM process will include real-time calculation of accumulated fatigue damage using individual aircraft usage and loads data acquired during flight and newer probabilistic safe life methods to determine when components should be retired based on established probabilistic reliability criteria. In this long-term vision, it may not be necessary to account for regimes, but use loads only to calculate fatigue damage. Furthermore, it may be possible to fully automate the calculations without an engineer in the loop.

However, the near-term implementation of UBM must coexist in a symbiotic way with the current fatigue substantiation practices and will require engineer-in-the-loop validation of UBM retirement time credits relative to published retirement times. These credits are backward-looking and are based only on the history of the aircraft on which a particular component was installed during its service life during the time it was installed.

6.3 Proposed Serial Number UBM Credit Process

Ensuring 6–9's reliability using measured usage and loads data requires a new way of calculating the probability of failure that can accommodate measured or estimated data. There has been much research into various probabilistic approaches to fatigue life analysis, much of which can be used to support UBM credit calculations. The objective in a UBM credit calculation that is the focus herein is to determine the retirement-time extension of a part that provides a reliability that is equal to the baseline reliability of a component when it was fielded and maintained according to traditional design CWC-load spectrum methods. The process takes credit for an updated model of uncertainty that is provided by historical measured usage and loads data.

Because a new reliability framework is needed to assess the probability of failure given fleet usage and loads data, it is important to also assess the baseline reliability of the original fielded part using the same framework. This ensures that any resulting extension of component retirement time is solely due to the measured usage and loads data. This process is shown in figure 33, which shows a baseline retirement time versus reliability curve calculated using traditional assumed uncertainties associated with strength, loads, and usage. The baseline reliability is determined by the intersection of the CWC-based retirement time with the baseline retirement time versus reliability curve. When HUMS-based measured usage and loads become available, the retirement time versus reliability curve is updated, which moves the curve to the right (less-aggressive usage and loads than assumed at design) or left (more aggressive). By measuring the percent change in retirement time at the baseline reliability, a retirement time credit can be applied based on the cumulative flight hours of the part at the time of the credit.

An adaptation of this process is proposed whereby, rather than computing the updated retirement time versus reliability curve for every fielded component in a UBM credit application, a usage monitor reliability factor (UMRF) is developed for the specific application using the reliability framework to ensure 6–9's. The UMRF is developed using a probabilistic fatigue modeling tool to understand the amount of conservatism that needs to be applied to usage data to maintain 6–9's reliability. This has the benefit of reducing the computation burden for each credit application and simplifying the approach. This modified process is shown in figure 34.
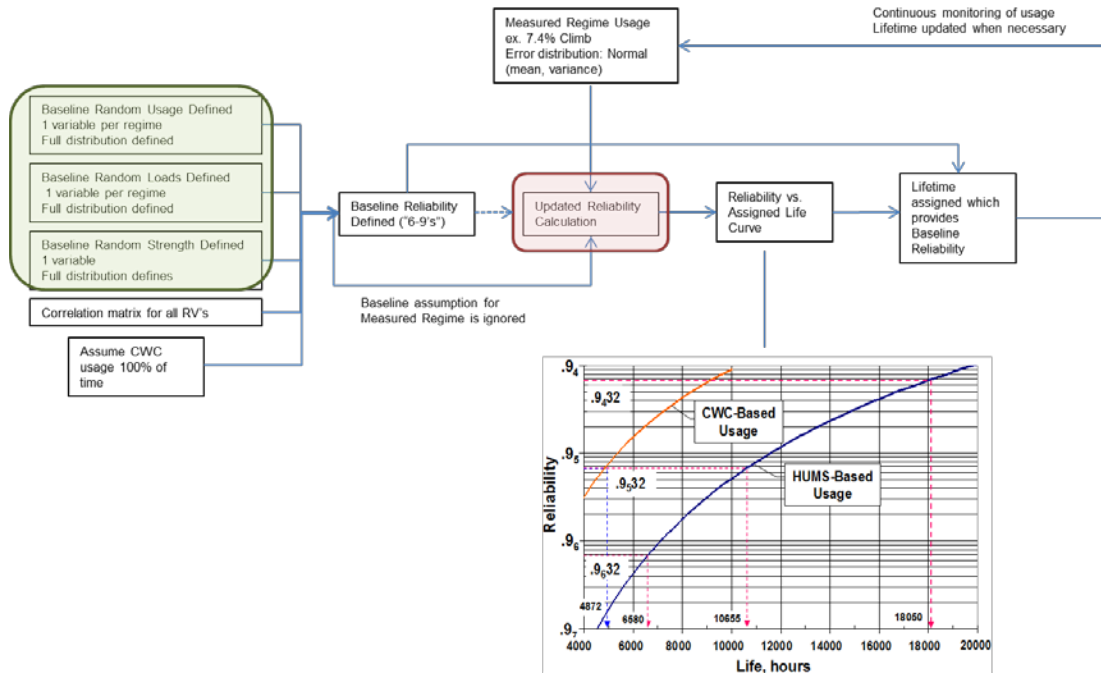
Figure 33. Proposed serial number UBM credit process
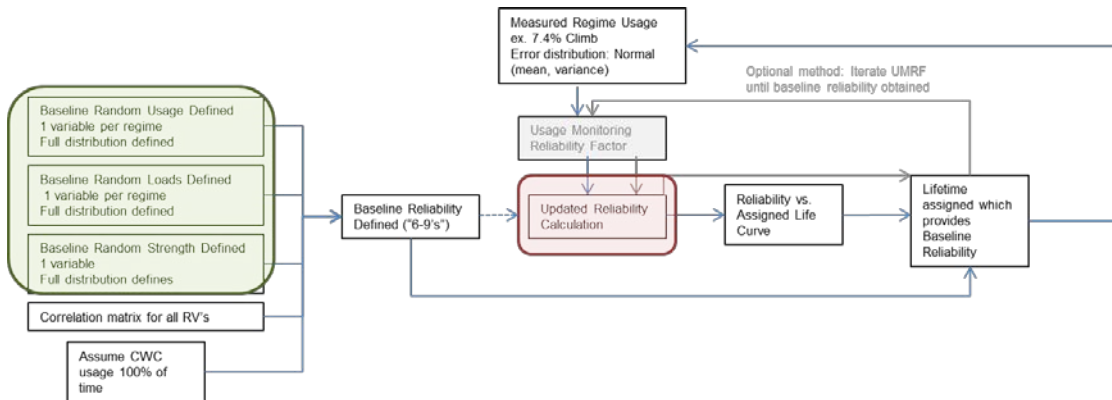
Figure 34. Proposed serial number UBM credit process with reliability factor

6.4 USAGE ERROR DISTRIBUTION THEORY

Though the updated retirement time versus reliability curve is based on measured or estimated usage and loads data, the data may still have some degree of uncertainty associated with it. Probabilistic approaches to fatigue analysis can accommodate these sources of uncertainty. The following methodology was developed to assess the uncertainty associated with a cumulative measurement of maneuver usage. This methodology provides a means to model the uncertainty in a cumulative fleet or tail number usage metric when the usage error distribution is known only at the individual occurrence or instance level. For example, if a particular regime algorithm was known to provide accuracy to within 5% on the duration of an individual occurrence of a regime, this methodology allows that to be used to assess the accuracy, or the error, in a fleet-wide or tail number accumulation of many occurrences. This is important because any

fleet- or tail-number-based retirement-time credit calculation will be concerned only with cumulative usage metrics and their errors, not individual occurrences. A similar approach will be developed for accounting for the uncertainty in loads in the next phase of this program.

Definitions:

$u_a =$ Actual usage, measured in seconds.

$u_m =$ Measured usage, measured in seconds. This could be from RR or the clustering algorithm.

$u_{a,I} =$ Single regime instance of actual usage, measured in seconds.

$u_{m,I} =$ Single regime instance of measured usage, measured in seconds.

$\varepsilon_t =$ Time-based usage measurement error, independent of actual length of regime (e.g., the error in the transition between regimes).

$\varepsilon_\% =$ Percentage-based usage measurement error, which is dependent on time spent in a regime.

$$\varepsilon_\% = \frac{u_a - u_m}{u_m}$$

$\mu =$ Various population means.

$\sigma =$ Various population standard deviations.

$\sigma^2 =$ Various population variances.

$T =$ Total aircraft flight time.

$n =$ Number of instances of a given regime.

Normal distribution: $p(x) = \frac{1}{\sigma\sqrt{2\pi}} e^{-\frac{(x-\mu)^2}{2\sigma^2}}, (-\infty, \infty)$

Coefficient of variation (COV) = μ/σ (non-dimensional).

Case A: Error is dependent only on time spent in regime. $\varepsilon\%$ is the correct error distribution to define and use.

$$u_a = \left(\frac{1}{T}\right) \sum_i \left[u_{m,i} \left(1 + \varepsilon_{\%,i} \right) \right] = \sum_i \frac{u_{m,i}}{T} + \sum_i \frac{u_{m,i}}{T} \cdot \varepsilon_{\%,i} \tag{6}$$

$$P(u_a) = P\left(\sum_i \frac{u_{m,i}}{T} + \sum_i \frac{u_{m,i}}{T} \cdot \varepsilon_{\%,i} \right) \tag{7}$$

If $\varepsilon_\%$ has normal distribution with mean μ and variance σ^2, then the distribution of u_a is also normal, with mean and variance given below:

$$\mu_{ua} = \Sigma_i \frac{u_{m,i}}{T} + \Sigma_i \frac{\mu \cdot u_{m,i}}{T} \tag{8}$$

$$\sigma^2_{ua} = \Sigma_i \left(\frac{u_{m,i}}{T}\right)^2 \sigma^2 \tag{9}$$

If $\varepsilon_\%$ has a non-normal but symmetric distribution, or a non-symmetric distribution with a large n ($n > 200$), then the distribution of u_a is approximately normal with mean and variance given below, where μ and σ^2 are the mean and variance of the non-normal distribution. This result is a form of the central limit theorem.

$$\mu_{ua} = \Sigma_i \frac{u_{m,i}}{T} + \Sigma_i \frac{\mu \cdot u_{m,i}}{T} \tag{10}$$

$$\sigma^2_{ua} = \Sigma_i \left(\frac{u_{m,i}}{T}\right)^2 \sigma^2 \tag{11}$$

If $\varepsilon_\%$ has a non-normal, skewed distribution with a relatively small n, then the central limit theorem does not apply. In this case, an exact distribution for the sum of random variables must be determined. Moment generating function methods are the key tool to be used. However, the exact distribution used must be known before any equations can be derived. The Weibull distributed for random variables does not have a closed form distribution.

Case B: Error is independent of the time spent in a regime. The correct error distribution to define and utilize is ε_t:

$$u_a = \frac{\Sigma_i u_{m,i} + \varepsilon_{t,i}}{T} = \frac{\Sigma_i u_{m,i}}{T} + \left(\frac{1}{T}\right)\Sigma_i \varepsilon_{t,i} \tag{12}$$

$$P(u_a) = P\left(\frac{\Sigma_i u_{m,i}}{T} + \left(\frac{1}{T}\right)\Sigma_i \varepsilon_{t,i}\right) \tag{13}$$

If ε_t has normal distribution with mean μ and variance σ^2, then the distribution of u_a is also normal, with mean and variance given below:

$$\mu_{ua} = \frac{\Sigma_i u_{m,i} + n\mu}{T} \tag{14}$$

$$\sigma^2_{ua} = n\left(\frac{\sigma^2}{T^2}\right) \tag{15}$$

If ε_t has a non-normal but symmetric distribution, or a non-symmetric distribution with a large n ($n > 200$), then the distribution of u_a is approximately normal with mean and variance given

below, where μ and σ^2 are the mean and variance of the non-normal distribution. This result is a form of the central limit theorem:

$$\mu_{ua} = \frac{\sum_i u_{m,i} + n\mu}{T} \tag{16}$$

$$\sigma^2_{ua} = n\left(\frac{\sigma^2}{T^2}\right) \tag{17}$$

If ε_t has a non-normal, skewed distribution with a relatively small n, then the central limit theorem does not apply. In this case, an exact distribution for the sum of random variables must be determined. Moment generating function methods are the key tool to be used. However, the exact distribution used must be known before any equations can be derived. The Weibull distributed for random variables does not have a closed form distribution.

<u>Case C:</u> The actual usage measurement error is not dominated by the time or % based errors, but is a combination of both.

$$u_a = \left(\frac{1}{T}\right)\sum\left(u_{m,i} + \varepsilon_{t,i}\right)\left(1 + \varepsilon_{\%,i}\right) \tag{18}$$

$$P(u_a) = P\left(\left(\frac{1}{T}\right)\sum\left(u_{m,i} + \varepsilon_{t,i}\right)\left(1 + \varepsilon_{\%,i}\right)\right) \tag{19}$$

As per this equation, the distribution of actual usage requires determination of the distribution of the product of random variables. This is an exceedingly complicated problem. For instance, the distribution of the product of two normal random variables with zero mean is given by the product normal distribution:

$$P(xy) = \iint_{-\infty}^{\infty} \frac{1}{\sigma\sqrt{2\pi}} e^{-\frac{x^2}{2\sigma_x^2}} \cdot \frac{1}{\sigma\sqrt{2\pi}} e^{-\frac{y^2}{2\sigma_y^2}} \cdot \delta(xy - u)dxdy \tag{20}$$
$$= \frac{\kappa_0\left(\frac{|u|}{\sigma_x\sigma_y}\right)}{\pi\sigma_x\sigma_y}$$

Where k_0 is the modified Bessel function of the second kind and δ is the delta function.

7. UBM PROCESS DEMONSTRATION

7.1 DESCRIPTION OF FLEET DATA

The Army-AED provided SAC with three sets, or populations, of sample fleet data from operational UH-60M aircraft. Each set of data was collected from a different location, with two overseas locations and one U.S. location. Table 24 shows the quantity of tail numbers and flight hours contained within each set of fleet data. A distribution of fleet hours by tail number for each location is shown in figures 35–37. Across all the data that were provided, there is an average of 60 hours per tail number, a maximum of 229 hours for one tail number, and an average usage

rate of 15 hours per month. These fleet data were used to assess the UH-60M CWC usage rates for climb and turns.

Table 24. The UH-60M fleet data sets

Location	Tail Numbers	Total Rotor Turning Hours
A	29	1,820
B	30	3,228
C	32	568
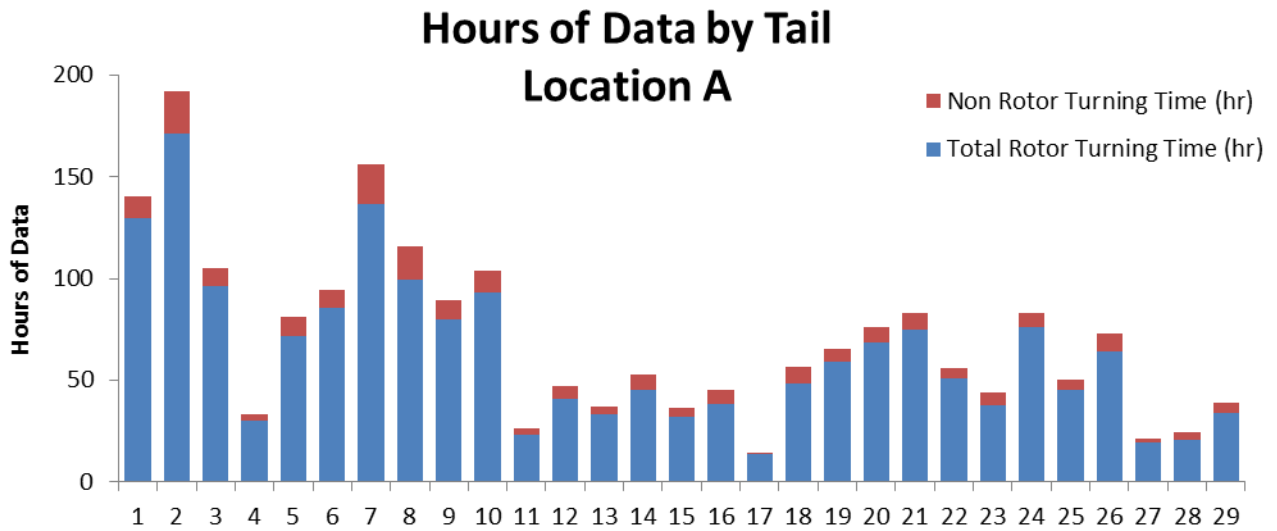
Figure 35. Fleet hours for location A by tail number
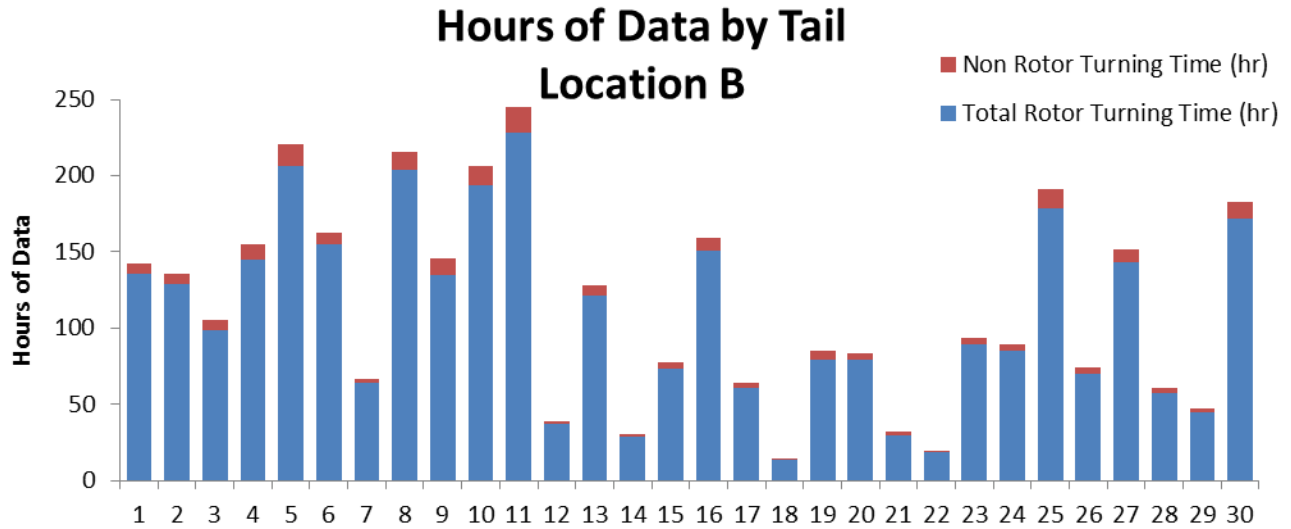
Figure 36. Fleet hours for location B by tail number
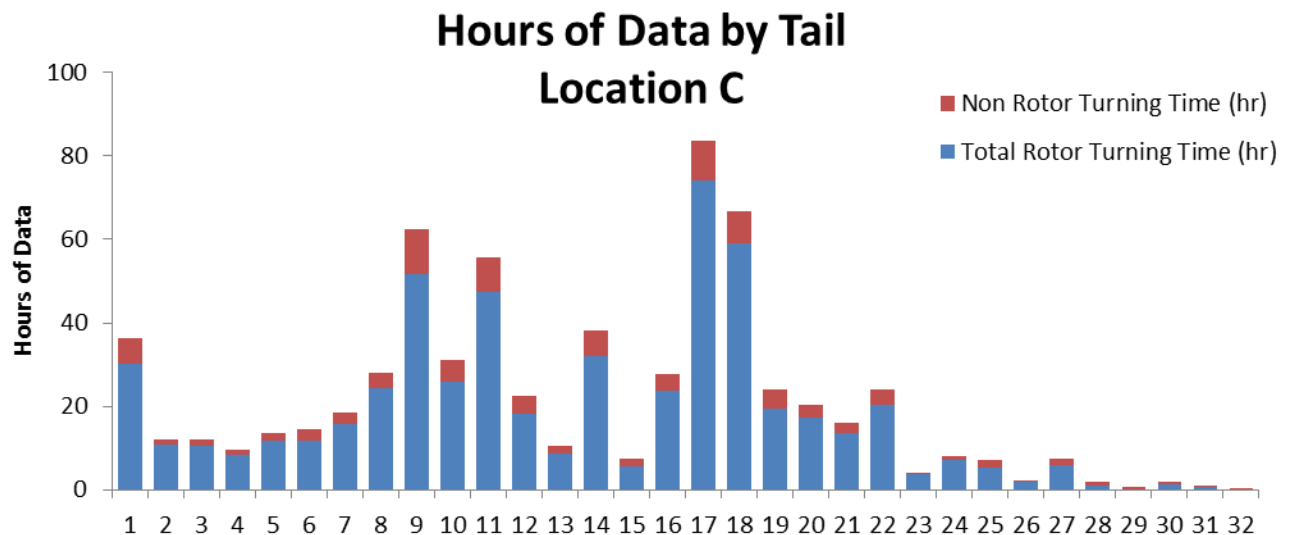
Figure 37. Fleet hours for location C by tail number

7.2 BASELINE REGIME USAGE STATISTICS

RR usage statistics based on current IVHMU onboard algorithms were collected and analyzed first, before applying any clustering methods, to arrive at a baseline set of data for comparison. For the climb and turn regimes, both the worst case usage and mean usage were calculated from the fleet data for each location. Duration of time in both climbs and turns were calculated as one usage statistic relevant to both steady (climb) and transient (turn) regimes. For the turn regime, occurrences were counted and related to the CWC turn entry and recovery regimes. The percent time associated with entry and recovery was added to the steady portion for purposes of comparison against the cluster results. Baseline usage duration statistics for both climbs and

turns are shown in table 25, and the occurrence statistics for turns is shown in table 26. Fleet usage statistics that violate the CWC usage are highlighted in red.

The most notable observation is that the worst case 30-degree turn occurrences for location C are more than double the CWC usage (see table 26). Also, the degree of exceedance of the occurrences is much worse than the associated duration statistics for turns. This is consistent with a known tendency of the current RR method to over-count occurrences and undercount duration. Also note that the usage statistics are much lower than CWC for the more damaging turn regimes having higher AOB.

Table 25. Baseline duration usage statistics for climb and turns

	CWC	Location A		Location B		Location C	
CWC Regime	%	Worst Case	Mean	Worst Case	Mean	Worst Case	Mean
CLIMB	4.20%	6.320%	4.090%	3.299%	2.208%	5.684%	3.716%
TURN 30 L	4.17%	3.518%	2.498%	2.923%	1.139%	5.953%	2.782%
TURN 30 R	4.17%	4.466%	2.512%	3.407%	1.101%	4.206%	2.089%
TURN 45 L	0.71%	0.378%	0.138%	0.120%	0.034%	0.205%	0.038%
TURN 45 R	0.71%	0.286%	0.117%	0.113%	0.025%	0.160%	0.036%
TURN 60 L	0.15%	0.024%	0.003%	0.005%	0.001%	0.009%	0.001%
TURN 60 R	0.15%	0.009%	0.001%	0.012%	0.001%	0.001%	0.000%

Table 26. Baseline occurrence statistics for turns

	CWC	Location A		Location B		Location C	
CWC Regime	Occ/100H	Worst Case	Mean	Worst Case	Mean	Worst Case	Mean
TURN 30 L	750	1248.3	850.8	957.8	435.6	2047.0	1045.4
TURN 30 R	750	1417.8	831.5	890.5	410.6	1827.7	865.3
TURN 45 L	170	156.2	51.8	51.0	15.3	151.6	27.5
TURN 45 R	170	81.7	37.3	35.4	9.8	94.4	22.4
TURN 60 L	77	12.2	2.1	7.5	0.9	25.4	1.1
TURN 60 R	77	4.7	0.7	3.3	0.4	11.6	0.5

7.3 CLUSTERING REGIME USAGE STATISTICS

The regime clusters developed in section 4.3 were processed on the Army fleet data using the hierarchical approach discussed in section 4.1. The fleet usage statistics after applying the cluster definitions are shown in table 27 for steady state climb and turn duration statistics and in table 28 for turn occurrence statistics. As anticipated, the turn duration statistics all increased while the turn occurrence statistics all decreased, or stayed the same in a few cases, as the result of

clustering. The largest reduction in occurrences was seen for 30-degree turns, because these regimes have the greatest opportunity for false positives during all higher AOB turns. Even after these reductions, however, the CWC usage for 30-degree turns is violated by the worst case tail number by both duration and counts in both locations A and C. Though the baseline results did not indicate any CWC violations for 45- and 60-degree turns, the clustering results show that locations A and C have several CWC duration violations by their respective worst case tail number.

For climb, however, the duration statistics decreased, which was not expected. This was a result of the hierarchical approach for processing many clusters simultaneously. The clustering process for turns was applied ahead of the clustering process for climb, and many climb indications that were originally part of a turn sequence were removed from the results. Without clustering turns ahead of climb, the climb regime usage would be artificially high because of the prevalence of climb indications during non-climbing turns. By processing the more critical turn regimes ahead of climb, the hierarchical process gives the turn a higher priority in clustering climb occurrences, which has the effect of taking these occurrences away from the climb regime.

To understand how the clustering algorithm performs on real-world fleet data relative to the baseline RR approach, a highly complex series of maneuvers was found within the fleet data. Within the sequence evaluated, three 45-degree turns, one 60-degree turn, and one severe pullout were flown within approximately 100 seconds. The roll angle from this maneuver sequence is shown in figure 38 with the baseline RR algorithm classifications overlaid. Figure 39 shows the same maneuver sequence classifications provided by the clustering approach, with the key transient maneuver classification labels enlarged and highlighted for readability. The non-highlighted regimes identified in this sequence are all either steady state level flight or partial power descent. This provides a visual example of how significantly improved the clustering approach is relative to the baseline RR approach at accurately detecting turns and pullouts even in a complex series of tightly packed maneuvers. The clustering results for this extended sequence of complex set of maneuvers agrees well with how a subject matter expert would classify it.

Table 27. Clustering duration usage statistics for climb and turns

	CWC	Location A		Location B		Location C	
CWC Regime	%	Worst Case	Mean	Worst Case	Mean	Worst Case	Mean
CLIMB	4.20%	6.26%	3.85%	2.87%	2.09%	5.44%	3.44%
TURN 30 L	4.17%	4.43%	3.19%	3.57%	1.49%	8.42%	4.02%
TURN 30 R	4.17%	5.63%	3.22%	4.42%	1.44%	5.81%	3.16%
TURN 45 L	0.71%	0.99%	0.35%	0.31%	0.09%	0.82%	0.14%
TURN 45 R	0.71%	0.66%	0.28%	0.21%	0.06%	0.68%	0.13%
TURN 60 L	0.15%	0.13%	0.02%	0.09%	0.01%	0.18%	0.01%
TURN 60 R	0.15%	0.03%	0.00%	0.02%	0.00%	0.05%	0.00%

Table 28. Clustering occurrence statistics for turns

CWC Regime	CWC Occ/100H	Location A Worst Case	Mean	Location B Worst Case	Mean	Location C Worst Case	Mean
TURN 30 L	750	888.4	623.8	651.0	368.6	1731.8	830.9
TURN 30 R	750	1000.5	629.0	673.5	347.4	1266.3	685.1
TURN 45 L	170	129.4	43.0	48.3	13.7	151.6	26.1
TURN 45 R	170	75.0	33.1	24.2	8.6	94.4	20.9
TURN 60 L	77	9.8	2.1	7.5	0.9	25.4	1.1
TURN 60 R	77	4.7	0.7	3.3	0.4	11.6	0.5
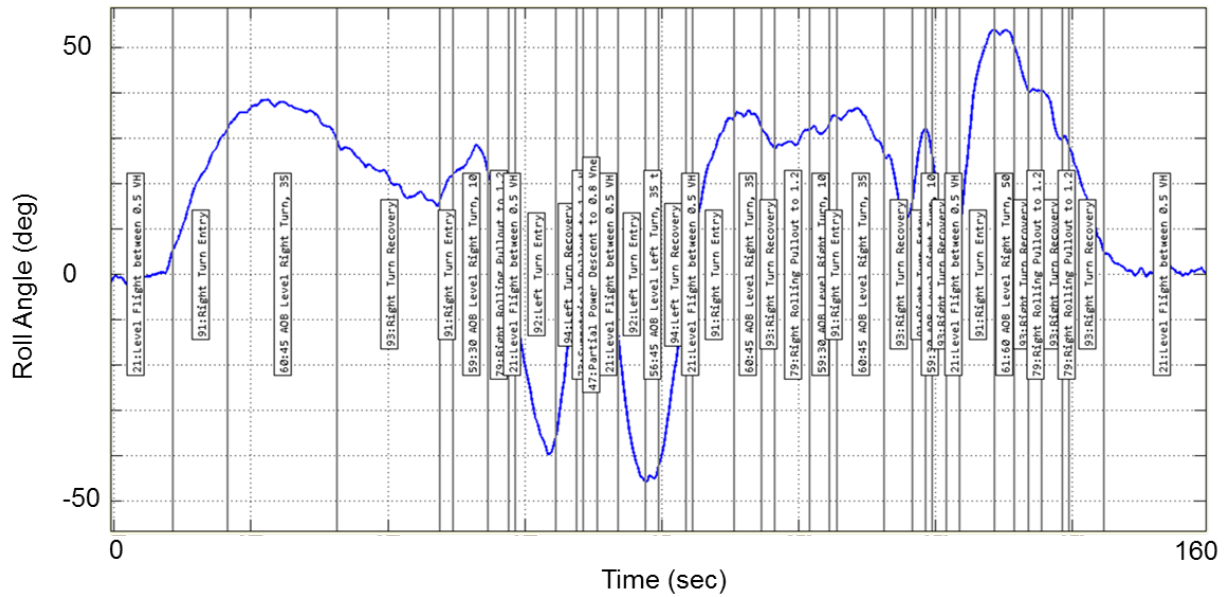
Figure 38. Baseline RR output during complex maneuver sequence
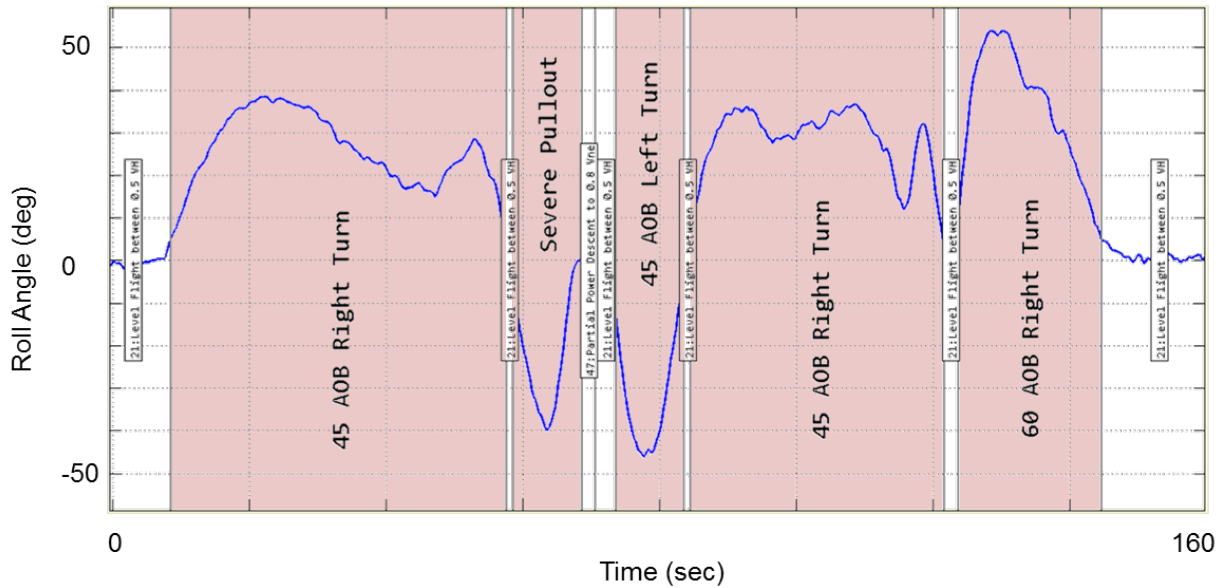
Figure 39. RR clustering output during complex maneuver sequence

7.4 UBM BENEFIT DEMONSTRATION

The largest potential UBM benefit was for location B, which also had the most flight hours evaluated in this study. Occurrence statistics for 45-degree left turns were evaluated for each tail number in location B, as shown in figure 40. It was found for all locations, but highlighted here, that the worst case tail number is often among the group with the lowest flight hours within the population. For this example, the worst case turn occurrences statistic of 48.3 per 100 flight hours was from an aircraft with less than 50 hours of flight history. When considering the two aircraft with the most flight hours, indicated as tail numbers B5 and B11, the occurrence statistics were less than half that of the worst case. This highlights the need for establishing flight-hour minimums when evaluating aircraft usage history, which may be dependent on the regime being studied. For regimes that occur relatively frequently or as part of normal usage, such as 30-degree turns, the minimum flight hours may be much lower than for regimes that rarely occur, such as severe pullouts and 60-degree turns. For this sample benefit analysis, a flight-hour minimum of 50 hours was imposed. Using the worst-case turn results from location B for all aircraft with more than 50 hours, a set of location-specific CWC adjustment factors were developed and incorporated into the retirement-time analysis for the UH-60M main gearbox housing as a representative example. A retirement-time benefit factor of 2.7 was achieved by adopting the sub-fleet usage history for location B into the CWC. This factor implies that the CRT of the main gearbox housing can increase by a factor of 2.7 if a new CRT were developed for the sub-fleet at location B, assuming that the available data is representative of a statistically significant population and it was known that usage data would not vary significantly for this location.

73
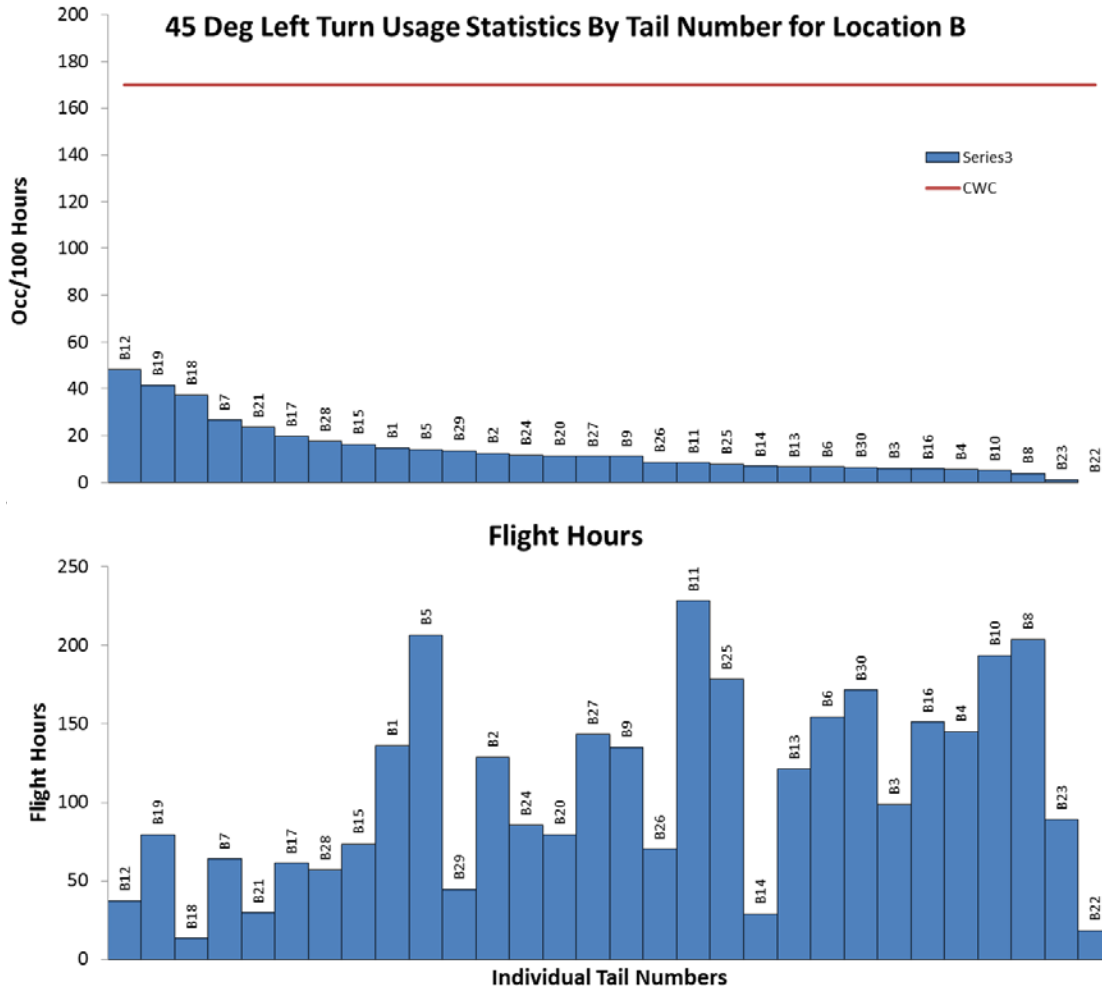
Figure 40. 45-degree left turn occurrences for location B

7.5 COMPARISON TO ARMY FLEET USAGE ANALYSIS

The Army-AED provided SAC with a final report documenting a CWC usage study [6] on the same set of fleet data that was described in section 7.1. This report documented a methodology to mine parametric fleet data, calculate regime usage statistics, and generate an updated CWC usage spectrum based on the fleet data. A comparison of some results from the AED report to results generated independently by SAC is presented in this section. These comparisons were focused on climb and turn flight regimes only, and were limited to the subset of fleet data from location B, which had the greatest proportion of total flight hours within the fleet dataset.

The first simple comparison is on the total flight hours from location B, which is identified as outside contiguous U.S. 1 in the AED report. For the UH-60, the CWC usage spectrum includes ground taxi conditions, which means that the accumulation of flight hours should include ground time with rotors turning. Both SAC and AED recognized this in the definition of flight hours. However, the actual count of flight hours did not precisely agree. SAC counted 3,228 "Rotor Turning Hours" using the duration metrics within RR output data for all regimes with the exception of "1:Power on Aircraft, Rotors Not Turning." The AED report documented that there

74

were 3367 flight hours for the same location, but did not describe the method of counting. Therefore, a difference in methodology resulted in an approximately 4%, or 139 hours, difference in calculating flight hours alone.

For the climb and turn regimes, the AED report did not provide tabulated results for average usage for each location, however it did provide mean plus 2-sigma updated CWC spectrum for each location. Following the same mean plus 2-sigma methodology for the climb and turn regimes, SAC generated results that can be directly compared to the tabulated results in the AED report. These results are shown in table 29. For the SAC results, both the baseline RR results and the RR with clustering results are provided for comparison of before and after clustering. Because the AED regime algorithms and thresholds were modeled after the existing Goodrich onboard RR algorithms, the baseline RR should be more aligned with the AED results.

Several differences in the usage results were observed. For the climb regime, the AED result was 30% higher than both the SAC baseline and clustering results. SAC could not investigate this discrepancy because of the limited details of how regimes were classified by AED. For the turn regimes, even greater differences of up to 50% were seen for the 30-degree turns for both the baseline and clustering approach, with the AED result showing a higher usage rate. The AED and SAC baseline RR results agreed fairly well for the 45- and 60-degree turns, whereas the AED results have usage rates 25–50% less than the SAC RR clustering results.

The reason for the discrepancies seen in the turn results is understood to be a function of how percent time within turns is counted. The AED report shows a sample of regime definitions that defines a 30-degree turn to be when the roll attitude is between 10 and 35 degrees. Using this definition, any 45- and 60-degree turn would accumulate time within the 30-degree regime during the portion of time spent achieving and recovering from the target roll attitude. So if a 60-degree turn is initiated and completed within 20 seconds, but only 10 seconds were actually spent within the 60-degree roll angle band, then AED accumulates only 10 seconds into the 60-degree turn regime and the other 20 seconds into the 45- and 30-degree turn regimes. The RR algorithms onboard the IVHMS classify entire turns by the maximum roll angle, so the 20-second turn that achieves a maximum roll angle of 60 degrees is mapped to the 60-degree turn regime for the entirety of the 20-second maneuver, which is a conservative approach for fatigue damage calculation. The clustering approach uses the same methodology to define a complete turn and goes further to ensure that the complete turns are indeed counted as a single turn and mapped to the correct AOB. The SAC approach of defining a turn is consistent with how maneuver loads are acquired and mapped to the CWC because a 60-degree entry and recovery by definition includes time spent in the lower AOB bands. This discrepancy in the AED and SAC methodology appears to both explain why AED is counting more time in the 30-degree turn regimes and less time in the 45- and 60-degree turn regimes than the SAC RR clustering results.

Because the SAC methodology was developed with the intention of getting both accurate duration and occurrence statistics, the occurrences of turn entry and recovery regimes are derived from the occurrences of the recognized turns themselves. The AED results do not contain entry and recovery occurrences for comparison. The interesting observation in the SAC results, however, is the significant reduction in 30-degree turn occurrences after implementing clustering.

These results indicate that subtle differences in the implementation details of the RR algorithms can generate significantly different bottom line results. For fatigue analysis applications that are sensitive to the occurrence rates of banked turns, the various approaches can yield results that differ by up to 50% in assumed damage rates, and therefore generate different results for remaining useful life. It is recommended that these discrepancies be investigated further and reconciled between SAC and AED. However, it should be noted that both approaches are valid for determining usage as long as the methods used are well-documented and serve as the basis for calculating reliability factors to ensure safety.

Table 29. The SAC-AED comparison of CWC usage results for location B

Regime	CWC Usage	AED "μ+2σ" CWC	SAC Baseline RR "μ+2σ" CWC	SAC RR with Clustering "μ+2σ" CWC
CLIMB	4.2%	4.17%	2.99%	2.81%
TURN 30 L*	4.17%	3.770%	1.970%	2.480%
TURN 30 R*	4.17%	3.880%	2.117%	2.726%
TURN 45 L*	0.71%	0.100%	0.093%	0.235%
TURN 45 R*	0.71%	0.070%	0.073%	0.144%
TURN 60 L*	0.15%	0.010%	0.003%	0.039%
TURN 60 R*	0.15%	0.005%	0.005%	0.011%
E&R TURN 30 L	750	N/A	686	539
E&R TURN 30 R	750	N/A	644	518
E&R TURN 45 L	170	N/A	41	37
E&R TURN 45 R	170	N/A	24	19
E&R TURN 60 L	77	N/A	4	4
E&R TURN 60 R	77	N/A	2	2

*Includes entry and recovery time

8. DEFINITIONS

Cluster: A grouping of neighboring HUMS regimes that represent a single CWC regime occurrence. This may be subject to a minimum length requirement corresponding to flight characteristics to minimize false detection.

Cluster regime: A HUMS regime often found in close proximity to a target regime in a HUMS regime sequence report.

Cluster set: The set of cluster regimes selected as part of the defining cluster parameters.

Cross-over: Time padded to the beginning and end of the cluster to accommodate possible errors due to HUMS RR resolution or update rate (typically 1 sec per current S-92 HUMS RR algorithm refresh rate).

CWC regime: Standard maneuver used to develop CWC usage spectrum and to establish CRTs for life-limited components.

CWC mapping: The general process being developed to take HUMS RR output and transform it into CWC maneuvers for the purpose of calculating CRT adjustments using existing life calculation methodology. The mapping can be accomplished by post processing the HUMS output with the clustering algorithm.

HUMS regime: A regime determined by the onboard HUMS RR algorithms.

Persistence: The maximum time in seconds to allow inclusion of a HUMS regime as part of a cluster vs. considering it as a legitimate separate entity.

Target regime: A HUMS regime that is physically close to the CWC regime of interest, usually a principal damaging regime, which must be identified by HUMS RR to form a cluster. This may be subject to a minimum length requirement corresponding to flight characteristics to minimize false detection.

Target set: The set of target regimes selected as part of the defining cluster parameters, if more than one target regime is used to identify with the CWC regime of interest.

Validation matrix: A table that contains data to quantify RR and clustering methodology accuracy for a set of CWC maneuvers of interest.

9. CONCLUSIONS

This report documents the technical work done under delivery order (DO) 0001 with a focus on developing and demonstrating methods for validating and applying several usage and loads monitoring technologies to fleet data to achieve meaningful results to support a usage-based fatigue life management or usage-based maintenance (UBM) process. Using a regime recognition (RR) clustering approach, regime cluster definitions were developed and validated for two critical regimes using a unique set of flight test data generated by the Army Communications-Electronics Research, Development and Engineering Center during their flight test. An enhanced regime validation approach was developed in response to the challenges encountered when analyzing regime performance and interactions among a large set of regimes. It was shown how RR can be used to capture maneuver load statistics by using the RR data as a capture window, similar to how flight loads are collected in a flight loads survey program. This approach provided valuable insight into the performance of regime algorithms and their ability to capture the significant damaging load events. The RR clustering algorithm was shown to be a viable approach for refining raw RR output data to support either fleet-wide usage calculated retirement time (CRT) adjustments or individual tail number CRT adjustments without having to modify existing onboard software. The clustering algorithm provides a more realistic picture of helicopter usage than the baseline Integrated Vehicle Health Management System RR algorithms, even in the presence of a complex series of maneuvers.

Virtual monitoring of loads (VML), gross weight (GW), and center of gravity (CG) estimation algorithms were shown to be viable approaches for monitoring actual aircraft usage and loads. Though neither of these virtual methods is perfect, the error distributions are reasonable and well-behaved, such that error models can be created for use in a probabilistic framework for establishing reliability factors to ensure safety and reliability associated with UBM processes and credits.

A serial-number-based UBM approach was proposed that leverages a probabilistic reliability method to maintain 6–9's reliability when applying these methods to fleet data to calculate usage credits. This process maintains the reliability inherent in the traditional fatigue retirement time and handles the residual uncertainties present in RR, VML, or GW/CG-based fleet usage metrics.

Applying these usage monitoring technologies to fleet data uncovered some challenges that are unique to an operational fleet environment. The focus of work conducted within DO 0002 will be to apply these methods to operational fleet data within a production framework in support of a specific mock UBM certification that will be shown to be in compliance with Advisory Circular 29-2C, MG-15 [7]. This effort is ongoing and will be documented in a separate technical report for that DO.

10. REFERENCES

1.   Bradley, Natasha C., "Federal Aviation Administration Health and Usage Maintenance Mock Certification Pilot Variability Written Documentation," Army Research Labs, ARL-TR-6922, May 2014.

2.   Goodrich Document S01122-CDDD0101, "Configuration Detailed Design for the UH-60M Integrated Vehicle Health Management System Operational Usage and Regime Processing."

3.   Bates, P., Davis, M., and Sadegh, P., "Structural Usage Monitoring and Flight Regime Recognition—Compliance Validation and Demonstration Using the HUMS Advisory Circular, AC 29-2C Section MG-15," FAA report DOT/FAA/AR-12/4, 2012.

4.   Davis, M.W., Isom, J.D., Cycon, J.P., and Fletcher, J.W., "Flight Test of Technology for Virtual Monitoring of Loads," *Proceedings of the American Helicopter Society 69th Annual Forum*, Phoenix, Arizona, May, 2013.

5.   Beale, R., "Applications of Virtual Monitoring of Loads to Engineering Decision Making," *Proceedings of the American Helicopter Society 70th Annual Forum*, Montréal, Québec, Canada, May, 2014.

6.   Zion, L., Chandler, M., and White, D., "Results of Health and Usage Monitoring System Fleet Data Analysis for Usage Credits," FAA Report DOT/FAA/AR-15/15, to be published.

7.   Federal Aviation Administration, "Airworthiness Approval of Rotorcraft Health and Usage Monitoring Systems (HUMS)," Advisory Circular 29-2C MG 15, January 2011.